

**An integrated systems approach to understanding
distortion and residual stress during thermal processing:
design for heat treating**

by

Haixuan Yu

WORCESTER POLYTECHNIC INSTITUTE

In partial fulfillment of the requirements for the

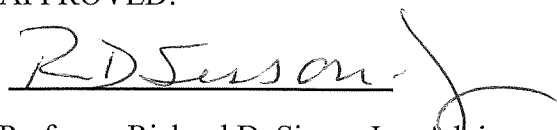
Degree of Doctor of Philosophy

in

Materials Science and Engineering

December 2019

APPROVED:



Professor Richard D. Sisson Jr. Advisor

George F. Fuller Professor

Director, Center for Heat Treating Excellence, Worcester Polytechnic Institute



Professor Brajendra Mishra

Kenneth G. Merriam Professor

Program Director, Materials and Manufacturing Engineering

Abstract

Heat treatment processes are used to develop the desired mechanical properties for steels. Unfortunately, heat treatment, especially quenching, can cause distortion. Failure to meet geometry specifications can result in extensive rework or rejection of the parts. A series of quenching simulations, using DANTE [1], have been conducted on an AISI 4140 steel Navy C-ring distortion coupon [2] and a WPI designed plate with a hole [3] to determine the effects of quenching process parameters including part geometry, agitation during quenching, and quench start temperatures on distortion. The heat transfer coefficients (HTC) of the quenchant with selected pump speeds were measured by CHTE quench probe system [4], which is the key input for heat treatment simulation. The maximum HTC of the quenching oil was increased from 2350 W/m²K to 2666 W/m²K with higher pump speed. Quenching experiments were also conducted. It was found that the experimental measured gap opening of the standard Navy C-rings increased from 0.307mm without agitation to 0.536mm at a high agitation. Quench start temperature does not have a significant effect on the gap opening. The experimental results showed good agreement with simulation results.

The important processing parameter identification was conducted using design of experiments (DoE) coupled with analysis of variance (ANOVA). The effect of processing parameters in decreasing order of importance were determined to be: quenchant type, part geometry, agitation speed, quenching orientation, quenchant temperature, immersion rates, and quench starts temperature.

Based on the simulation and experimental results, it was found that the two most important parameters are:

1. The part geometry and size (product design)
2. The temperature dependent heat transfer coefficients between the part and the quenchant (process design)

The coupling of these product and process parameters is necessary to apply the systems analysis that must be accomplished to understand the interaction between the part design and process design parameters. This coupling can be accomplished by locally applying the well-known Biot number [4].

$$Bi(T) = h(T) * L / k(T)$$

Where

$h(T)$ = film coefficient or convective heat transfer coefficient [W/m²*K].

L_c = characteristic length, which is generally described as the volume of the body divided by the surface area of the body [m].

$k(T)$ = thermal conductivity of the body [W/m*k]

The concept of a local Biot number is introduced to quantify the local variations of part size, geometry and heat transfer coefficient. First, a large Bi indicates large temperature gradients within the part. Second, large local (geometry dependent) variations in Bi number will lead to large lateral temperature gradients. Therefore, variations in local Bi can lead to large temperature gradients and therefore high stress during quenching and finally distortion. This local Bi concept can be used in a systems approach to designing a part and the quenching system. This systems approach can be designated as design for heat treating.

References

1. Ferguson, B. L., Li, Z., & Freborg, A. M. (2005). Modeling heat treatment of steel parts. *Computational Materials Science*, 34(3), 274-281.
2. Totten, G. E. (Ed.). (2002). *Handbook of residual stress and deformation of steel*. ASM international.
3. Warke, V. S. (2008). *Predicting the response of powder metallurgy steel components to heat treatment*. Worcester Polytechnic Institute. Worcester, USA.
4. Maniruzzaman, M., Chaves, J., McGee, C., Ma, S., & Sisson Jr, R. (2002, July). CHTE quench probe system: a new quench characterization system. In 5th International Conference on Frontiers of Design and Manufacturing (ICFDM) (pp. 619-625).
5. Mills, A. F. Heat Transfer, 1992. Irwin, IL.

Acknowledgements

The Ph.D. thesis could not be finished without support and extensive collaboration. I really appreciate all the helps.

First of all, I would like to express my appreciation to my advisor, Prof. Richard D. Sisson, Jr. He provides me the opportunity to work on this project and helps me to start my research career. Thanks for your encouragement and mentoring, which was not only helpful for my research study but also for school life. I am still impressed that you can give us an hour lecture base on a simple temperature versus time curve. You are the most knowledgeable person I ever met.

Thanks to my colleagues of the CHTE group, Mei Yang, Lu Yuan, Richard Smith, Lei Zhang, Anbo Wang, Xiaoqing Cai, Yangzi Xu, and Lin Yuan, who have been supportive all the time. I am so grateful to work with them and I appreciate their help, ideas, and sense of humor.

I would like to acknowledge all the members of CHTE who support my project. Particularly Olga Rowan and Mohammed Maniruzzaman from Caterpillar Inc. for their help with the quenching experiments. Also, I would like to thank Justin Sims, Charlie Li from Dante-Solution and Jean-Philippe A. Thomas from Pratt & Whitney for their suggestions.

Thanks to my friends at WPI (Xuejian Lyu, Tao Yan, Song Zhang, Piao Liu, Songge Yang, Xiaoye Qi...) that makes the life far from home become pleasurable. Special thanks to Xuejian, my best brother, for the supporting and struggling we experienced together in the past seven years.

Special thanks to Dr. Boquan Li and Michael Collins, for allowing me to use the equipment and giving me the proper training.

Last but not least, I would like to thank my parents, Zhiwei Yu and Xiaolei Xu, for your strong support. I could not have done it without you.

Table of contents

Abstract.....	2
Acknowledgements	4
Table of contents	5
CHAPTER 1 Introduction.....	8
CHAPTER 2 Literature review.....	12
CHAPTER 3 Paper I: Applications of the Navy C-ring Specimen to Study the Distortion During Quenching	19
1 Introduction.....	21
2 Experimental Procedure.....	23
2.1 CHTE quench probe system	23
2.1.1 Data Acquisition	23
2.1.2 Thermocouple connection	23
2.1.3 CHTE quench probe	23
2.1.4 Calculation of surface heat transfer coefficient using CHTE quench probe	24
2.2 Quenching experiments	26
2.2.1 FEM simulation.....	29
3 Results and Discussion.....	32
3.1 Heat transfer coefficient	32
3.2 Microstructure and crystallography	34
3.3 Gap opening.....	40
3.4 Heating and cooling behaviors	42
4 Conclusion.....	53
References.....	54

CHAPTER 4 Paper II: Identification of the important processing parameters on distortion in AISI 4140 steel	57
1 Introduction.....	59
2 Experimental Procedure.....	60
2.1 CHTE quench probe system	60
3 Results and Discussion.....	66
3.1 Rectangular component specimen	66
3.2 The effect of immersion orientation on quenching induced distortion	68
3.3 The effect of part thickness of rectangular specimen on quenching distortion.....	71
3.4 The effect of gravity on quenching induced distortion.....	74
3.5 The effect of agitation on quenching induced distortion	76
4 Navy C-ring specimen.....	80
4.1 The effect of specimen geometry and agitation speed on quenching induced distortion of Navy C-ring.....	80
4.2 Using DoE to determine the important processing parameters on distortion.....	85
5 Conclusions.....	91
References.....	92
CHAPTER 5 Paper III: The effect of heat transfer coefficient on distortion of Navy C-ring specimen.....	94
1 Introduction.....	96
2 Numerical simulation.....	98
3 Results and Discussion.....	99
3.1 Sensitivity study of HTC value on distortion of Navy C-ring specimen during quenching.....	99
3.2 Sensitivity study of HTC max on distortion of Navy C-ring specimen during quenching.....	101

3.3	Sensitivity study of HTC at convection stage on distortion of Navy C-ring specimen during quenching	103
3.4	Sensitivity study of quench starts temperature on distortion of Navy C-ring specimen during quenching.....	104
3.5	Sensitivity study of carbon content on distortion of Navy C-ring specimen during quenching.....	105
3.6	The sensitivity study of the effect of the HTC curve on distortion of the Navy C-ring using the DoE method	108
3.6.1	Significant features of HTC curves	108
3.6.2	Using DoE to determine the important processing parameters on distortion.....	110
4	Conclusions.....	114
	References.....	115
	CHAPTER 6 Summary.....	116
	CHAPTER 7 Recommendations for future work.....	118
	CHAPTER 8 Relevant presentations and publications.....	119
	Appendix 1: Full factorial design table to identify the important processing parameters on quenching distortion	121
	Appendix 2: Fractional factorial design table to study the effect of HTC curve on quenching distortion of the Navy C-ring specimen.....	127

CHAPTER 1 Introduction

Steel parts that are used in the aerospace, automotive, and heavy equipment industry rely on heat treatment, especially quenching, to acquire the desired mechanical properties. Unfortunately, during heat treating the parts may distort and develop residual stress, especially during quenching. The economic importance of distortion during heat treatment in the manufacturing industry is very high. For example, the bearing industry spends approximately 30% of production cost to eliminate the distortion by hard machining [1]. For the steel industry, heat treatment distortion is a great burden, but at the same time, it is a good opportunity for the engineers to understand the mechanisms to save time and money. The quenching process is often regarded as the 'black hole' of heat treatment [2] because residual stress and deformation induced by quenching are a consequence of complex interaction among the parameters of phase transformation, heat transfer, and strain in the steel. The phase distribution is temperature-dependent, at the same time, the phase transformation induced latent heat affect the temperature distribution.

During quenching, the significant thermal gradient can produce large thermal stress/strain. Furthermore, transformation induced stress/strain would arise due to significant volume difference between austenite and product phases especially martensite.

Numerical modeling is one of several ways being used to study the interactions that happen during heat treatment, especially, quenching [3], [4]. Seok-Jae et al. [5] used an asymmetrically cut cylinder as a distortion coupon to understand the relationship between the distortion and transformation kinetics. Li et al. [6] minimized the distortion of the as-quenched component by changing the heat transfer coefficient between the circulated gas and the surface of the component in selected regions. The distortion of disks with different carburized case depth was examined by Steinbacher et al. [7].

The Navy C-ring coupon [8] is a specimen used for characterizing dimensional changes after heat treatment. By experiment and simulation, Da Silva, A. D., et al. [9] observed an increase in both ring gap and outside diameter after quenching the Navy C-rings made of AISI 4140 steel in oil. Junwan Li, Yuan Feng, et al. [10] performed experimental and numerical investigations of deep cryogenic treatment (DCT) on SDC99 steel Navy C-rings. The retained austenite content was reduced from 15.5% to 2.3% when the part was cooled in liquid

nitrogen after conventional quenching. By modifying the hardening temperature, H. Farivar [11] introduced ferrite into the core of the carburized Navy C-ring made of AISI 8620 steel. Finite element analysis (FEA) is one of several effective methods to understand the mechanisms causing distortion and help develop a heat treatment procedure that can minimize distortion, cost as well as processing time [12]. Heat treatment analysis software including DANTE [13], DEFORM-HT [14], HEARTS [15], and SYSWELD [16] have been well developed to predict the microstructure and final distortion after heat treatment. In the heat treatment industry, design of experiment (DoE) has been widely used as an efficient approach to collect enough data using the minimum number of experiments [17]. Analysis of variance (ANOVA), mathematical technique, is usually used to investigate the relative impact of each factor in DoE [18]. Juan Dong et al. [19] used statistical analysis of the DoE to show that the most important factor influencing distortion in the process of induction hardening of AISI 1045 steel is the drawing process. The gear wheels made from SAE 5120 steel were studied by B. Clausen et al. [20], which showed volume, carburizing depth, carburizing temperature and flow velocity of the quenching gas had significant effect on distortion.

This thesis is focused on the identification and potential control of the important process parameters that affect the distortion during heat treatment. The overall project goals are:

- Determine the important heat-treating process parameters that affect the distortion in industrial parts.
- Develop a ranking of these processing parameters based on their impact.
- Provide processing guidelines to control distortion.

References

1. Zoch, H. W. (2009). Distortion engineering: vision or ready to application?. *Materialwissenschaft und Werkstofftechnik: Entwicklung, Fertigung, Prüfung, Eigenschaften und Anwendungen technischer Werkstoffe*, 40(5-6), 342-348.
2. Canale, L. D. C. F., & Totten, G. E. (2005). Quenching technology: a selected overview of the current state-of-the-art. *Materials Research*, 8(4), 461-467.
3. Jung, M., Kang, M., & Lee, Y. K. (2012). Finite-element simulation of quenching incorporating improved transformation kinetics in a plain medium-carbon steel. *Acta Materialia*, 60(2), 525-536.
4. Şimşir, C., & Gür, C. H. (2008). 3D FEM simulation of steel quenching and investigation of the effect of asymmetric geometry on residual stress distribution. *Journal of materials processing technology*, 207(1-3), 211-221.
5. Lee, S. J., & Lee, Y. K. (2008). Finite element simulation of quench distortion in a low-alloy steel incorporating transformation kinetics. *Acta Materialia*, 56(7), 1482-1490.
6. Li, Z., Grandhi, R. V., & Srinivasan, R. (2006). Distortion minimization during gas quenching process. *Journal of Materials Processing Technology*, 172(2), 249-257.
7. Steinbacher, M., Clausen, B., Hoffmann, F., & Zoch, H. W. (2009). New challenges in heat treatment and surface engineering. In Smoljan, Božo & Liščić, Božidar (Eds.), *conference in honour of prof. Liščić, Božidar* (pp. 343-349). Dubrovnik - Cavtat, Croatia.
8. Totten, G. E. (Ed.). (2002). *Handbook of residual stress and deformation of steel*. ASM international.
9. Da Silva, A. D., Pedrosa, T. A., Gonzalez-Mendez, J. L., Jiang, X., Cetlin, P. R., & Altan, T. (2012). Distortion in quenching an AISI 4140 C-ring-Predictions and experiments. *Materials & Design*, 42, 55-61.
10. Li, J., Feng, Y., Zhang, H., Min, N., & Wu, X. (2014). Thermomechanical Analysis of Deep Cryogenic Treatment of Navy C-Ring Specimen. *Journal of materials engineering and performance*, 23(12), 4237-4250.
11. Farivar, H., Prahl, U., Hans, M., & Bleck, W. (2019). Microstructural adjustment of carburized steel components towards reducing the quenching-induced distortion. *Journal of Materials Processing Technology*, 264, 313-327.
12. Wallis, R. A., & Forgings, W. G. (2010). Modeling of quenching, residual-stress formation, and quench cracking. *ASM handbook*, 22, 547-585.
13. Ferguson, B. L., Li, Z., & Freborg, A. M. (2005). Modeling heat treatment of steel parts. *Computational Materials Science*, 34(3), 274-281.
14. Arimoto, K. (1998). Development of heat treatment simulation system Deform-HT. In *Proceeding of 18th Heat Treating Conference, ASM International*, 1998.
15. Inoue, T. (1992). Metallo-thermo-mechanical Simulation of Quenching Process-Theory, and Implementation of Computer Code" HEARTS". In *Proc. 1st Int. Conf. Quenching and Control of Distortion*, 1992.

16. Jarvstrat, N., & Sjostrom, S. (1993, June). Current status of TRAST; a material model subroutine system for the calculation of quench stresses in steel. In ABAQUS User's Conference Proceedings.
17. Rani, R. M., & Seshan, S. (1998). Studies on abrasive jet machining through statistical design of Experiments. *Experimental techniques*, 22(2), 28-30.
18. Ross, P. J. (1996). *Taguchi techniques for quality engineering: loss function, orthogonal experiments, parameter and tolerance design*.
19. Dong, J., Epp, J., da Silva Rocha, A., Nunes, R. M., & Zoch, H. W. (2016). Investigation of the influence factors on distortion in induction-hardened steel shafts manufactured from cold-drawn rod. *Metallurgical and Materials Transactions A*, 47(2), 877-888.
20. Clausen, B., Frerichs, F., Kohlhoff, T., Lübben, T. H., Prinz, C., Rentsch, R., & Klein, D. (2009). Identification of process parameters affecting distortion of disks for gear manufacture Part I: casting, forming and machining. *Materialwissenschaft und Werkstofftechnik: Entwicklung, Fertigung, Prüfung, Eigenschaften und Anwendungen technischer Werkstoffe*, 40(5-6), 354-360.

CHAPTER 2 Literature review

Heat transfer during quenching process

As shown in Fig. 1, Maniruzzaman et al. used CHTE quench probe system [1] to measure the cooling rate and calculate the heat transfer coefficient of Houghton T7A quenching oil. It shows that the heat transfer during quenching with a liquid medium is a process, which is controlled by four distinct cooling stages [2, 3].

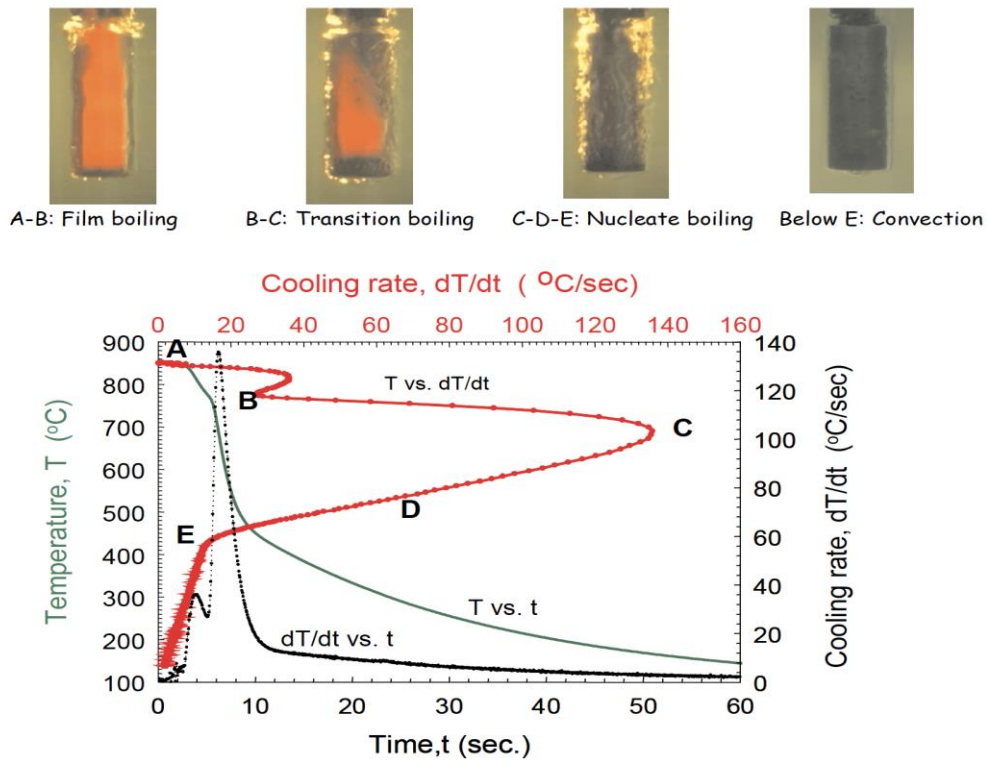


Figure 1: Temperature-Time and Cooling Rate-Temperature curves of a CHTE 4140 steel probe quenched in Houghton T7A quenching oil

At the beginning of the quenching procedure, the hot surface becomes surrounded by a vapor blanket, which is shown in range A-B. The film boiling stage has the lowest heat transfer rate, and the heat transfer occurs mainly by radiation through the vapor blanket. The vapor film is stable, and it can be removed by speed improving additives or agitation during quenching [4].

The second phase of the quenching process is called transition boiling or partial film boiling, which is shown by range B-C. In the second phase, the vapor film becomes unstable, and the

heat transfer coefficient increases. The onset of the partial film boiling stage is known as Leidenfrost point (LF).

The range C-D is the nucleate boiling regime. With a further decrease in temperature, the partial film collapses into numerous bubbles, and the quenchant contacts the part directly, which corresponds to rapid heat transfer. In this stage, the heat transfer rate reaches its maximum, which is known as critical heat flux (CHF). The nucleate boiling regime stops when the surface temperature of the part is lower than the boiling point of the liquid quenchant.

The fourth regime is the natural convection regime, where the heat is transferred by the natural convection of the liquid. Heat is removed by convection and is controlled by quenchant's conductivity and specific heat. The convection stage usually has the lowest heat transfer rate among the four stages of quenching.

The heat transfer coefficient (HTC) is the most important boundary condition for the quenching process simulation.

Modeling heat treatment of steel parts

As one of the most important heat-treating processes, quenching can generate high thermal gradients and rapid phase transformation. Such rapid processes are hard to experimentally investigate the sequence of events, for instance, internal stress states and phase fraction during quenching. In recent years, different heat treatment simulation software including HEARTS [5], TRAST [6], SYSWELD [7], DEFORM-HT [8], and DANTE [9] has been developed. Ferguson et al. [10] used DANTE to simulate a 3-D test bar with different heat treatment steps including furnace heating, carburization, air transfer, quenching, cryogenic treatment, and tempering. Rectangular bar with a "V" notch made of Pyrowear 53 is shown in Fig. 2. A finer mesh was applied on the surface due to the higher cooling rate and carbon gradient. There were 9045 nodes and 7672 elements in the meshed part. The part was simulated to heat up to 900°C with 0.8% carbon potential for 4 hours, followed by oil quenching, deep freeze to liquid nitrogen and tempered at 230°C.

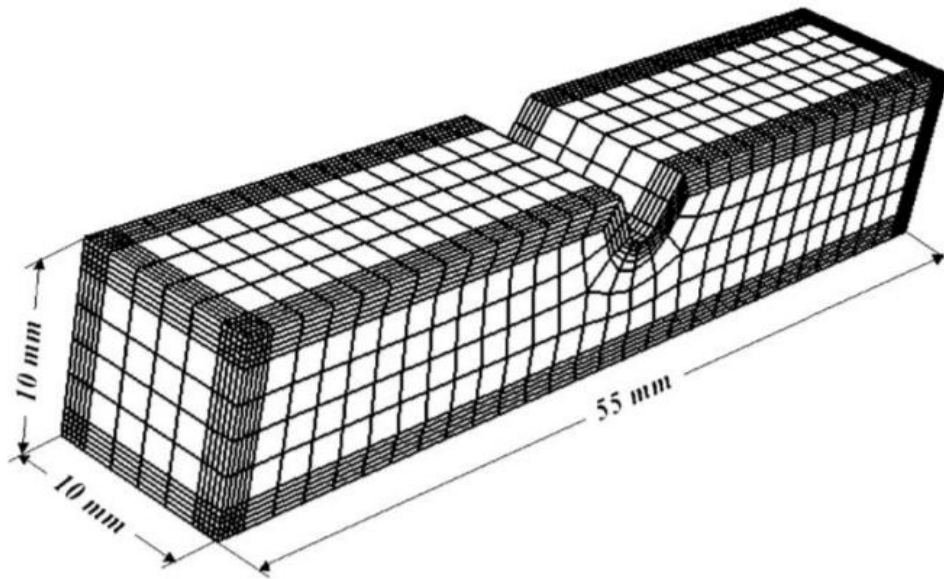


Figure 2: Rectangular bar and finite element mesh.

From the simulation results, the retained austenite composition was largely reduced after cryogenic treatment (Fig. 3).

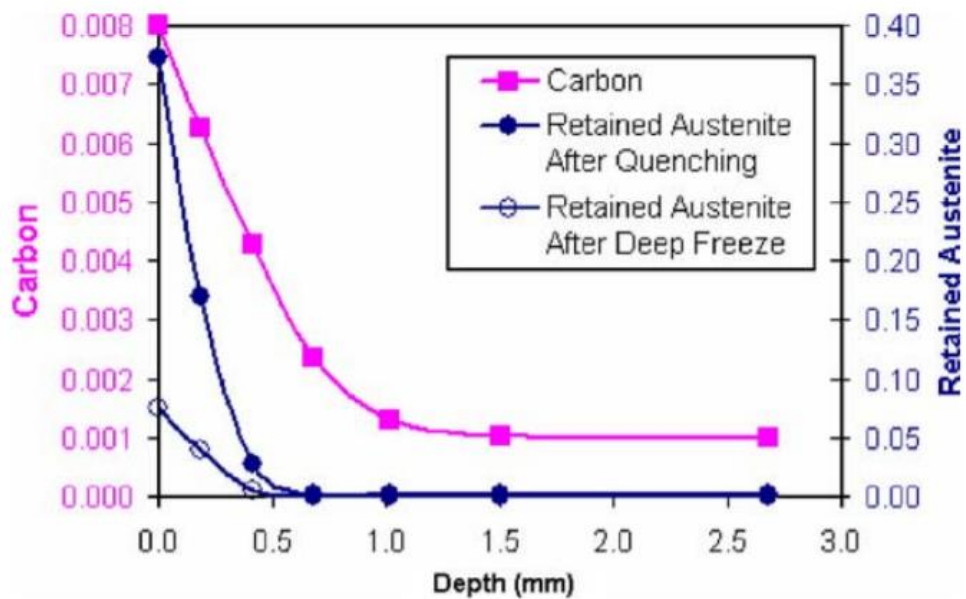


Figure 3: Carbon distribution and retained austenite content before and after deep freezing.

Fig. 4 shows the residual stress distribution in the carburized case. Compressive residual stress is generated near the surface. And the modeling results showed good agreement with the residual stress measured by X-ray diffraction.

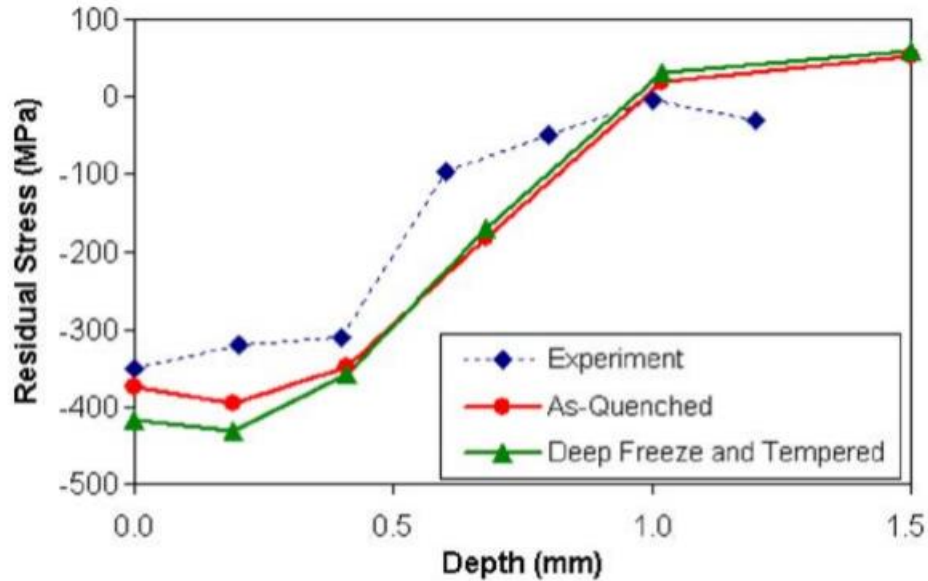


Figure 4: Comparison between modeling results and experimental results.

Microstructural adjustment of carburized steel components towards reducing the quenching-induced distortion

Farivar et al. [11] used Navy C-ring specimen made of AISI 8620 steel [12] as a distortion coupon to study the effect of hardening temperature on gap opening during heat treatment. Fig. 5 illustrates that instead of holding the parts at 860°C, the hardening temperature was dropped down to 775°C, which ferrite could nucleate and grow in the core, meanwhile, the carburized case remained in a single austenite region.

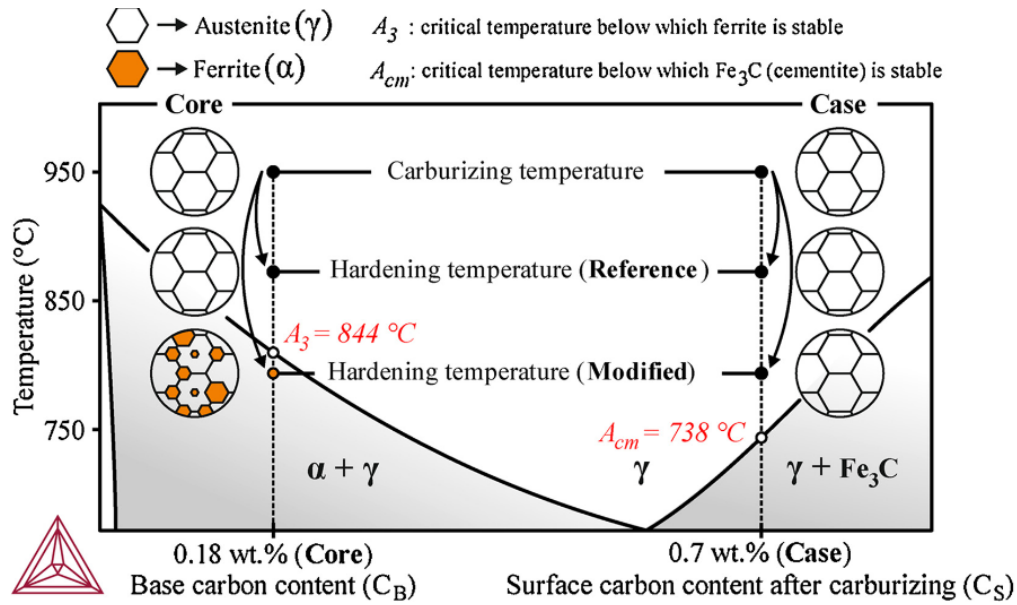


Figure 5: Schematic representation of the cycles before and after modified.

Fig. 6 shows that the gap width distortion decreased with lower hardening temperature and longer holding time, which correspond to the higher fraction of ferrite in the core of the Navy C-ring specimen. Due to the lower density of the martensite compared to ferrite, lower volume fraction of martensite would make the gap opening smaller.

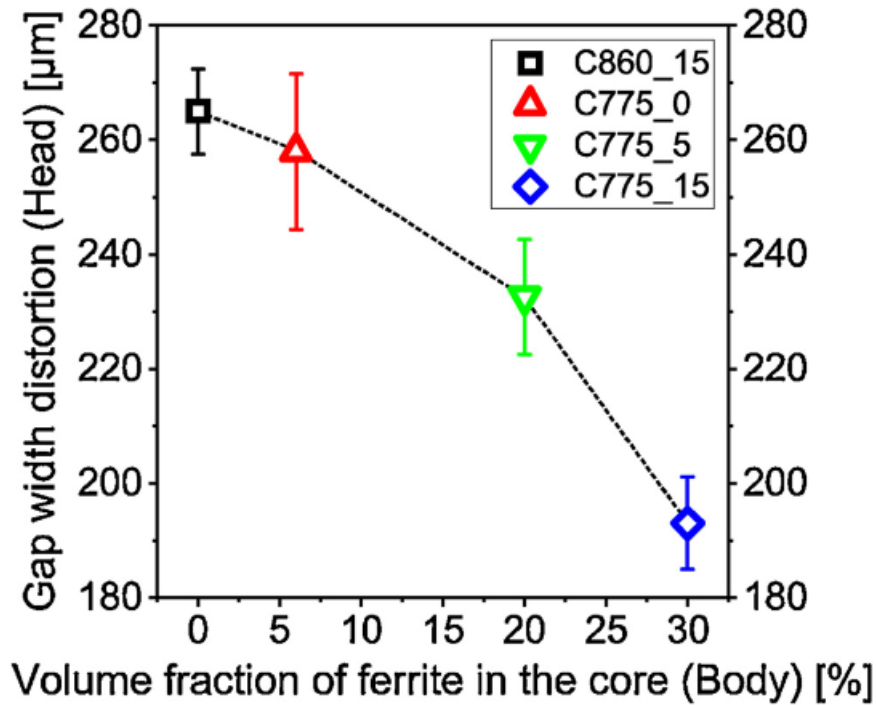


Figure 6: Correlation between ferrite fraction in the core and gap opening.

Table 1 shows that after the modification. The formation of ferrite in the core of the part only slightly bring down the tensile properties. The strain rates among the samples with selected hardening temperatures and time are very similar.

Table 1: The tensile properties of the samples with selected heat treatment conditions [11].

Specimen	σ_y (MPa)	UTS (MPa)	ϵ_u (%)	ϵ_{total} (%)
C860_15	660 \pm 7	958 \pm 9	6.2 \pm 0.9	20.2 \pm 1.0
C775_0	658 \pm 25	942 \pm 29	6.8 \pm 0.4	22.1 \pm 0.6
C775_5	658 \pm 19	978 \pm 18	7.2 \pm 0.5	22.7 \pm 0.9
C775_15	645 \pm 23	989 \pm 7	7.4 \pm 0.3	21.9 \pm 0.8

References

6. Maniruzzaman, M., Chaves, J., McGee, C., Ma, S., & Sisson Jr, R. (2002, July). CHTE quench probe system: a new quenchant characterization system. In 5th International Conference on Frontiers of Design and Manufacturing (ICFDM) (pp. 619-625).
7. Bergles, A. E. (1992). Elements of Boiling Heat Transfer. In *Boiling Heat Transfer* (pp. 389-445). Elsevier.
8. Totten, G. E., Bates, C. E., & Clinton, N. A. (1993). *Handbook of quenchant and quenching technology*. ASM international.
9. Faulkner, C. (2017, Oct). Aqueous quenchant for induction hardening. *Proceedings of the 29th Heat Treating Society Conference* (pp. 141-143). Columbus, Ohio, USA
10. Inoue, T. (1992). Metallo-thermo-mechanical Simulation of Quenching Process-Theory, and Implementation of Computer Code" HEARTS". In *Proc. 1st Int. Conf. Quenching and Control of Distortion, 1992*.
11. Jarvstrat, N., & Sjostrom, S. (1993, June). Current status of TRAST; a material model subroutine system for the calculation of quench stresses in steel. In *ABAQUS User's Conference Proceedings*.
12. SYSWELD-A predictive model for heat treat distortion, *Southwest Research Institute, 1992*.
13. Arimoto, K. (1998). Development of heat treatment simulation system Deform-HT. In *Proceeding of 18th Heat Treating Conference, ASM International, 1998*.
14. Ferguson, B. L., Freborg, A., & Petrus, G. J. (2000). Software simulates quenching. *Advanced Materials & Processes (USA)*, 158.
15. Farivar, H., Prahl, U., Hans, M., & Bleck, W. (2019). Microstructural adjustment of carburized steel components towards reducing the quenching-induced distortion. *Journal of Materials Processing Technology*, 264, 313-327.
16. Totten, G. E. (Ed.). (2002). *Handbook of residual stress and deformation of steel*. ASM international.

CHAPTER 3 Paper I: Applications of the Navy C-ring Specimen to Study the Distortion During Quenching

Haixuan Yu · Mei Yang · Richard D. Sisson, Jr

Accept by: Metal Science and Heat Treatment (Oct 2019)

Highlights:

1. CHTE quench probe system was used to measure the HTC of alphaquenched 5300 quenching oil as a function of temperature, which was a key input for heat treatment simulation.
2. Navy C-ring experiments were conducted with selected quench start temperatures and pump speeds during quenching. The simulation results showed excellent agreement with the experimental results.
3. Higher agitation levels can produce higher cooling rates in the bottom section of the Navy C-ring and transform more austenite to martensite instead of lower bainite, which enlarges the gap opening due to the relatively lower density of martensite.
4. Selected quench start temperatures do not have a significant effect on the gap opening since they have no influence on HTC of the quenchant during quenching.

Applications of the Navy C-ring Specimen to study the Distortion During Quenching

Haixuan Yu¹ · Mei Yang¹ · Richard D. Sisson, Jr.^{*1}

¹*Center for Heat Treating Excellence, Worcester Polytechnic Institute, 100 Institute Road, Worcester, MA 01609, USA*

hyu2@wpi.edu, yhxates@gmail.com (H. Yu)

meiy@wpi.edu (M. Yang)

sisson@wpi.edu (R.D. Sisson, Jr)

Abstract

Heat treating, especially quenching, is used to develop the desired properties of steels. Quench-induced distortion can result in extensive rework or rejection. A series of quenching simulations, using DANTE [1] have been conducted on an AISI 4140 steel Navy C-ring distortion coupon [2] to determine the effects of agitation and quench start temperature on quenching distortion. Heat transfer coefficients (HTC) of the quenchant with selected pump speeds were measured by CHTE quench probe system [3], which is the key input for heat treatment simulation. The maximum HTC of the quenching oil was increased from 2350 W/m²K to 2666 W/m²K with higher pump speed. Quenching experiments were also conducted. It was found that the experimental gap opening of the standard Navy C-rings increased from 0.307mm without agitation to 0.536mm at a high agitation. Quench start temperature does not have significant effect on the gap opening. The experimental results showed good agreement with simulation results.

Keywords quenching distortion · FEM · heat transfer coefficient · AISI 4140 steel · Navy C-ring

1 Introduction

The economic importance of distortion during heat treatment in the manufacturing industry is very high. For example, the bearing industry spends approximately 30% of production cost to eliminate the distortion by hard machining [4]. For the steel industry, heat treatment distortion is a great burden, but at the same time, it is a good opportunity for the engineers to understand the mechanisms to save time and money. Quenching process is often regarded as the ‘black hole’ of heat treatment [5] because residual stress and deformation induced by quenching are a consequence of complex interaction among the parameters of phase transformation, heat transfer, and strain in the steel (Fig. 1). The phase distribution is temperature-dependent, at the same time, the phase transformation induced latent heat would affect the temperature distribution.

During quenching, the significant thermal gradient can produce large thermal stress/strain. Furthermore, transformation induced stress/strain would arise due to significant volume difference between austenite and product phases especially martensite. The change in volume during phase transformation from austenite into martensite can be as high as 3.8%, and the relationship between thermal expansion after quenching and carbon content can be expressed by (Eq. 1) [6]:

$$(\Delta V_{\gamma \rightarrow \alpha} / V_{\gamma})_{20^{\circ}\text{C}} = 3.216 + 0.859 \text{ wt. \%C} - 0.343 (\text{wt. \%C})^2 \quad (1)$$

With higher carbon content, the thermal expansion due to phase transformation is higher. In fact, the phase transformation induced deformation can be more dominant than thermal-induced distortion in quenching processes [7] for most types of steel.

Numerical modeling is one of several ways being used to study the interactions that happen during heat treatment, especially, quenching [8], [9]. Seok-Jae et al. [10] used an asymmetrically cut cylinder as a distortion coupon to understand the relationship between the distortion and transformation kinetics. Li et al. [11] minimized the distortion of the as-quenched component by changing the heat transfer coefficient between the circulated gas and the surface of the component in selected regions. In the work of Fabijanic and Hilditch [12], the quenching induced distortion by nitrogen and helium gas quenching on toothed gears was compared. Gas quenching with helium obtained lower distortion than quenching

using nitrogen. The distortion of disks with different carburized case depth was examined by Steinbacher et al. [13].

The Navy C-ring coupon [2] is a specimen used for characterizing dimensional changes after heat treatment. By experiment and simulation, Da Silva, A. D., et al. [14] observed an increase in both ring gap and outside diameter after quenching the Navy C-rings made of AISI 4140 steel in oil. Junwan Li, Yuan Feng, et al. [15] performed experimental and numerical investigations of deep cryogenic treatment (DCT) on SDC99 steel Navy C-rings. The retained austenite content was reduced from 15.5% to 2.3% when the part was cooled in liquid nitrogen after conventional quenching. By modifying the hardening temperature, H. Farivar [16] introduced ferrite into the core of the carburized Navy C-ring made of AISI 8620 steel. The quenching induced distortion decreased, and the mechanical properties were still comparable to the unmodified samples. The distortion of the ferritic nitrocarburizing was studied by C. Nan, D. O. Northwood., et al. [17]. The gap tended to close, and a small expansion of the outer diameter (OD) was obtained after ferritic nitrocarburizing.

This chapter is presented in three sections. First, the measurement of the heat transfer coefficient of alphaquench 5300 quenching oil [18] as a function of temperature with selected agitation and quench start temperature using CHTE quench probe system [3] is presented. Second, the quenching experiment with the Navy C-ring specimen is described and discussed. Finally, heat treatment modeling, using commercial heat treatment code, DANTE, is presented.

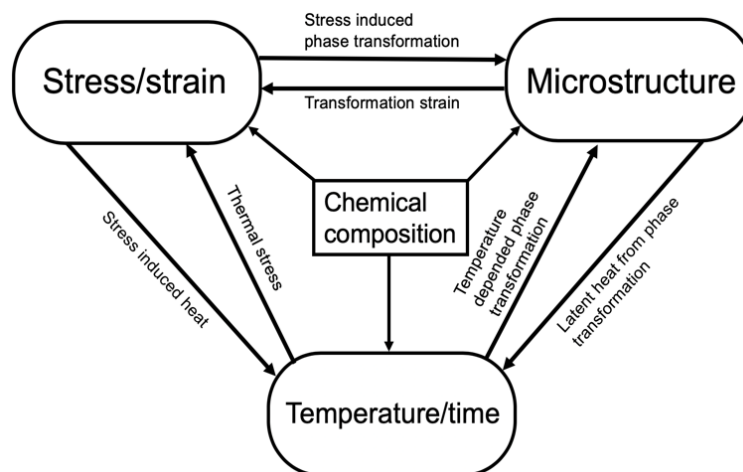


Figure 1: The interaction among stress, strain, microstructure, and temperature.

2 Experimental Procedure

2.1 CHTE quench probe system

2.1.1 Data Acquisition

The OMB-DAQ-2408 data acquisition and Tracer DAQ software were used for collecting the time-temperature data from the CAXL-116U-144-UHX-M K type thermocouple, which was placed in the center of the CHTE quench probe. The A/D analogue to digital data rate can be as high as 3000 counts per second in OMB-DAQ-2408 module. For measuring the cooling curve, 80 HZ A/D data rate was used.

2.1.2 Thermocouple connection

CAXL-116U-144-UHX-M K type thermocouple with a 1/16-inch diameter and 12-foot length was used for recording cooling data. Before inserted into the CHTE quench probe, graphite powder was applied on the probe tip so that there would be a better contact between the thermocouple and quench probe.

2.1.3 CHTE quench probe

The geometry of the CHTE quench probe, along with the coupling, is shown in Fig. 2. The diameter of the probe is 3/8 inch, and the length of probe and coupling is 3/2 inch. An Allen set screw of 1/16 inch (#6-32) was used in the coupling to tighten thermocouple and probe. Resbond 989, high-purity alumina ceramic, was applied to the interface between the probe and coupling to eliminate the oil leakage during quenching. The fabricated CHTE quench probe made by Hass ST-30Y CNC lathe is shown in Fig. 3a. The assembled CHTE quench probe is shown in Fig. 3b.

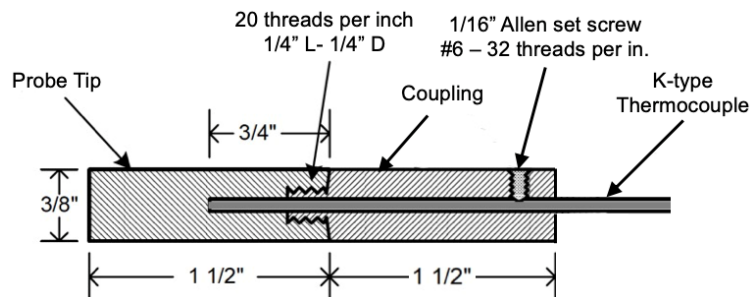


Figure 2: CHTE quench probe-coupling assembly [3].

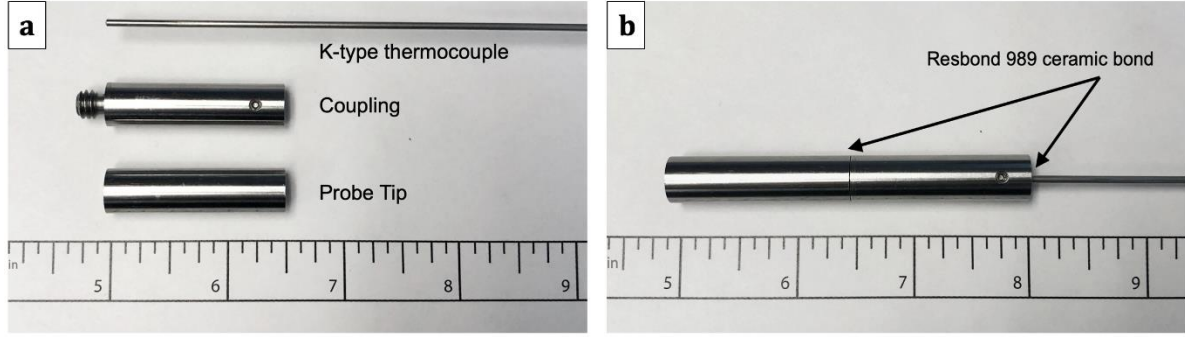


Figure 3: Fabricated CHTE quench probe by CNC lathe (a), assembled probe (b).

2.1.4 Calculation of surface heat transfer coefficient using CHTE quench probe

When the difference of temperature within a rod is small enough to ignore, the changes in internal energy can then be expressed in terms of changes of the average temperature of the system. Such approximation is named the lumped thermal capacity model [19]. The lumped-capacity model is valid for parts when the Biot number is less than 0.1, and CHTE quench probe satisfies this condition. The heat balance is expressed by equation (2):

$$\rho V C_p \frac{dT}{dt} = -\bar{h}_c A (T - T_e) \quad (2)$$

where, ρ = Density of the material, kg/m^3

V = volume, m^3

C_p = specific heat, $\text{J/kg} \cdot ^\circ\text{C}$

dT/dt = cooling rate, $^\circ\text{C/s}$

\bar{h} = heat transfer coefficient averaged over the surface area, $\text{W/m}^2 \text{K}$

A = surface area, m^2

T = temperature of the probe surface, $^\circ\text{C}$

T_e = temperature of the oil, $^\circ\text{C}$

Equation (2) can be re-written as:

$$\bar{h}_c = \frac{\rho V C_p(T) \frac{dT}{dt}}{A(T_e - T)} \quad (3)$$

For 304 stainless steel, three linear segments [20] can be used for specific heat calculation.

When $T < 83.2\text{ }^{\circ}\text{C}$,

$$C_p = 0.3542 T + 492.58$$

$83.2\text{ }^{\circ}\text{C} < T < 315.5\text{ }^{\circ}\text{C}$,

$$C_p = 0.1665 T + 508.2$$

$T > 315.5\text{ }^{\circ}\text{C}$,

$$C_p = 0.2551 T + 408.26$$

The CHTE quench probe system is shown in Fig. 4. In order to safely handle the probe and maintain the connections with the thermal acquisition, a 12-foot-long thermocouple was used.

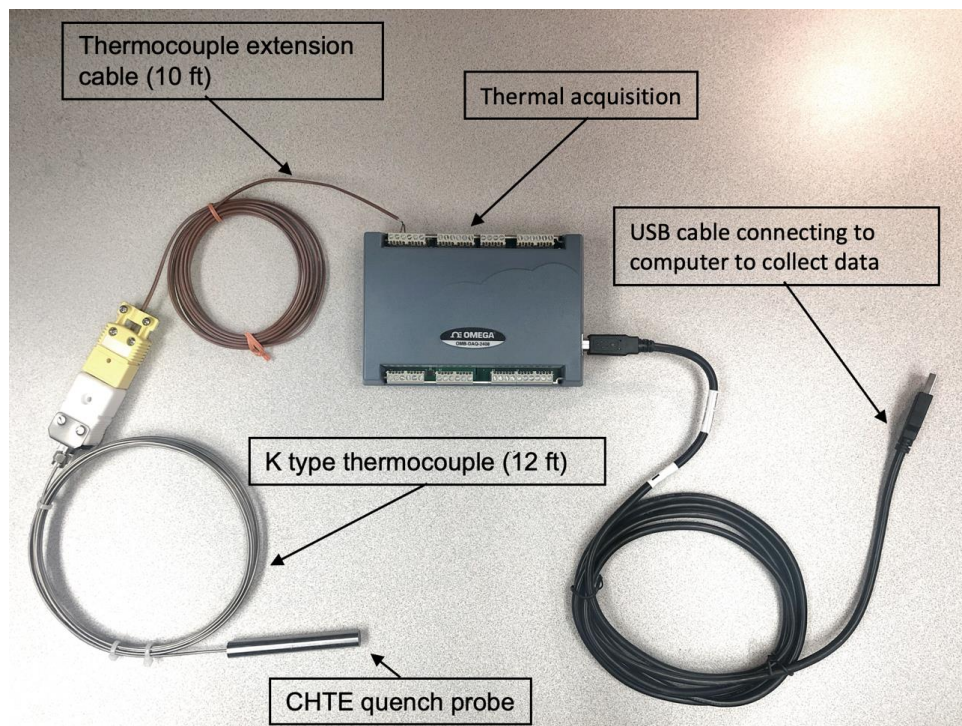


Figure 4: CHTE quench probe system to measure the heat transfer coefficient.

2.2 Quenching experiments

To study the correlation between processing parameters and quenching induced distortion, Navy C-ring specimens were fabricated from AISI 4140 hot rolled steel round bars using Hass ST-30Y CNC lathe in Worcester Polytechnic Institute (Fig. 5). The chemical composition of the steel was measured by SPECTROMAXx optical emission spectroscopy (OES), and the results are given in Table 1. The geometry of Navy C-ring is shown in Fig. 6. The fabricated parts by CNC lathe are shown in Fig. 7. Twenty-two Navy C-ring specimens were manufactured for quenching experiments, and the test plan is presented in Table 2. Test parts and quench probe were tied to a quenching basket, heated up in AFC-Holcroft CJ-4718 atmospheric furnace at selected quench start temperatures in 40 minutes and quenched in alphaquench 5300 quenching oil with various pump speeds and quenching orientations (Fig. 8). The gap opening was measured by Fowler electronic IP54 inside micrometer [21] after quenching experiments. The flow rate of the quenchant with selected pump speeds was measured by Swoffer current velocity meters [22].

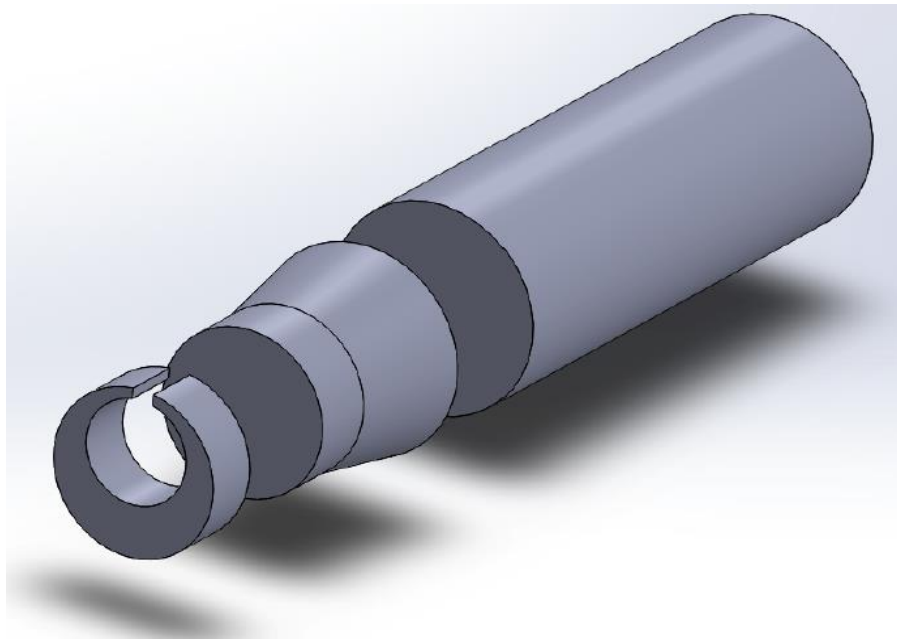


Figure 5: Illustration of fabrication of Navy C-ring specimen by CNC lathe.

Table 1: Chemical composition of AISI 4140 steel measured by OES (wt.%)

Fe	C	Si	Mn	Cr	Ni	Mo	Cu
Rest	0.396	0.225	0.920	0.860	0.090	0.169	0.214

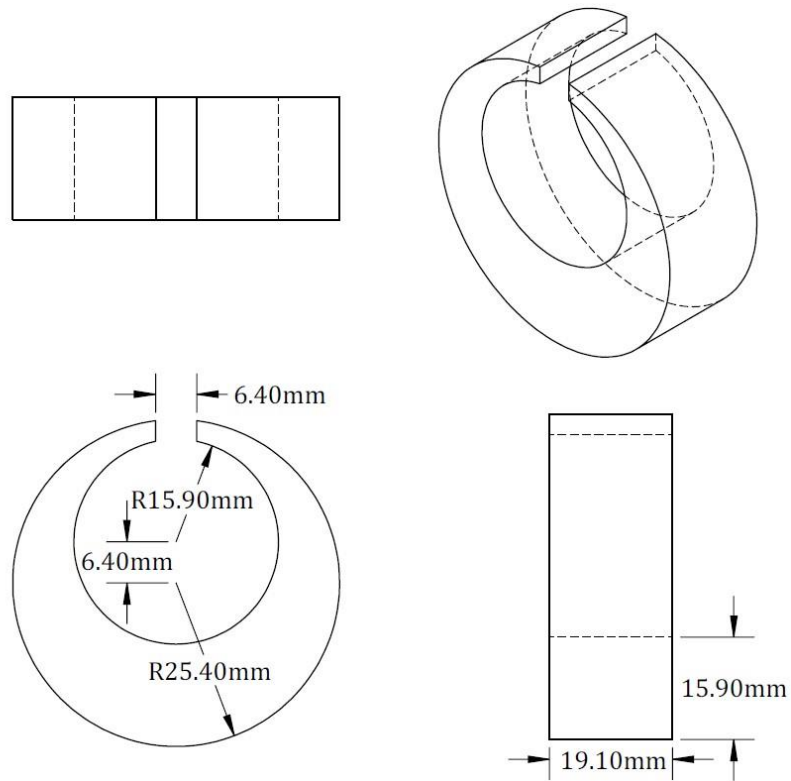


Figure 6: Dimensions of the Navy C-ring specimen.

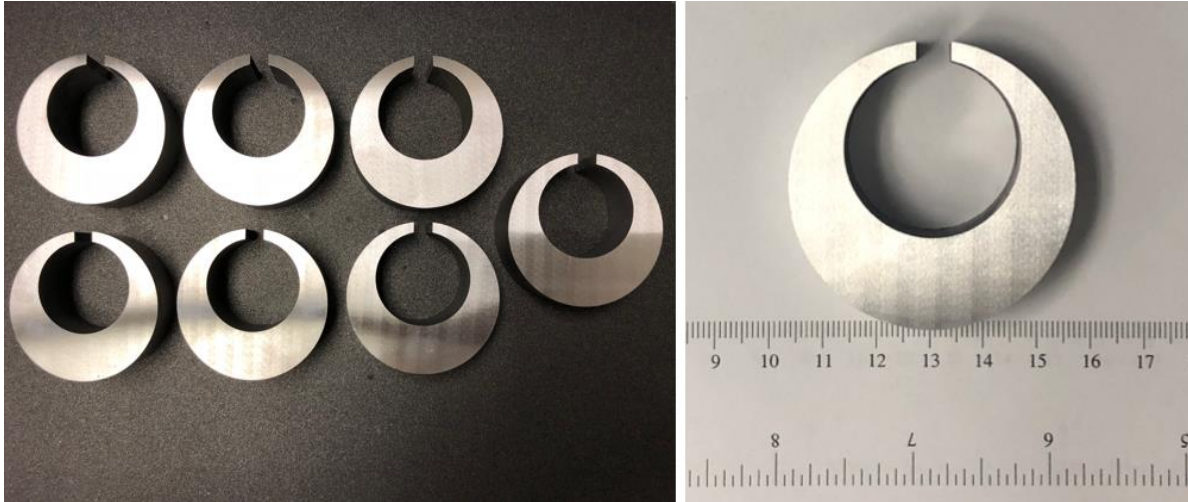


Figure 7: Fabricated specimens made by AISI 4140 steel using CNC lathe.

Table 2: Test plan of quenching experiments

Test No.	Sample No.	Pump speed	Quench start temperature, °C
1	1, 2	no agitation	850
2	3, 4	25% agitation	850
3	5, 6	55% agitation	850
4	7, 8	25% agitation	900
5	9, 10	25% agitation	950



Figure 8: Setup of Navy C-ring and CHTE quench probe before heat treatment.

2.2.1 FEM simulation

The heat treatment modeling of the Navy C-ring was carried out using finite element analysis (FEA) software ABAQUS coupled with heat treatment analysis software DANTE. Fig. 9 gives the three-dimensional finite element (FE) model of the steel part for heat treatment simulation. In order to have accurate simulation results, a finer mesh was applied near the surface. Due to the symmetry of the specimen, only one-quarter of the part was simulated. The finite element mesh consisted of 21584 nodes and 18900 quad elements. Node A was used to measure the distortion of the gap after heat treatment simulation. Node B, C, D, E, and F were used to track the temperature, cooling rate, and phase fraction in quenching simulation. The finite element (FE) setup for the simulation is summarized in Table 3. The air transfer time is as same as the time measured in quenching experiment. Constant HTC as a function of temperature was applied to all surfaces of the part.

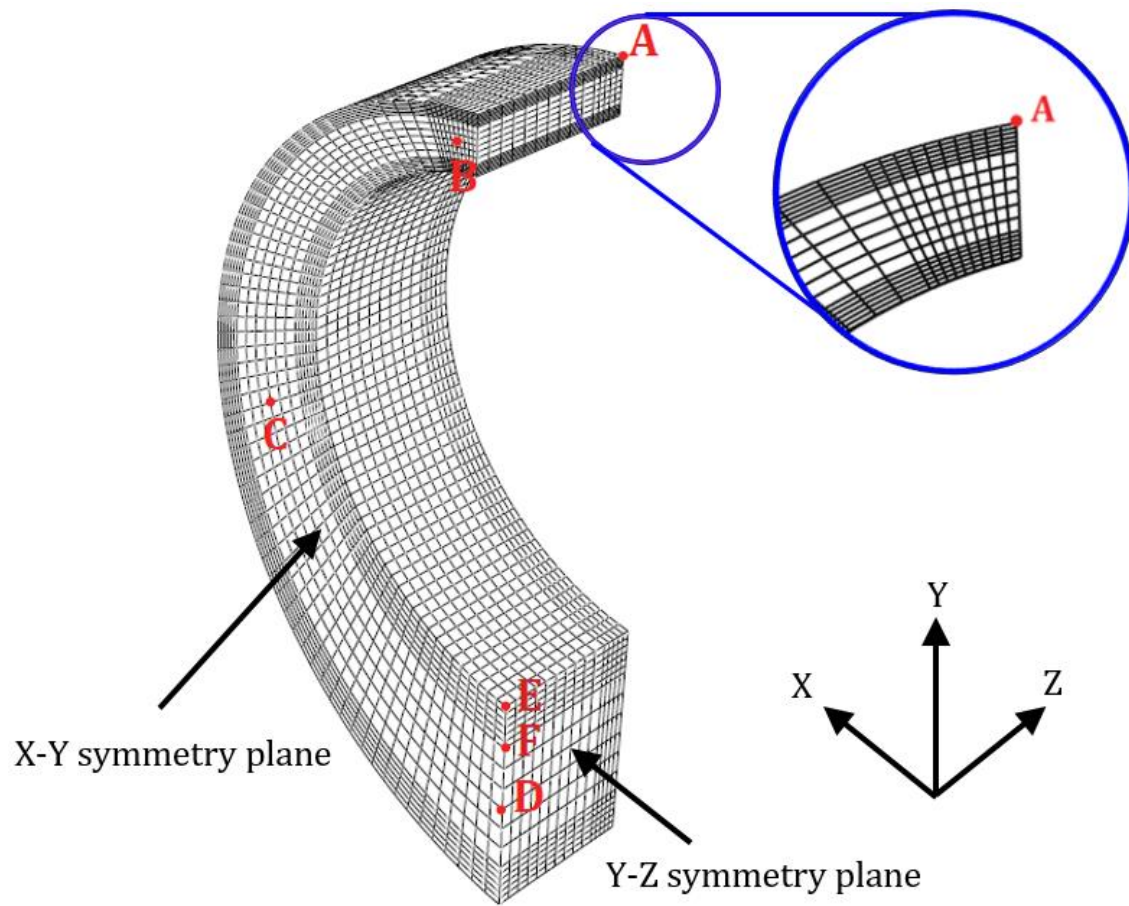


Figure 9: Solid model and finite element mesh used for heat treatment simulation.

Table 3: FE setup for the simulations.

Operation	Parameter	Value
Step 1: Heating	Code	DANTE
	Specimen geometry	Fig. 6
	Material Property	AISI 4140 steel from DANTE data base
	Initial temperature	20°C
	Austenitizing temperature	850°C, 900°C, 950°C
	Time	40 minutes
Step 2: Air transfer	Code	DANTE
	Time	15 seconds
Step 3: Immersion quenching	Code	DANTE
	Time	2 seconds
Step 4: Quenching	Code	DANTE
	Heat transfer coefficient	Function of temperature measured by CHTE quench probe
	Quenchant	Alphaquench 5300
	Time	5 minutes

3 Results and Discussion

3.1 Heat transfer coefficient

The heat transfer coefficient of alphaquench quenching oil measured by CHTE quench probe system with selected quenching conditions is shown in Fig. 10, and Fig. 11. With increasing pump speed, the HTC increases in both nucleated boiling region and convection region. By increasing agitation speed during quenching, the maximum HTC changes from 2350 W/m²K to 2666 W/m²K. The details of HTC with selected pump speeds are shown in Table 4. The HTC in convection region also increases with higher pump speed. Higher agitation level breaks down the vapor blanket faster comparing with lower agitation level and forces the transition to nucleate boiling. It also cools the liquid near the workpiece faster. Therefore, higher HTC is obtained in both nucleation stage and convection stage. On the other hand, with selected quench start temperature, there is no difference in both nucleation boiling and convection regions. The correlation between pump speed and flow rate measured by flow meter is shown in Table 5. It was expected that the flow rate increased with the pump speed of the quench tank.

Table 4: The heat transfer coefficient with selected pump speeds.

Pump speed, %	Maximum HTC, W/m ² K	HTC at Martensite start Temperature, W/m ² K
0	2350	735
25	2470	976
55	2666	1700

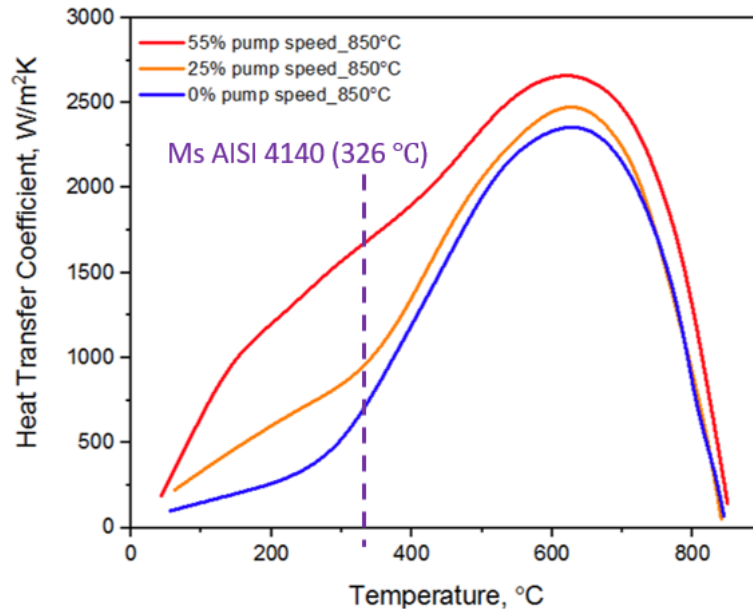


Figure 10: Heat transfer coefficient of alphaquench 5300 quenching oil with selected pump speed.

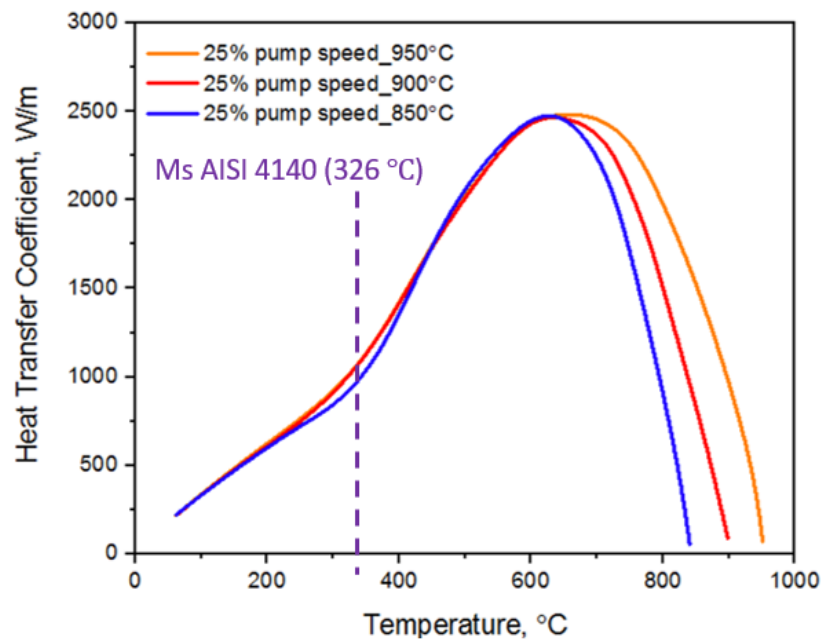


Figure 11: Heat transfer coefficient of alphaquench 5300 quenching oil with selected quench start temperature.

Table 5: The relationship between pump speed and flow rate.

Pump speed, %	Velocity, feet/second
25	0.41
35	0.82
45	1.55
55	2.08

3.2 Microstructure and crystallography

Fig. 12a, and Fig. 12b show one of the tested Navy C-ring specimens before and after heat treatment. The samples were cut, mechanically ground, polished, and etched with 4% nitric acid solution. The microstructure from the bottom center of the cross-section (Fig. 13) of the as-fabricated and as-quenched Navy C-ring specimens were characterized. The quenching orientation is also shown in Fig. 13. OLYMPUS DP73 optical microscope and JEOL JSM-7000F Scanning Electron Microscope (SEM) were used for microstructure investigation. The microstructure of Navy C-ring specimens with selected pump speed are very similar. As shown in Fig. 14, and Fig. 15, the microstructures of as-received material mainly consisted of pearlite and ferrite (Fig. 14a, b and Fig. 15a, b). After quenching into the oil with 25% pump speed, the lath martensite was obtained (Fig. 14c, d, and Fig. 15c, d). As it is shown in Fig. 16. The microhardness profile on the cross-section of Navy C-ring specimens with the selected pump speeds was taking along the x-axis by Wilson VH3300 automatic hardness tester. The average hardness and the standard deviation for each measurement are shown in Table 6. The approximately homogeneous microhardness was present in various locations with each quenching condition. With higher pump speed, the average hardness of the cross section was slightly increased, which was likely related to the increased martensite amount in the bottom part of the Navy C-ring. This is due to the higher cooling rate in the core of the part.

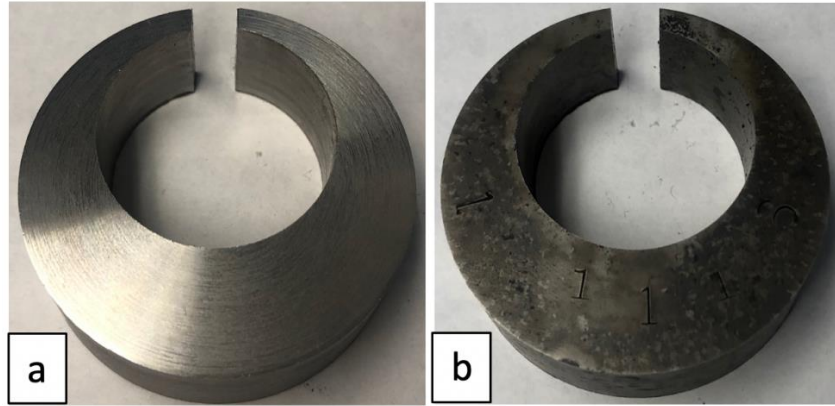


Figure 12: The Navy C-ring sample before and after heat treatment at a pump speed of 25%.

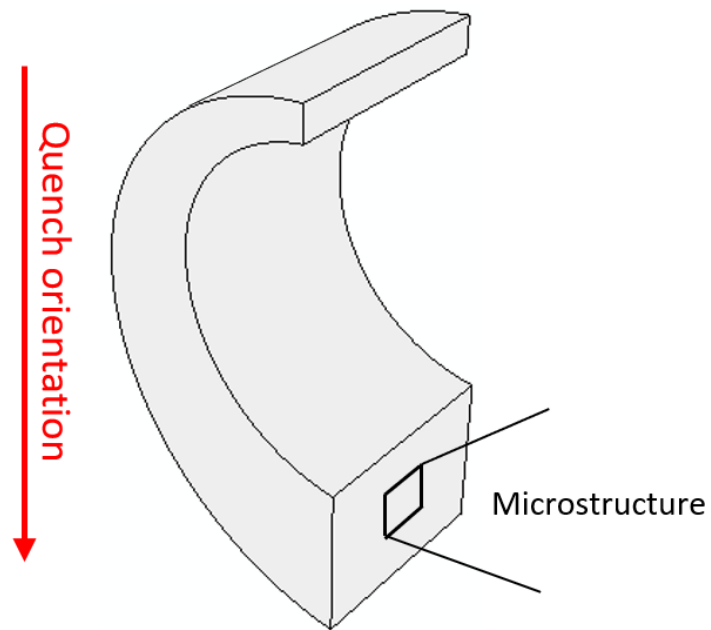


Figure 13: Quenching orientation of the Navy C-ring.

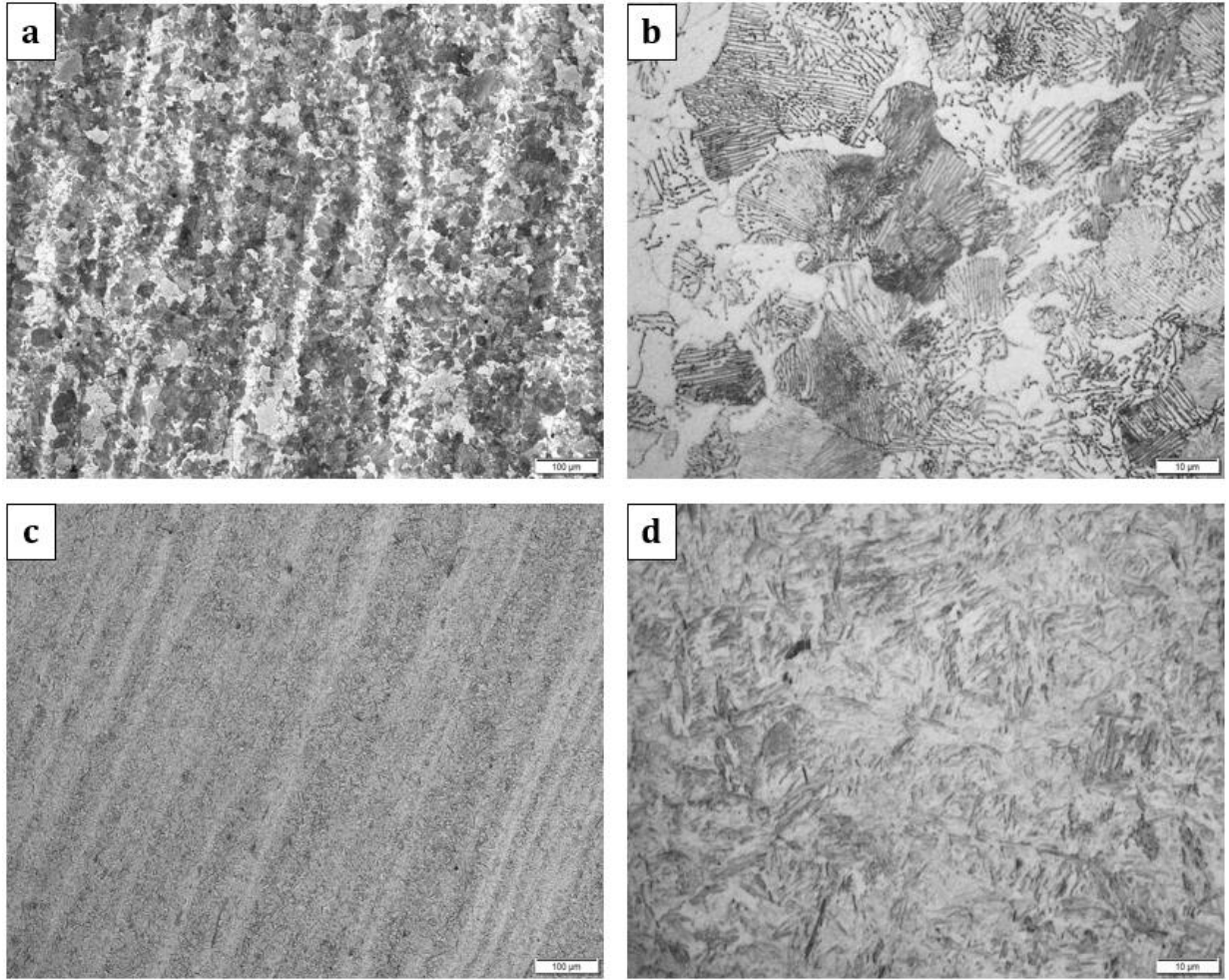


Figure 14: The optical micrographs near Node D of Navy C-ring: (a) and (b): as-fabricated, (c) and (d): as-quenched

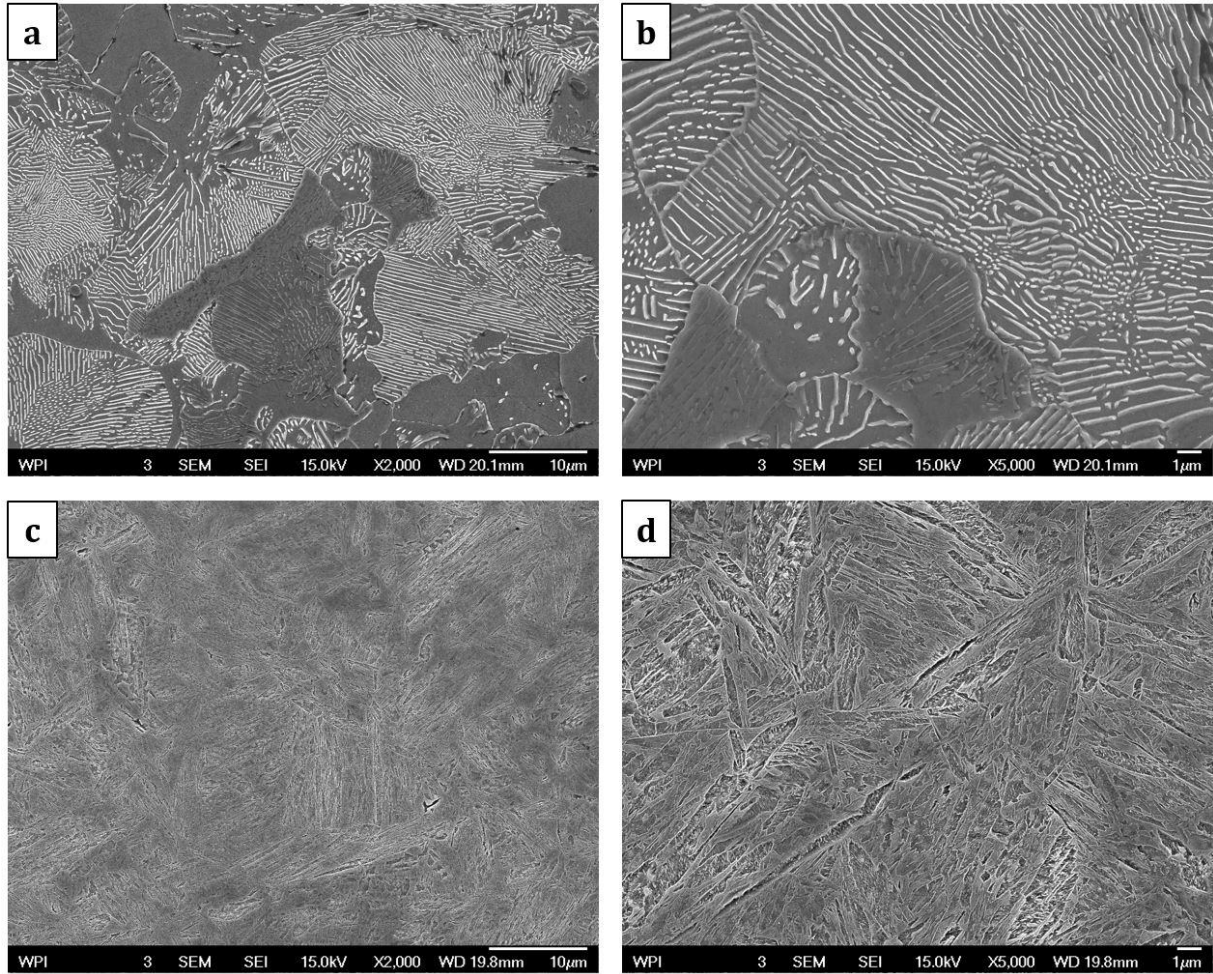


Figure 15: The scanning electron micrographs near Node D of Navy C-ring: (a) and (b): as-fabricated, (c) and (d): as-quenched

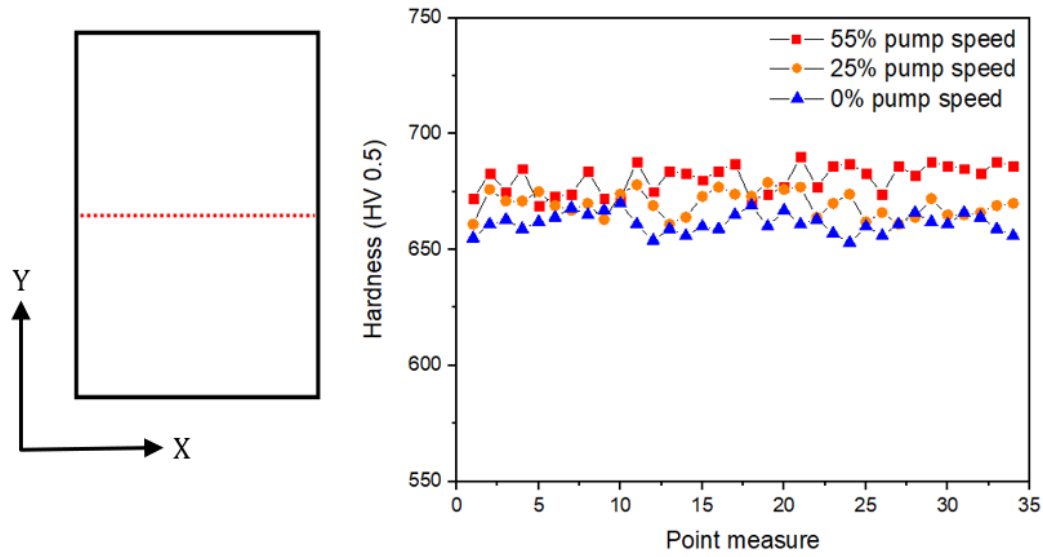


Figure 16: Microhardness of the cross-section of Navy C-ring with selected pump speeds.

Table 6: The average and standard deviation of the hardness with selected pump speeds.

Pump speed, %	Average Hardness, HV	Standard Deviation, HV
0	661.44	4.36
25	669.59	5.41
55	680.68	6.22

The high-resolution PANalytical Empyrean X-ray diffractometer was also used to characterize the crystal structure of the parts before and after quenching. To obtain a better resolution of the XRD pattern, Cr-K α radiation was used at 30 kV voltage and 55 mA current. In order to reduce the effect of the deformation layer due to sample preparation [23], the sample was vibratory polished using Buehler Vibromet 2 Vibratory Polisher with colloidal silica suspension (0.05 μm with 9.8 pH). The XRD patterns from the bottom center of the Navy C-ring specimens with selected pump speeds are very similar and no retained austenite was found by XRD. (Fig. 17). The XRD patterns with 25% pump speed before and after heat treatment is shown in Fig. 18. The peaks get broadened due to the smaller grain

size of the martensite and micro-strain present in the martensite comparing to ferrite. The positions of the peaks moved to the left due to the supersaturation of carbon in martensite, which gives larger d spacing. Rietveld refinement analysis [24, 25] was conducted by HighScore Plus 4.1 software. Martensite is a body-centered tetragonal structure with I4/mmm space group. The c/a ratio of martensite is calculated to be 1.012. According to the modified equation, $c/a = 1 + 0.031 \text{ wt\%C}$ from Yuan and Sisson [26], the carbon content in the martensite is 0.39%.

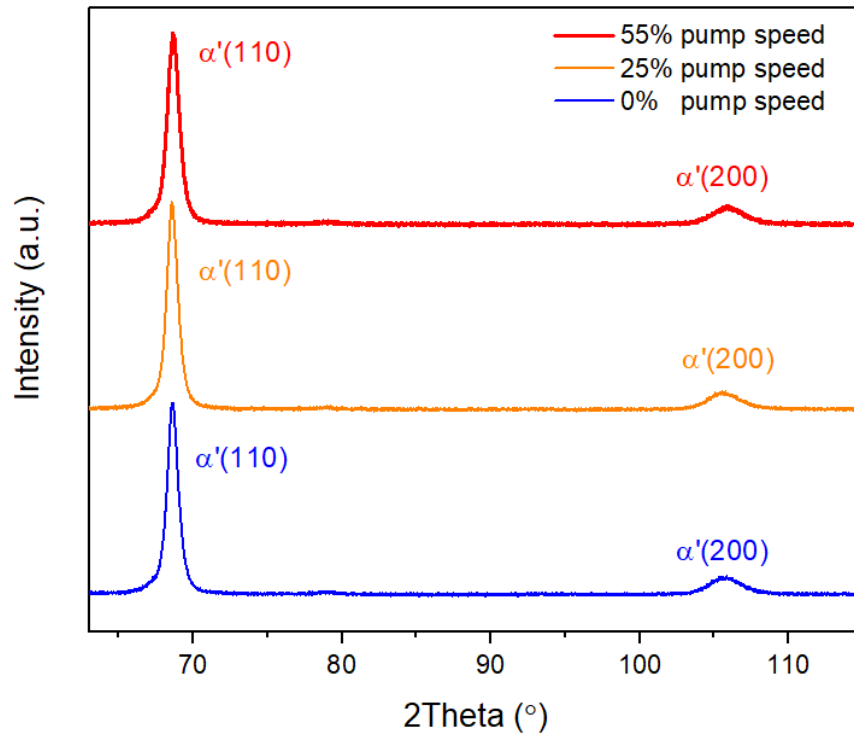


Figure 17: The XRD patterns from the bottom center of the Navy C-ring specimens with selected pump speeds.

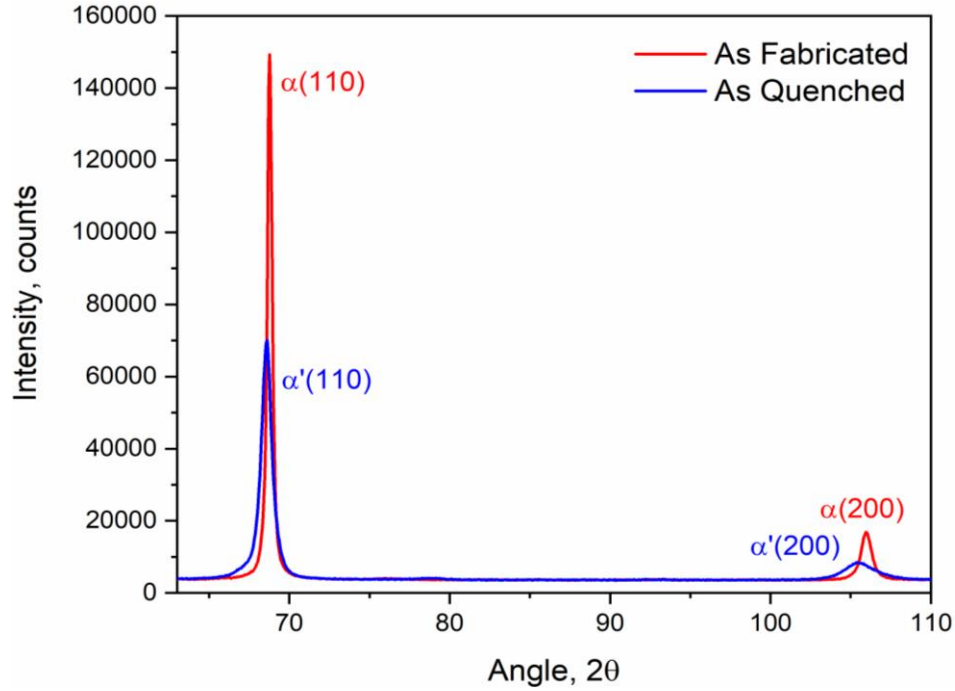


Figure 18: The comparison of the XRD pattern before (red) and after quenching (blue).

3.3 Gap opening

The gap openings of Navy C-ring specimens are representative of distortion with selected pump speed. Fig. 19 illustrates the effect of pump speed on distortion of Navy C-ring. A larger gap opening was obtained with higher pump speed in both modeling and experiment results. The difference between both methods is small. Increasing pump speed can generate a higher cooling rate in the core of the Navy C-ring, which would transform more austenite to martensite instead of lower bainite, and because of the relatively lower density of martensite, the gap opening tends to become larger. As it is shown in Fig. 20, the modeling results show that higher pump speed increases the volume fraction of martensite and decreases the volume fraction of lower bainite in Node D, which has a good agreement with the microhardness result.

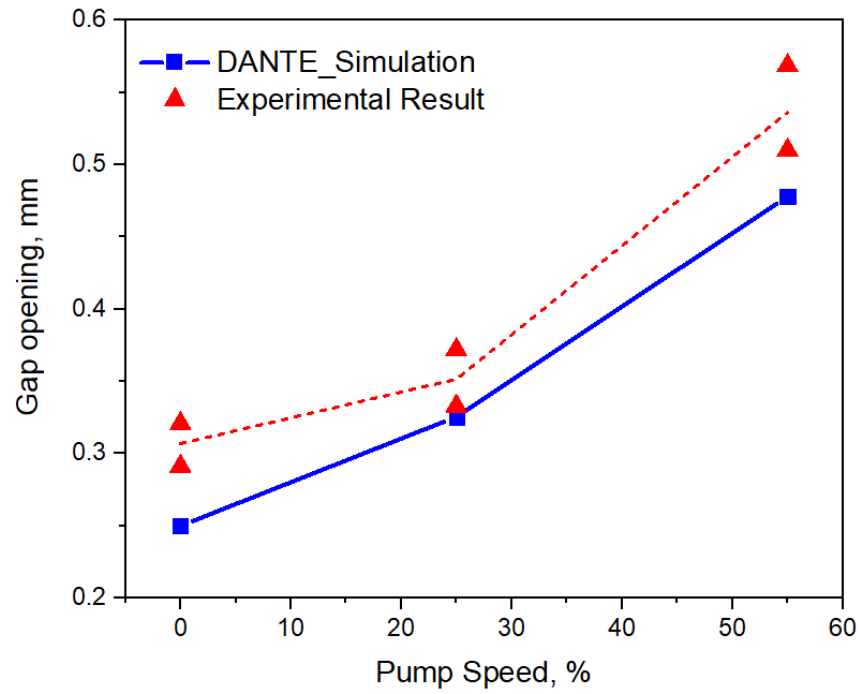


Figure 19: The gap opening with selected pump speeds after quenching.

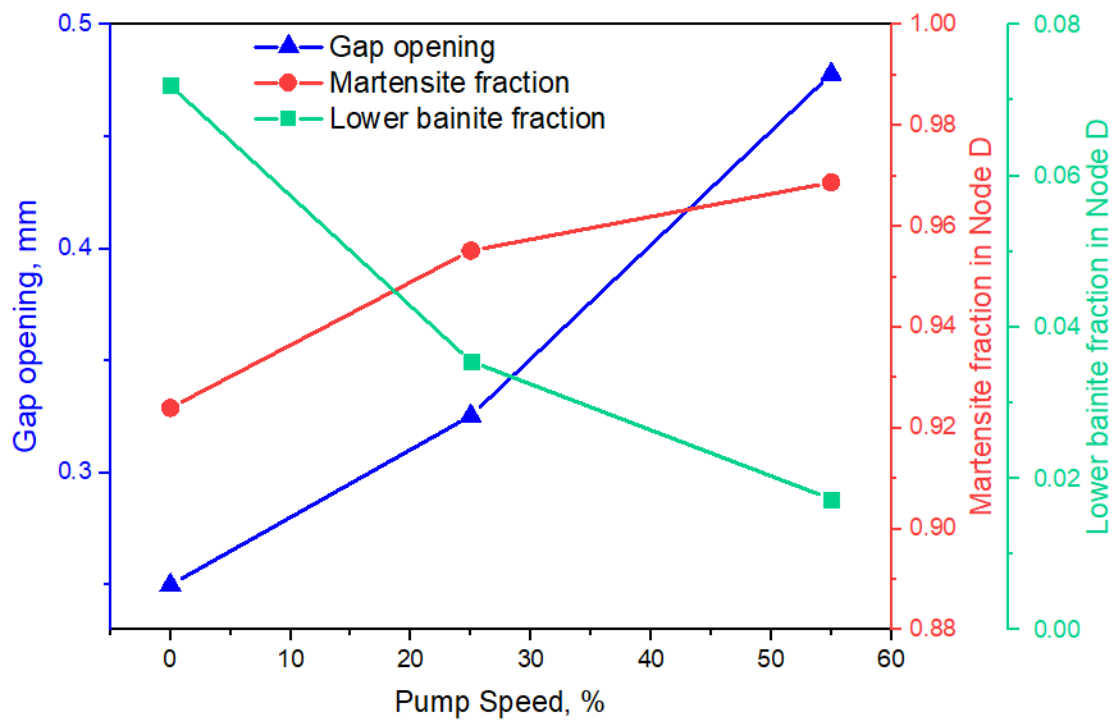


Figure 20: The correlation among gap opening, martensite fraction, and lower bainite fraction in Node D after quenching.

3.4 Heating and cooling behaviors

As it is shown in Fig. 21, the calculated cooling curves of Node D with selected pump speeds are plotted on the continuous cooling transformation (CCT) diagram of AISI 4140 steel from the DANTE material database. It illustrates that with lower pump speed, the cooling curve of Node D moves to the right side, and more austenite is transformed to bainite instead of martensite during quenching. For each curve, there is a plateau at the martensite start temperature due to the latent heat of phase transformation from the surrounding material of Navy C-ring.

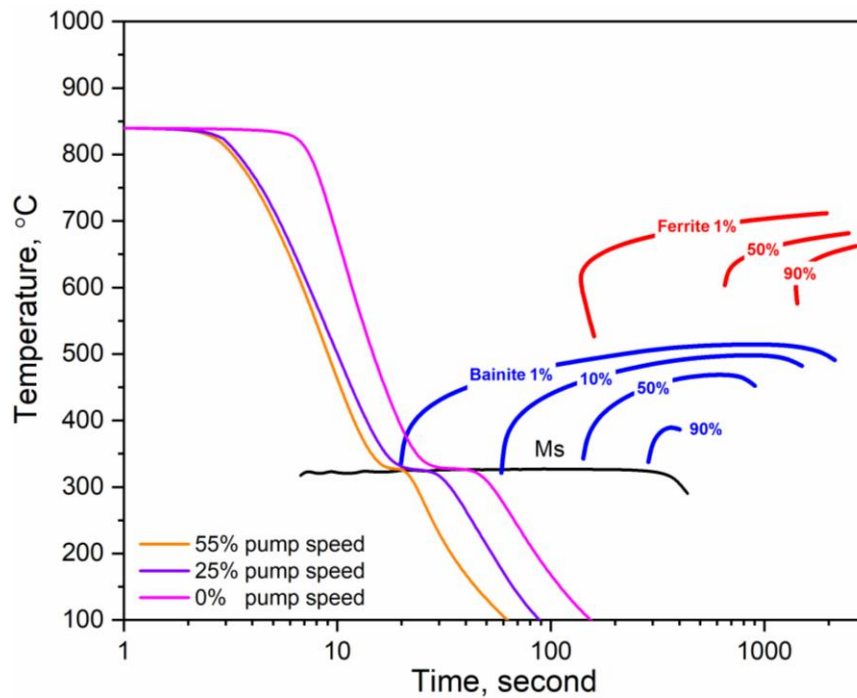


Figure 21: The cooling curves of Node D with selected pump speeds in the CCT diagram of AISI 4140 steel.

Fig. 22 presents the effect of quench start temperature on Navy C-ring distortion. There is no significant difference among gap opening with selected quench start temperatures in both experiment and simulation results. This is because with selected quench start temperature, the HTC of alphaquench 5300 quenching in both nucleation boiling and convection regions is the same.

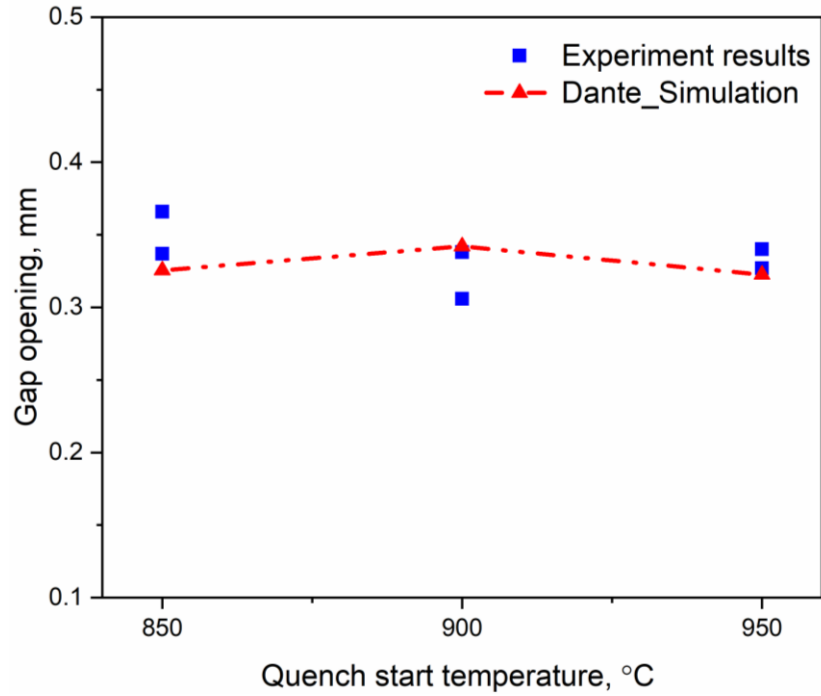


Figure 22: The gap opening with selected quench start temperatures.

In Fig. 23, the cooling curves of Node D with selected quench start temperatures at a pump speed of 25% are plotted on AISI 4140 CCT diagram. With selected quench start temperatures, the cooling curves of Node D are very similar to each other after 10 seconds. The quench start temperature does not have a significant effect on the gap opening after quenching since each case produces similar cooling behavior and bainite fraction in Node D.

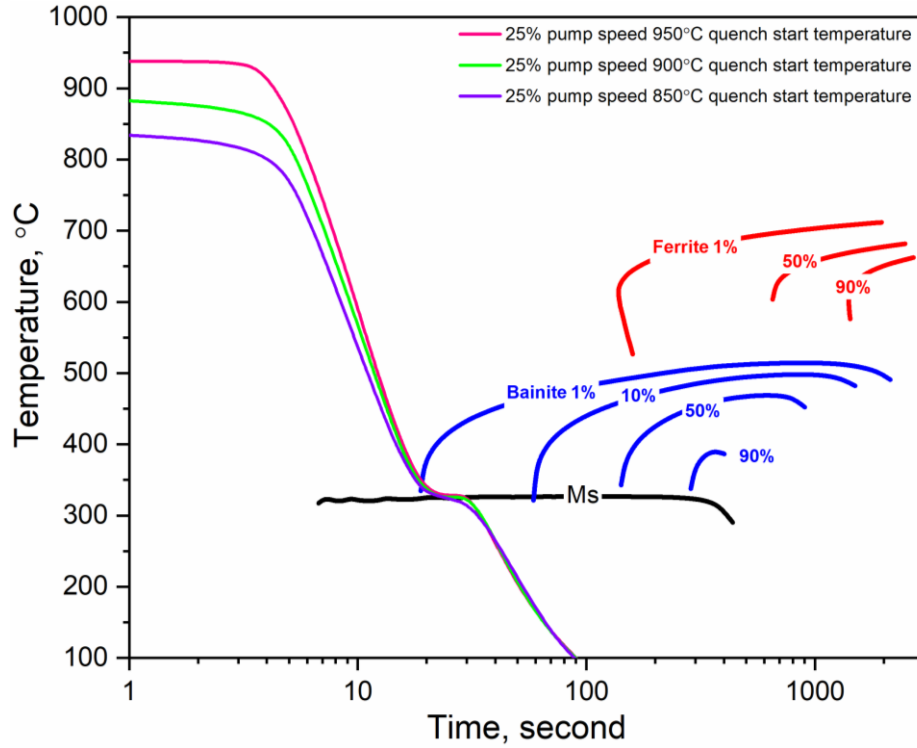


Figure 23: The cooling curves of Node D with selected pump speeds in CCT diagram of AISI 4140 steel.

Fig. 24 and Fig. 25 show the calculated cooling curves and cooling rate curves of a Navy C-ring specimen at selected locations in the simulation of quenching the specimen in oil at a pump speed of 25%. Due to the relatively thinner thickness, the cooling rate of node B can be as high as 260°C/s, while the cooling rate for Node D is less than 100°C/s. The calculated cooling rate as a function of temperature is shown in Fig. 26. According to the time-dependent martensite volume fraction curves (Fig. 27), the austenite starts to transform to martensite after 20 seconds for node B, meanwhile, after 80 seconds, the whole part transforms to martensite.

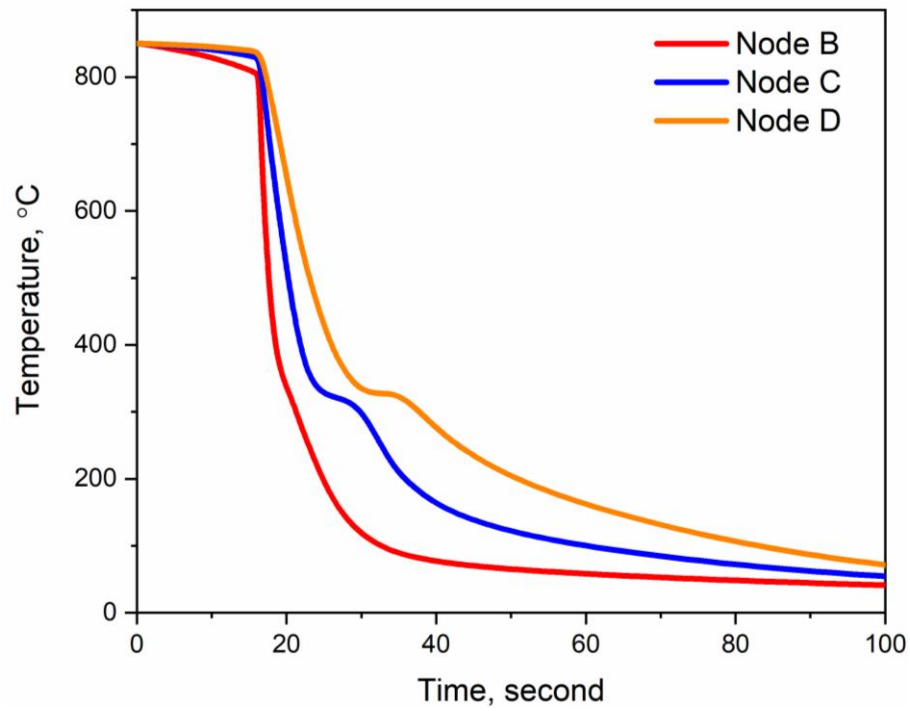


Figure 24: Calculated cooling curves at Node B, C, and D of Navy C-ring during quenching.

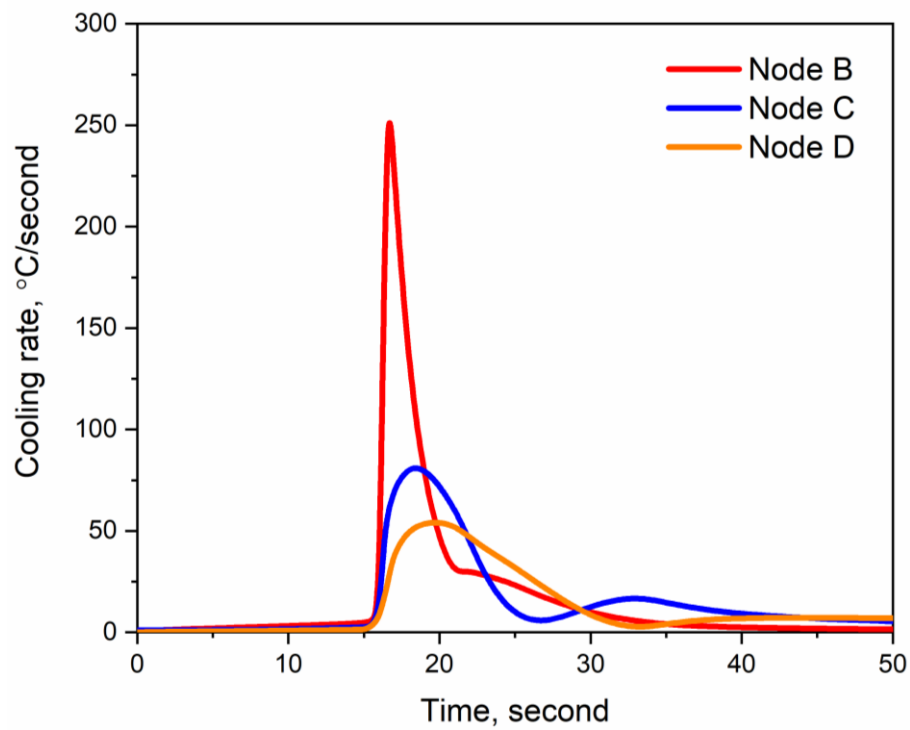


Figure 25: Calculated cooling rate curves at Node B, C, and D of Navy C-ring during quenching.

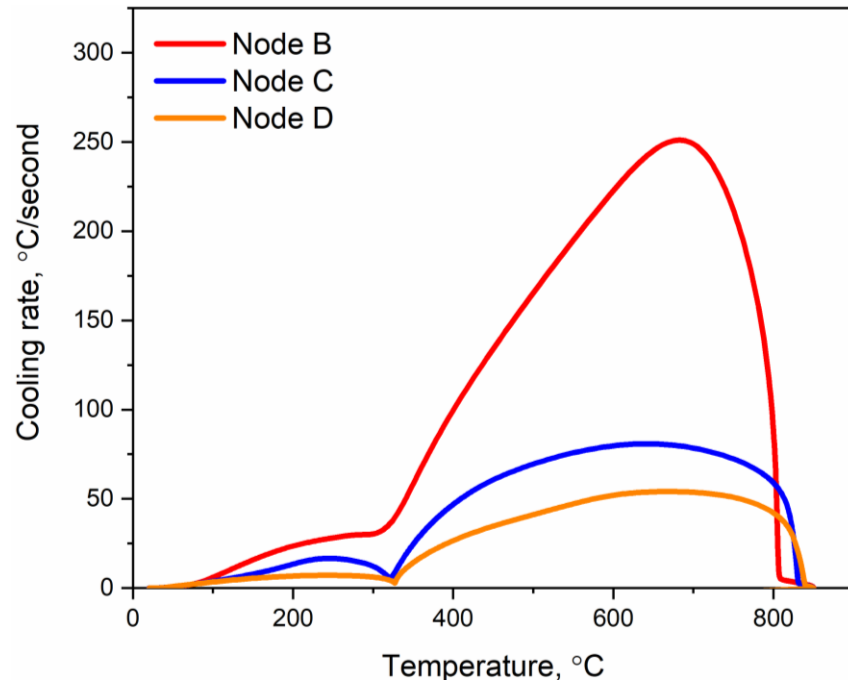


Figure 26: Calculated cooling rate versus temperature at Node B, C, and D of Navy C-ring during quenching.

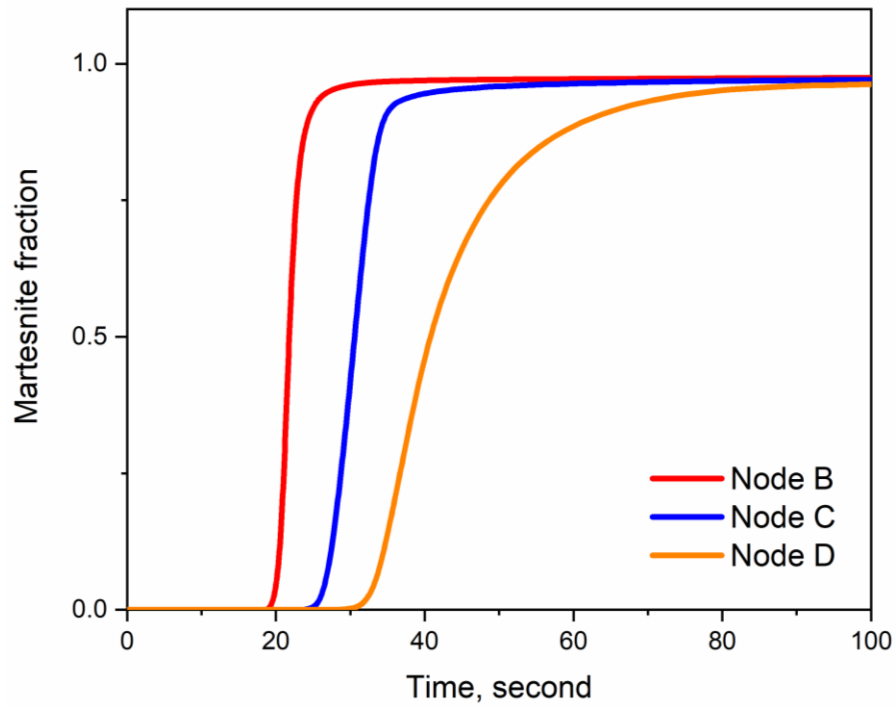


Figure 27: Calculated martensite fraction at Node B, C, and D of Navy C-ring during quenching.

Fig. 28a, and Fig. 28b show the simulated heating curve, the displacement of Node A in the x-axis (gap opening), and the phase fraction at Node D. At the beginning of the heating, because the upper part of the Navy C-ring is relatively thinner, it is heated faster than the lower part. The gap width becomes smaller because of the thermal expansion from the upper portion. At point 1 (Fig. 28), the temperature for the core of the Navy C-ring begins to take over, and due to the thermal expansion from the lower part, the gap starts to open. When it comes to point 2, the core part of the Navy C-ring starts to transform to austenite. Due to the higher density of austenite compared to martensite, ferrite, and pearlite, the specimen shrinks as a result of the transformation, which makes the gap width smaller. When the heating time reaches to point 3, the whole specimen transforms to austenite, and the gap width becomes larger again because of the thermal expansion.

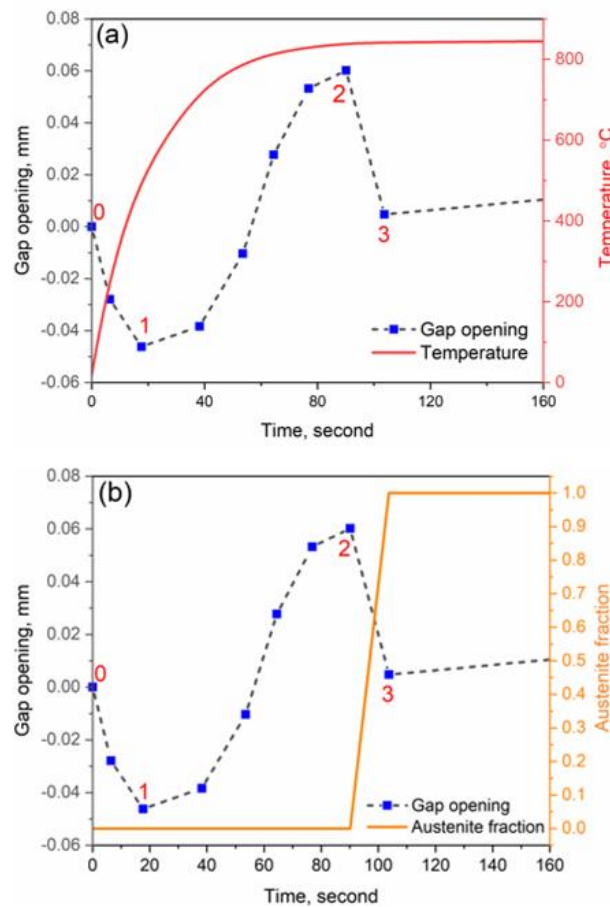


Figure 28: (a) The simulated heating curve and the displacement of Node A in x-axis versus time during heating. (b) The phase fraction of austenite at Node D during heating.

The simulated cooling curve, the opening (closing) of the gap, and the phase fraction of the core part are shown in Fig. 29a, and Fig. 29b. At the beginning of the quenching process (point 4), because of the thinner section on the tip, the upper part of the Navy C-ring cooled faster than the lower part. The gap continues opening because of the thermal contraction of the upper portion. When it reaches to point 5, the temperature of the upper part is close to quenchant temperature, and the thermal contraction from the lower part of the specimen begins to dominate, and that is why the gap starts to close. When point 6 is reached, the lower part of the distortion coupon starts to transform from austenite to martensite, and because of the relatively lower density of martensite, the lower portion begins to expand and make the gap larger. After 43 seconds (point 7), the whole part transformed to martensite.

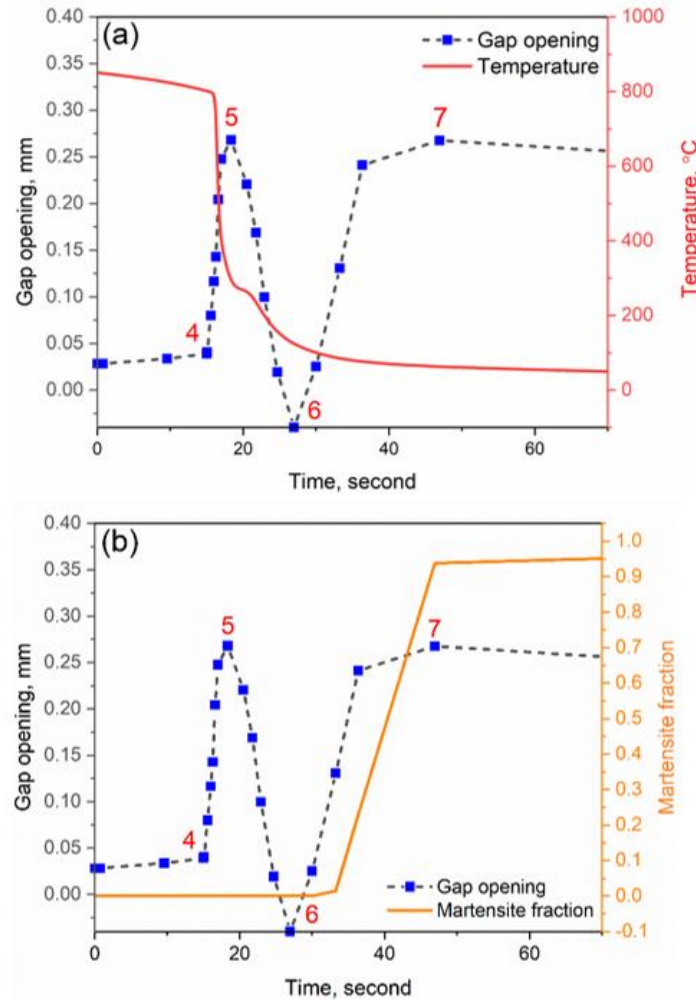


Figure 29: (a) The simulated cooling curve and the distortion of Node A in x-axis versus time during quenching, (b) the phase fraction of martensite at Node D during quenching.

The von Mises criterion [27] has been widely used as a mathematical description for the yielding of materials [28]. The material starts to yield when the von Mises stress is greater than the yield strength, σ_y . The yield strength of austenite as a function of temperature generated by DANTE [29] is shown in Fig. 30. With increasing temperature, the yield strength of the austenite decreases.

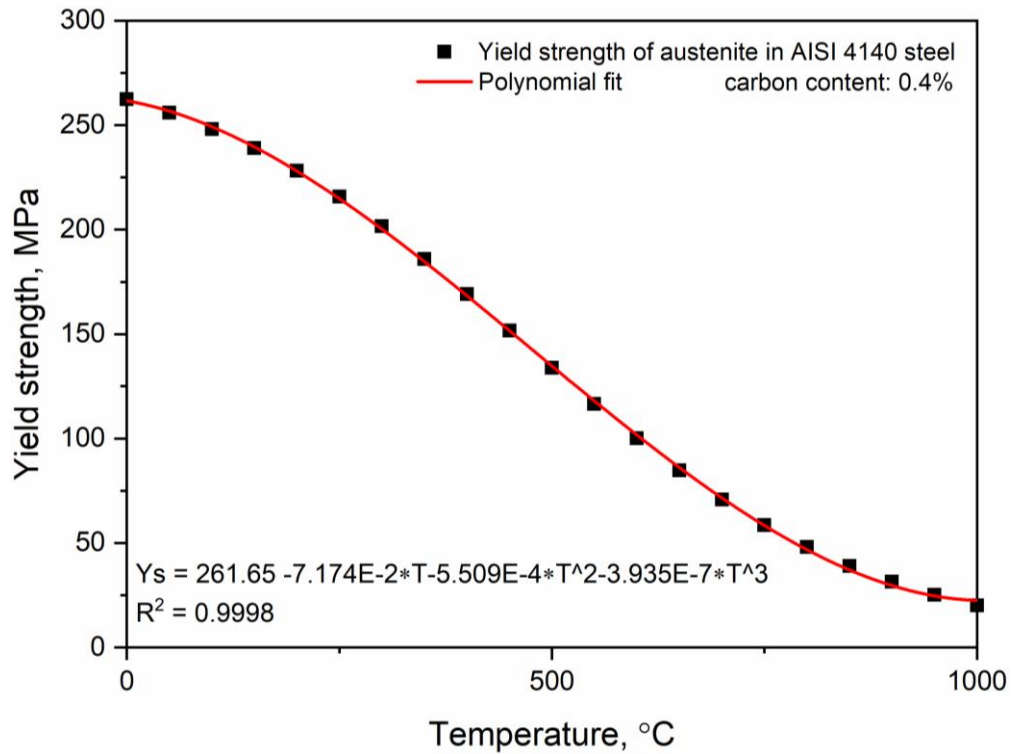


Figure 30: Yield strength of austenite in AISI 4140 steel as a function of temperature.

With the help of the effective plastic strain, the temperature and time at which the distortion happened during quenching for each node can be identified. Fig. 31 shows the relationship among von Mises stress, yield stress of austenite, and effective plastic strain as a function of time for Node E. After quenching to 800°C, the von Mises stress due to thermal contraction exceeded the yield strength, and the steel part began to deform. The deformation due to thermal stress stopped at 581°C and resumed at 436°C. The plastic strain continued increasing up to the martensite start temperature of 327°C and continued increasing until the completion of martensite transformation. Similar distortion behavior near the surface (Node F) is shown in Fig. 32.

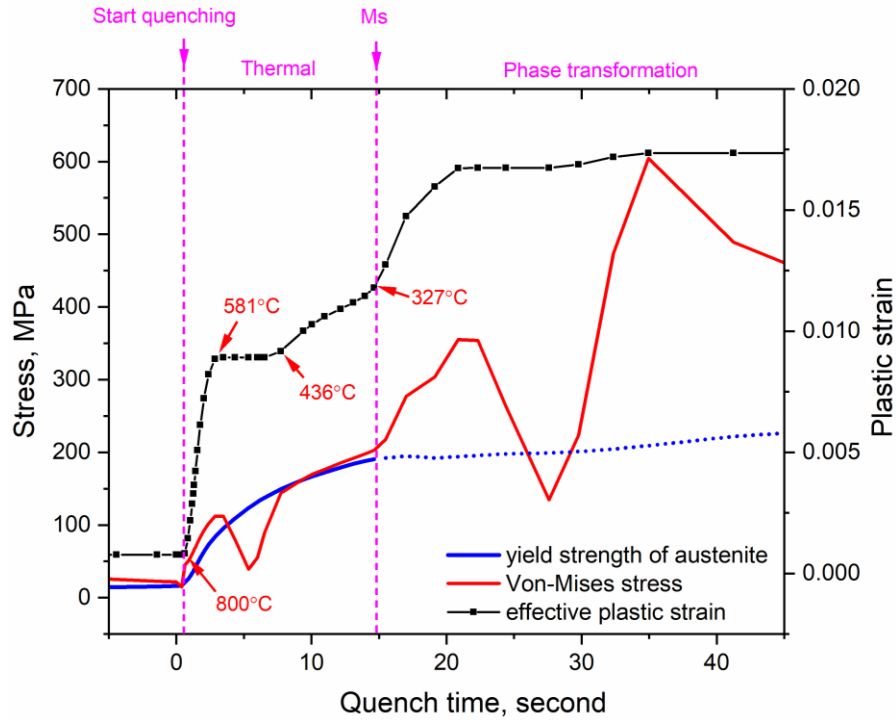


Figure 31: The relationship among von Mises stress, σ_y , and plastic strain as a function of time for Node E.

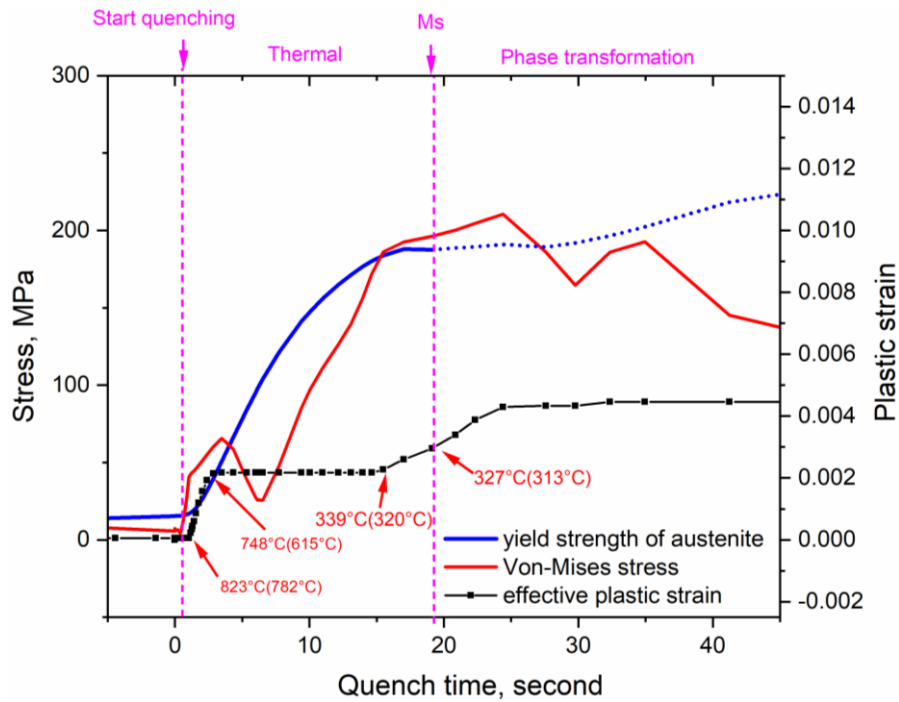


Figure 32: The relationship among von Mises stress, σ_y , and plastic strain as a function of time for Node F.

Fig. 33 presents the temperature distribution for the Navy C-ring during heating. It is shown that the thermal expansion from the upper part dominates at the beginning of the heating, which leads to the closing of the gap. When the thermal expansion of the lower part dominates, the gap tends to open. When the lower part of the Navy C-ring starts to form austenite, the gap closes again because austenite has a relatively higher density than pearlite and ferrite.

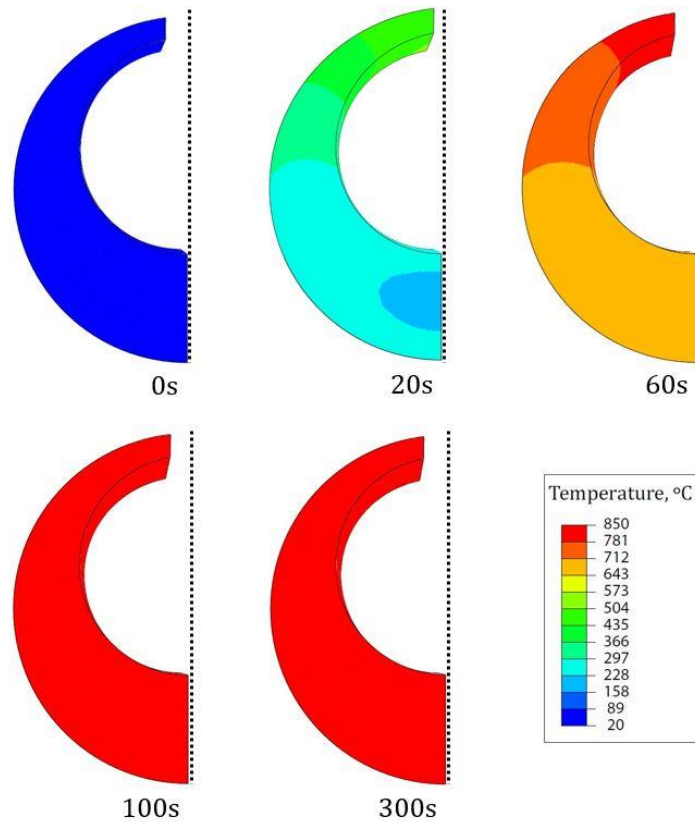


Figure 33: Temperature distribution of specimen during heating (0 s to 300 s).

Fig. 34 presents the temperature distribution for the Navy C-ring during quenching and the domination of the thermal contraction from the upper part to the lower part. When the thermal contraction of the upper portion dominates, the gap tends to open. When thermal contraction of the lower part dominates, the gap tends to close.

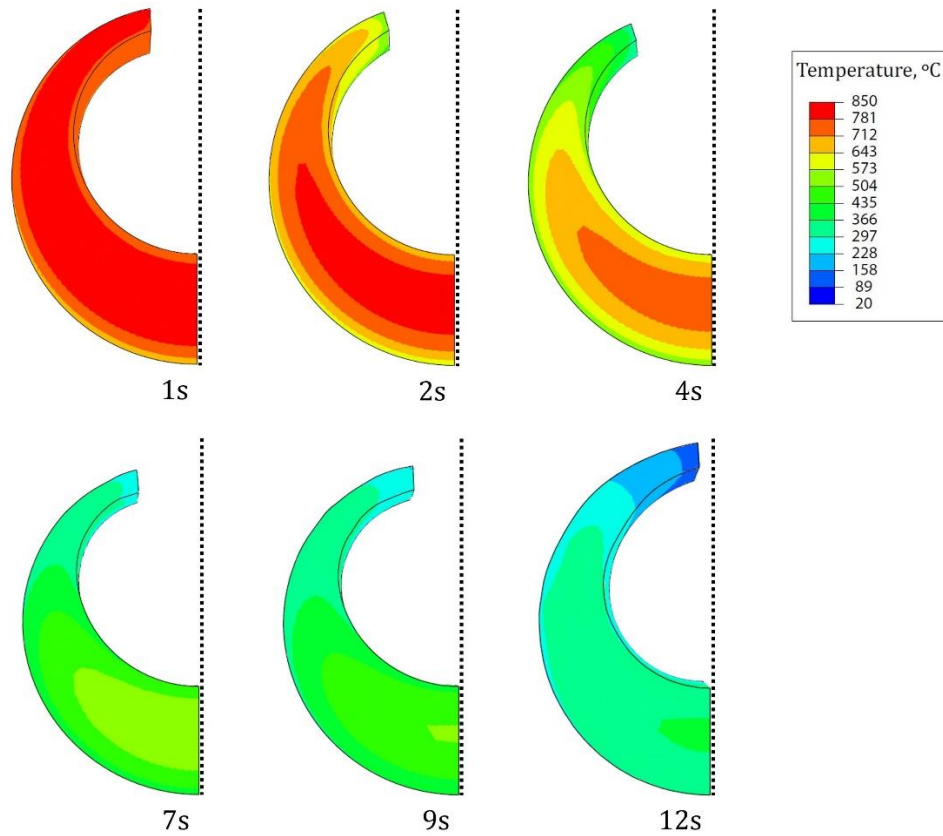


Figure 34: Temperature distribution of specimen during quenching (1 s to 12 s).

Fig. 35 presents the martensite distribution for the Navy C-ring during quenching. It is shown that after 15 seconds of quenching, martensite starts to form in the lower part of the specimen, which makes the gap begin to open.

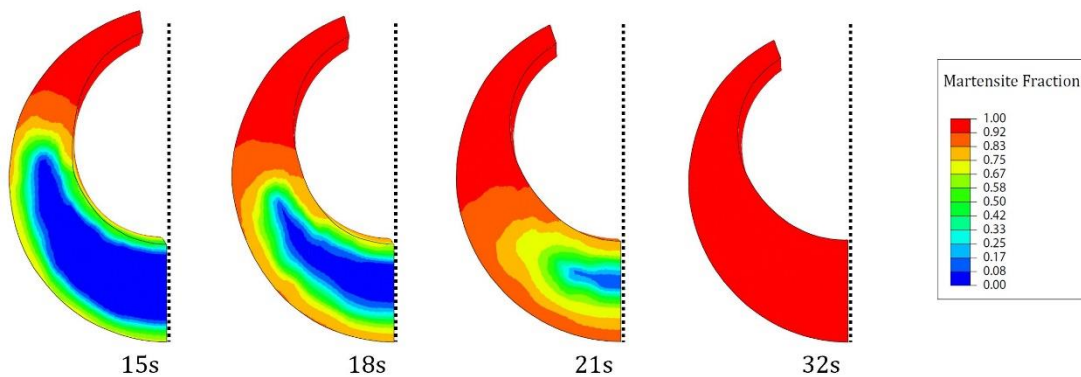


Figure 35: Martensite distribution of the specimen during quenching (15 s to 32 s).

4 Conclusion

In this study, the heat treatment experiments and modeling of AISI 4140 steel Navy C-ring are conducted. The conclusions are summarized as follows:

- The heat transfer coefficient of quenching oil was measured by CHTE quench probe system, and Navy C-ring experiments were also conducted. The simulation results showed excellent agreement with the experimental results.
- Because of the geometry of the Navy C-ring, the difference of cooling behavior between tip and core is significant. The cooling rate in the tip region is much higher than the cooling rate in the core region, and the occurrence of distortion is related to the presence of phase transformation at various locations during quenching.
- Higher agitation levels can produce higher cooling rates in the bottom section of the Navy C-ring and transform more austenite to martensite instead of lower bainite, which enlarges the gap opening due to the relatively lower density of martensite.
- Selected quench starts temperatures do not have a significant effect on the gap opening since they have no influence on HTC of the quenchant during quenching.
- Plastic deformation occurs in the Navy C-ring specimen either when the von Mises stress exceeds the yield strength or when phase transformation happens.

References

1. Ferguson, B. L., Li, Z., & Freborg, A. M. (2005). Modeling heat treatment of steel parts. *Computational Materials Science*, 34(3), 274-281.
2. Totten, G. E. (Ed.). (2002). *Handbook of residual stress and deformation of steel*. ASM international.
3. Maniruzzaman, M., Chaves, J., McGee, C., Ma, S., & Sisson Jr, R. (2002, July). CHTE quench probe system: a new quench characterization system. In *5th International Conference on Frontiers of Design and Manufacturing (ICFDM)* (pp. 619-625).
4. Zoch, H. W. (2009). Distortion engineering: vision or ready to application?. *Materialwissenschaft und Werkstofftechnik: Entwicklung, Fertigung, Prüfung, Eigenschaften und Anwendungen technischer Werkstoffe*, 40(5-6), 342-348.
5. Canale, L. D. C. F., & Totten, G. E. (2005). Quenching technology: a selected overview of the current state-of-the-art. *Materials Research*, 8(4), 461-467.
6. Moyer, J. M., & Ansell, G. S. (1975). The volume expansion accompanying the martensite transformation in iron-carbon alloys. *Metallurgical Transactions A*, 6(9), 1785.
7. Surm, H., Frerichs, F., Lübken, T., Hoffmann, F., & Zoch, H. W. (2012). Distortion of rings due to inhomogeneous temperature distribution. *Materialwissenschaft und Werkstofftechnik*, 43(1-2), 29-36.
8. Jung, M., Kang, M., & Lee, Y. K. (2012). Finite-element simulation of quenching incorporating improved transformation kinetics in a plain medium-carbon steel. *Acta Materialia*, 60(2), 525-536.
9. Şimsir, C., & Gür, C. H. (2008). 3D FEM simulation of steel quenching and investigation of the effect of asymmetric geometry on residual stress distribution. *Journal of materials processing technology*, 207(1-3), 211-221.
10. Lee, S. J., & Lee, Y. K. (2008). Finite element simulation of quench distortion in a low-alloy steel incorporating transformation kinetics. *Acta Materialia*, 56(7), 1482-1490.
11. Li, Z., Grandhi, R. V., & Srinivasan, R. (2006). Distortion minimization during gas quenching process. *Journal of Materials Processing Technology*, 172(2), 249-257.

12. Atraszkiewicz, R., Januszewicz, B., Stachurski, W., Dybowski, K., & Rzepkowski, A. (2012). High pressure gas quenching: Distortion analysis in gears after heat treatment. *Materials Science and Engineering: A*, 558, 550-557.
13. Steinbacher, M., Clausen, B., Hoffmann, F., & Zoch, H. W. (2009). New challenges in heat treatment and surface engineering. In Smoljan, Božo & Liščić, Božidar (Eds.), *conference in honour of prof. Liščić, Božidar* (pp. 343-349). Dubrovnik - Cavtat, Croatia.
14. Da Silva, A. D., Pedrosa, T. A., Gonzalez-Mendez, J. L., Jiang, X., Cetlin, P. R., & Altan, T. (2012). Distortion in quenching an AISI 4140 C-ring—Predictions and experiments. *Materials & Design*, 42, 55-61.
15. Li, J., Feng, Y., Zhang, H., Min, N., & Wu, X. (2014). Thermomechanical Analysis of Deep Cryogenic Treatment of Navy C-Ring Specimen. *Journal of materials engineering and performance*, 23(12), 4237-4250.
16. Farivar, H., Prahl, U., Hans, M., & Bleck, W. (2019). Microstructural adjustment of carburized steel components towards reducing the quenching-induced distortion. *Journal of Materials Processing Technology*, 264, 313-327.
17. Nan, C., Northwood, D. O., Bowers, R. J., Sun, X., & Bauerle, P. (2009). The use of navy C-ring specimens to study distortion in ferritic nitrocarburized 1010 steel. *WIT Transactions on Engineering Sciences*, 62, 13-25.
18. <http://objects.eanixter.com/PD365571.PDF>
19. Mills, A. F. Heat Transfer, 1992. *Irwin, IL*.
20. Rothman, M. F. (1987). High-temperature property data: ferrous alloys.
21. <http://www.fowlerprecision.com/Products/Inside-Micrometers/1-2-Electronic-IP54-Inside-Micrometer-54-860-276.html>
22. https://www.forestry-suppliers.com/product_pages/products.php?mi=33981&itemnum=
23. Yu, H., Lu, Y., Xu, Y., & Sisson, R. (2019). The Effect of Surface Preparation on Retained Austenite Measurement. In *100 Years of E04 Development of Metallography Standards*. ASTM International.
24. Rietveld, H. (1969). A profile refinement method for nuclear and magnetic structures. *Journal of applied Crystallography*, 2(2), 65-71.

25. Rietveld, H. M. (1967). Line profiles of neutron powder-diffraction peaks for structure refinement. *Acta Crystallographica*, 22(1), 151-152.
26. Lu, Y., Yu, H., & Sisson Jr, R. D. (2017). The effect of carbon content on the c/a ratio of as-quenched martensite in Fe-C alloys. *Materials Science and Engineering: A*, 700, 592-597.
27. Von Mises, R. (1913). Göttingen Nachrichten, Math. Phys. Klasse, 582.
28. Yang, W. H. (1980). A generalized von Mises criterion for yield and fracture.
29. Li, Zhichao. Private communication, 2019.

CHAPTER 4 Paper II: Identification of the important processing parameters on distortion in AISI 4140 steel

Haixuan Yu · Richard D. Sisson, Jr

To be submitted to: Materials Science and Engineering: A

Highlights:

1. CHTE quench probe system was used to measure the heat transfer coefficient (HTC) of Houghton-Quench G quenching oil as a function of temperature, which was a key input for heat treatment simulation.
2. The most important processing parameters is HTC, which is a function of quenchant, agitation speed, quenchant temperature and quenching orientation.
3. The second most important processing parameters is part geometry. The part geometry can be coupled with HTC to calculate Biot number, where the larger the Biot number, the greater the distortion of the quenched part.

Identification of the important processing parameters for distortion in AISI 4140 steel

Haixuan Yu¹ · Richard D. Sisson, Jr.^{*1}

¹*Center for Heat Treating Excellence, Worcester Polytechnic Institute, 100 Institute Road, Worcester, MA 01609, USA*

hyu2@wpi.edu, yhxates@gmail.com (H. Yu)

sisson@wpi.edu (R.D. Sisson, Jr)

Abstract

Steel parts are specified in terms of geometry and mechanical properties. Distortion during heat treating can result in scrap parts. Failure to meet these specifications can result in extensive rework or rejection of the parts. To identify of the important processing parameters for quenching induced distortion in AISI 4140 steel, a series of computer simulations, using DANTE [1], has been conducted on selected distortion coupons including Navy C-ring specimen [2]. To simulate the steel part quenched with different conditions, CHTE quench probe system [3] was used to measure the heat transfer coefficient (HTC) as a function of temperature of Hougto-Quench G quenching oil as a function of agitation speeds, quench starts temperatures, and quenchant temperatures. The important processing parameter identification was conducted using design of experiments (DoE) coupled with analysis of variance (ANOVA). The effect of processing parameters in decreasing order of importance were determined to be: quenchant type, part geometry, agitation speed, quenching orientation, quenchant temperature, immersion rates, and quench starts temperature, where the first five parameters have the greatest impact on the Biot number of the quenched part. Higher Biot numbers corresponded to larger temperature gradient and greater distortion of the Navy C-ring specimen after quenching. In this paper, the results of these simulations and the statistical analysis will be presented and discussed.

Keywords quenching distortion · FEM · heat transfer coefficient · AISI 4140 steel · Navy C-ring · DoE · ANOVA

1 Introduction

Steel parts that are used in the aerospace, automotive, and heavy equipment industry rely on heat treatment, especially quenching, to acquire the desired mechanical properties. Rapid phase transformation and high thermal gradients occurring during quenching can cause distortion [4], which can lead to costly hard-machining and rejection. The distortion of the steel part should be handled as a “system attribute”, not caused by a single factor. To reduce dimensional changes in the parts during quenching, understanding the impact of the processing parameters on quenching distortion is very important.

Finite element analysis (FEA) is one of several effective methods to understand the mechanisms causing distortion and help develop a heat treatment procedure that can minimize distortion, cost as well as processing time [5]. Heat treatment analysis software including DANTE [1], DEFORM-HT [6], HEARTS [7], and SYSWELD [8] have been well developed to predict the microstructure and final distortion after heat treatment. In the heat treatment industry, design of experiment (DoE) has been widely used as an efficient approach to collect enough data using the minimum number of experiments [9]. Analysis of variance (ANOVA), mathematical technique, is frequently used to investigate the relative impact of each parameter in DoE [10]. Using DoE method, Dan O. Macodiyo et al. [11] found out that cavitation number, which is defined by the ratio of upstream pressure to downstream pressure, had the biggest impact on the improvement of fatigue strength using cavitation shoeless peening method on carburized JJS SCM420 steel. Juan Dong et al. [12] used statistical analysis of the DoE to show that the most important factor influencing distortion in the process of induction hardening of AISI 1045 steel is the drawing process. The gear wheels made from SAE 5120 steel were studied by B. Clausen et al. [13], which

showed volume, carburizing depth, carburizing temperature and flow velocity of the quenching gas had significant effect on distortion.

In the previous paper, the experimental results showed good agreement with the simulation results from DANTE. Therefore, the discussion is mainly based on DANTE simulation. This chapter is presented in three sections. First, the measurement of the HTC as a function of temperature of alphaquench 5300 quenching oil, and Hougto-Quench G oil [14] with selected quenchant temperature, agitation speeds, and quench start temperatures using CHTE quench probe system are presented. Second, the heat-treating simulation using commercial heat treatment software, DANTE on selected distortion coupon, including Navy C-ring specimen is described and discussed. Finally, the DoE method is utilized to identify the important processing parameters on quenching induced distortion of AISI 4140 steel.

2 Experimental Procedure

2.1 CHTE quench probe system

The OMB-DAQ-2408 data acquisition and Tracer DAQ software were used for collecting the time-temperature data from the KQXL-116G-12 K type thermocouple, which was placed in the center of the CHTE quench probe. The A/D analog to digital data rate can be as high as 3000 counts per second in OMB-DAQ-2408 module. For measuring the cooling curve, 80 HZ A/D data rate was used. The setup of CHTE quench probe system is shown in Fig. 2. The 304 stainless steel quench probe was heat up to 850°C in F48015-60 muffle furnace for 10 minutes and then quenched in Hougto-Quench G quenching oil without agitation at 20°C. Fig. 3 shows the time-temperature data acquired from OMB-DAQ-2408 data-acquisition. By using the OriginPro 2018b, the acquired data can be reduced to a smaller size by applying data reduction filters. The cooling rate can be calculated based on the filtered data (Fig. 4).

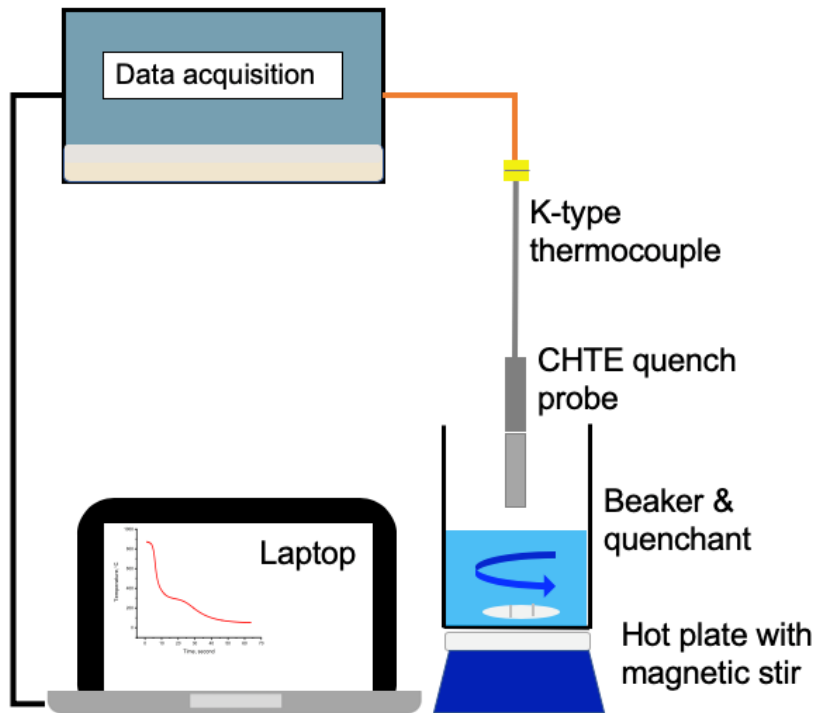


Figure 2: CHTE quench probe system to measure heat transfer coefficient [3].

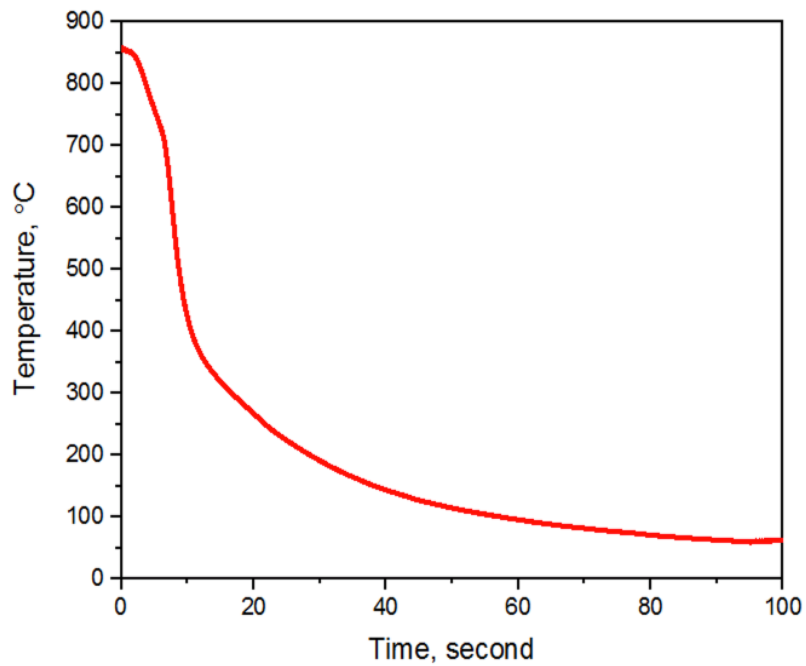


Figure 3: Time-temperature data measured by OMB-DAQ-2408 data-acquisition.

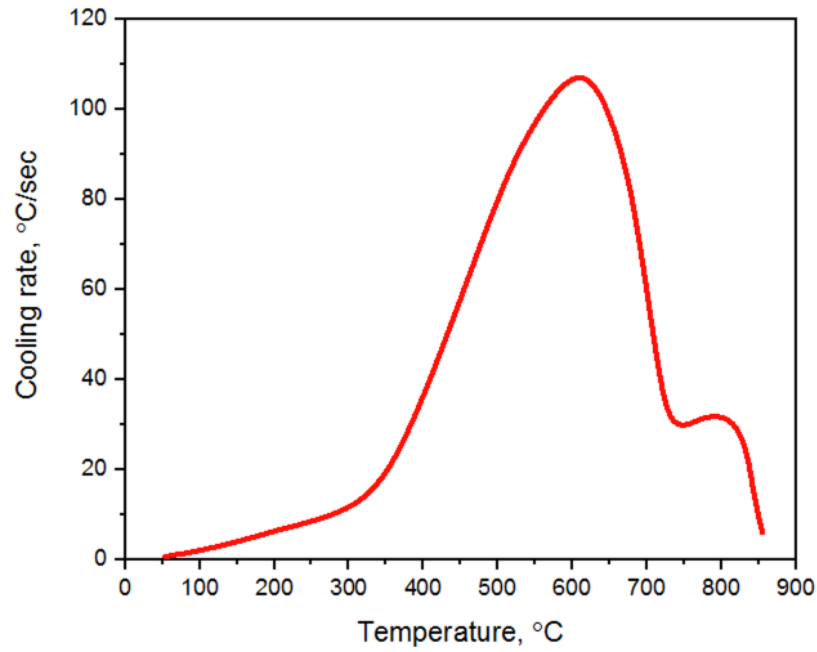


Figure 4: Cooling rate calculated by OriginPro 2018b based on time-temperature data.

After calculating the cooling rate, the heat transfer coefficient of Hougto-Quench G quenching oil can be obtained, which is shown in Fig. 5. The Leidenfrost temperature is approximately 750°C, and the maximum heat transfer coefficient was obtained when the temperature dropped to 600°C.

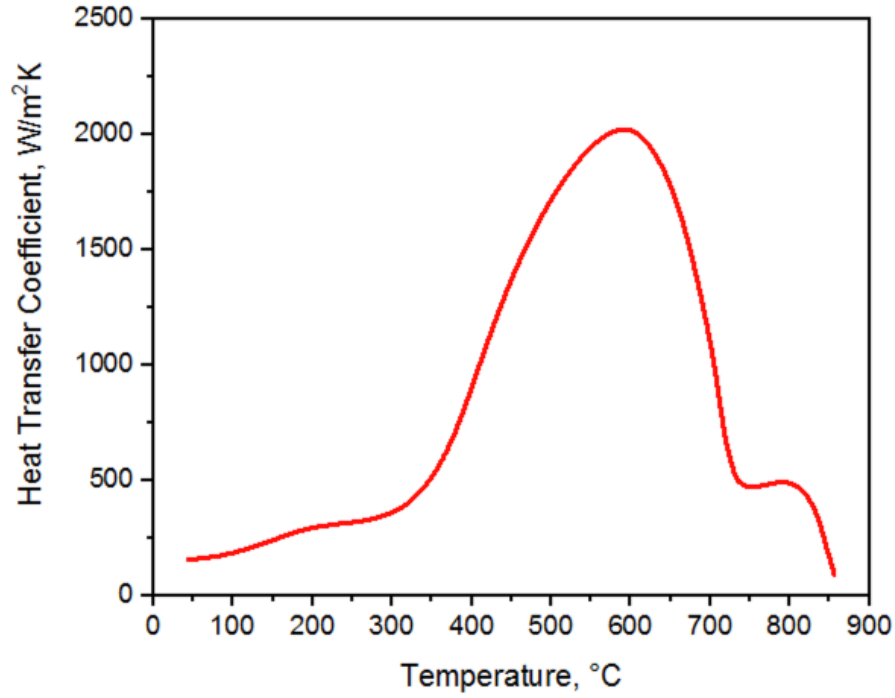


Figure 5: Calculated heat transfer coefficient of Houghton-Quench G quenching oil at 20°C without agitation.

Fig. 6 presents the calculated heat transfer coefficient as a function of temperature of Houghton-Quench G quenching oil held at 20°C, 40°C, 60°C and 80°C. The heat transfer coefficient at film boiling region and nucleate boiling region increase with increasing quenchant temperature. That is because higher temperature results in lower viscosity of the quench oil, which will improve heat transfer. It was also found that the temperature of the maximum heat transfer coefficient also shifts to higher temperature. A similar result is also reported by Scott et al. [15].

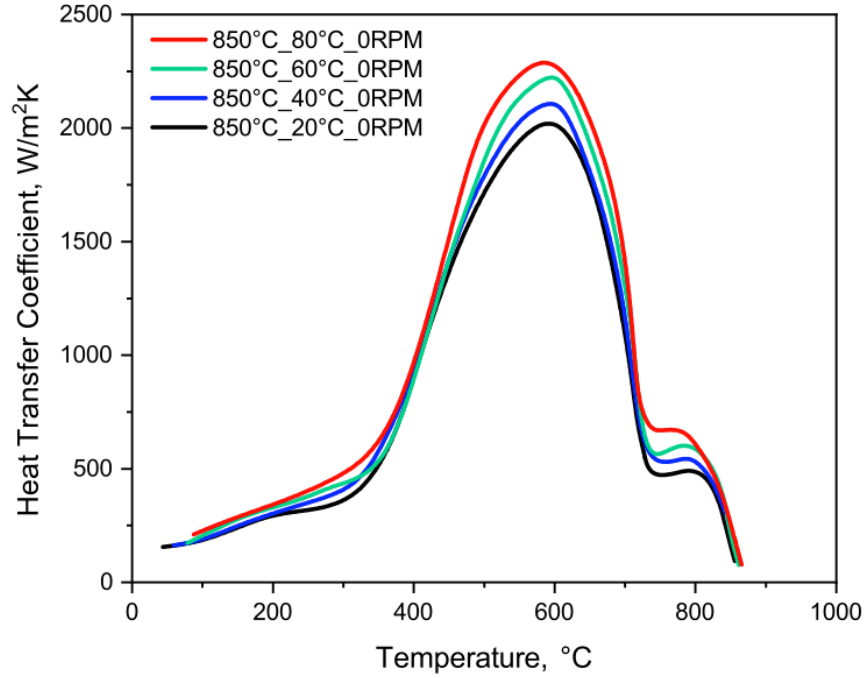


Figure 6: Calculated heat transfer coefficient of Houghto-Quench G quenching oil at selected oil temperatures without agitation.

Fig. 7 presents the calculated heat transfer coefficient of Houghto-Quench G quenching oil with selected agitation speed starts from 0 RPM to 1200 RPM. With a higher agitation level, the HTC in all three regions gets higher. It is also found that with higher agitation speed, the reduction of the Leidenfrost phenomenon is observed. That is because intensive agitation will break the thin vapor film around the probe at the beginning of the quenching.

In order to study the effect of quench start temperature on distortion, the heat transfer coefficient of Houghto-Quench G quenching oil with selected quench start temperature was also calculated (Fig. 8). HTC in the convection region and nucleate boiling region are the same. HTC in the film boiling region increase with higher quench starts temperature.

As the key input for heat treatment simulation, the heat transfer coefficient measured by CHTE quench probe was used to assess the important process parameters that affect the distortion during quenching in the following sections.

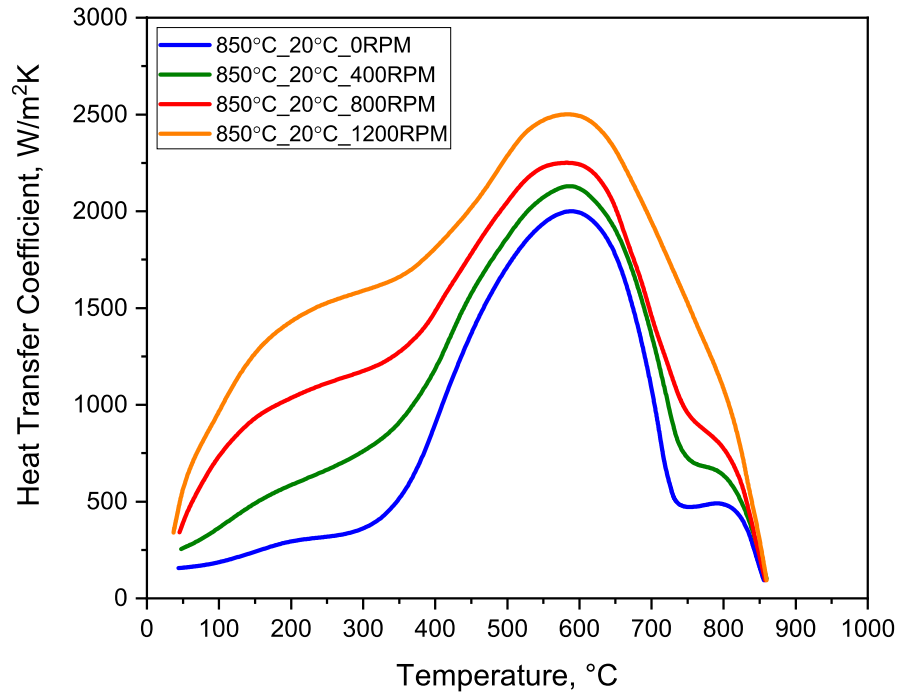


Figure 7: Calculated heat transfer coefficient of Hougto-Quench G quenching oil with selected agitation speeds at 20°C.

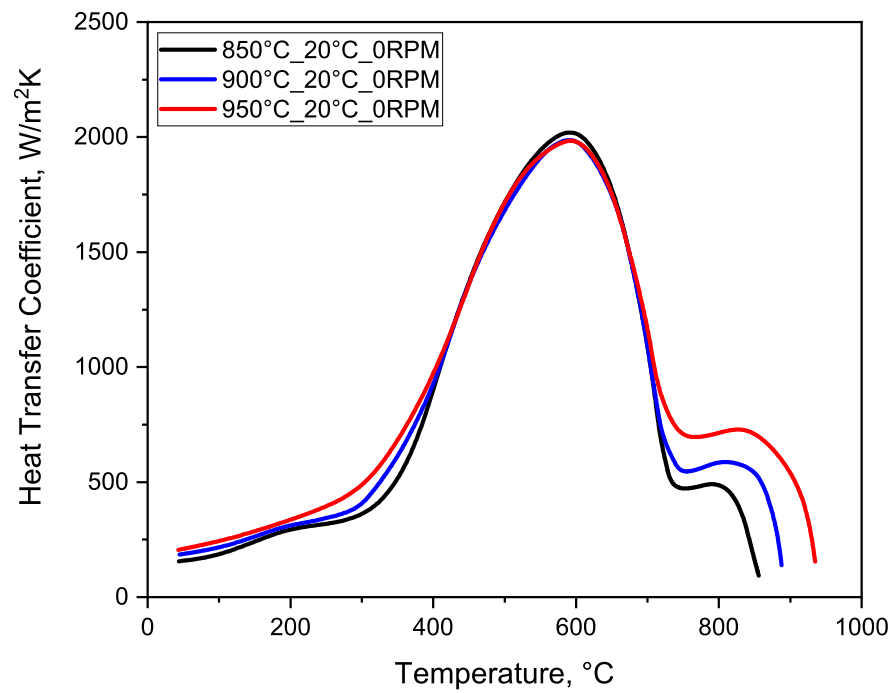


Figure 8: Calculated heat transfer coefficient of Hougto-Quench G quenching oil with selected quench start temperature.

3 Results and Discussion

A rectangular plate with a hole and the Navy C-ring specimen were selected as distortion test coupons to identify the important processing parameters for quenching distortion.

3.1 Rectangular component specimen

The first test part under consideration is rectangular plate with a hole (Fig. 9) [16]. The purpose of this design is to exaggerate distortion that may occur during heating and quenching of the steel part. The dimensional changes can be identified by measuring the radius change and circularity of the hole before and after quenching. The three-dimensional part geometry created and meshed by Abaqus pre-processor is shown in Fig. 10, which contained 34720 nodes and 30780 elements. To capture the fast change of temperature during quenching and accurately account for the final distortion prediction, the mesh with higher density of nodes was generated near the surface of the hole.

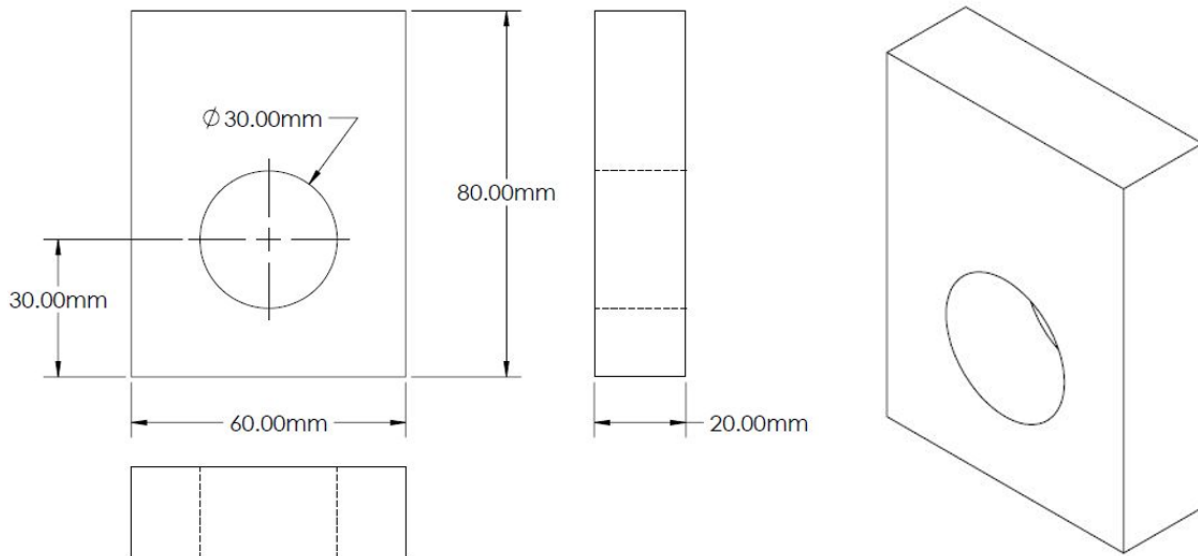


Figure 9: Three view drawing of the rectangular specimen.

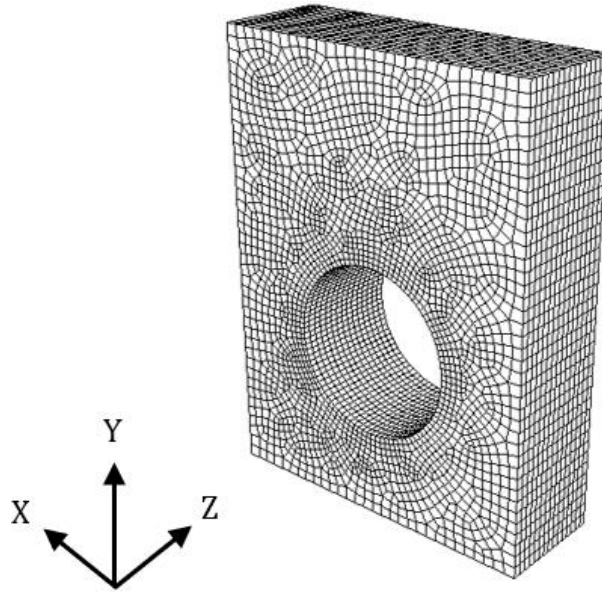


Figure 10: Finite element mesh of the rectangular specimen for heat treatment simulation.

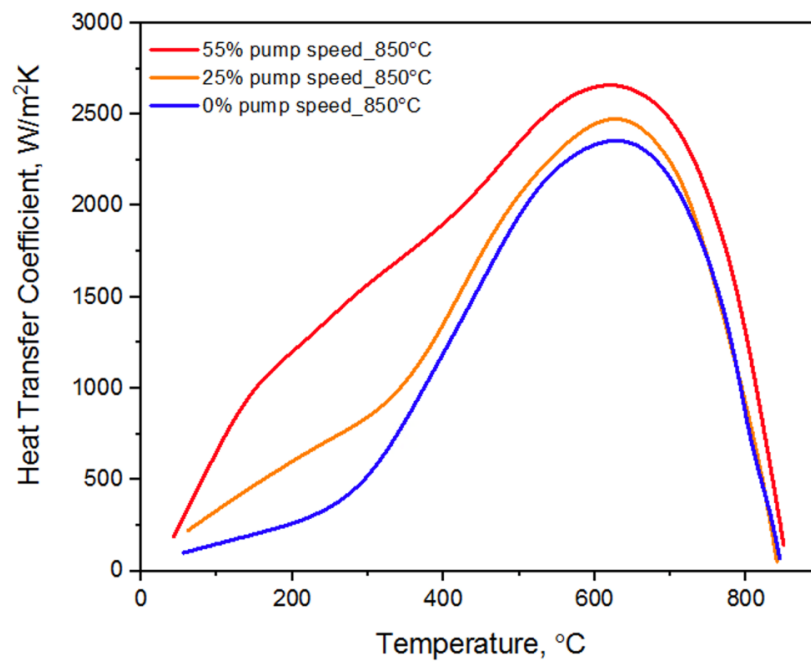


Figure 11: Heat transfer coefficient of alphaquench 5000 quenching oil with selected pump speeds.

The heat transfer coefficient of alphaquench quenching oil measured by CHTE quench probe system with selected pump speeds is shown in Fig. 11. As seen in Fig. 11, with increasing pump speed, the HTC increases in both the nucleated boiling region and convection region.

By increasing agitation speed during quenching, the maximum HTC increases from 2350 W/m²K to 2666 W/m²K. In the following section, the distortion coupon is simulated to quench in alphaquench 5300 quenching oil with selected processing parameters.

3.2 The effect of immersion orientation on quenching induced distortion

To identify the immersion orientation effect on distortion, the test part was simulated to quench in alphaquench 5300 quenching oil at the pump speed of 25% with selected immersion orientations. The rectangular specimen was simulated to quench along the x-axis, y-axis and z-axis. Fig. 12 through Fig. 14 show the heat transfer simulation with selected quenching orientations. In order to see the distortion behavior during quenching easily, the distortion was magnified sixty times. It is clear from the figure, the face that first contacts with the quenchant reaches to lower temperature more quickly. And the volume closes to that face shrinks first.

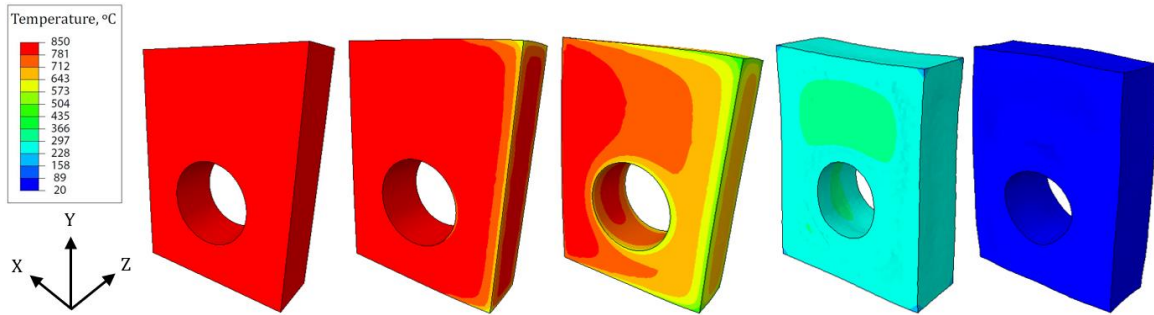


Figure 12: Heat transfer simulation of the rectangular specimen: quench along the x-axis.

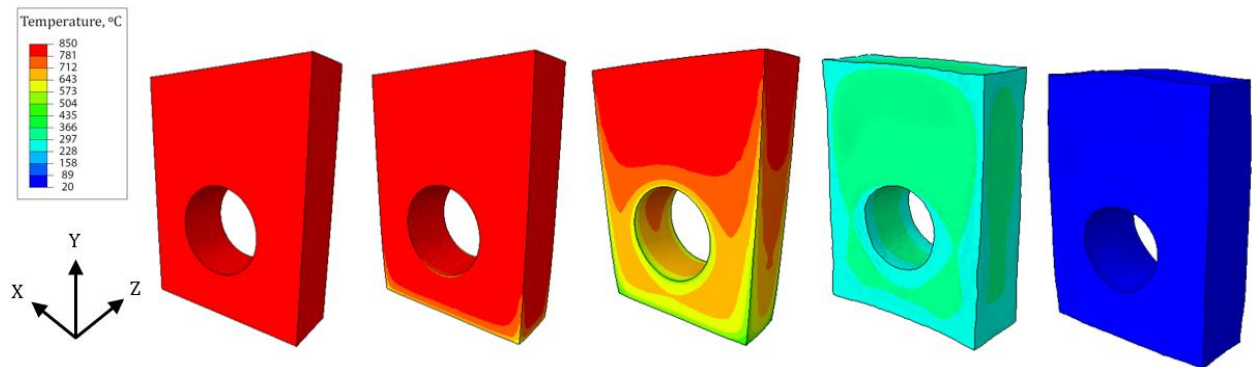


Figure 13: Heat transfer simulation of the rectangular specimen: quench along the y-axis.

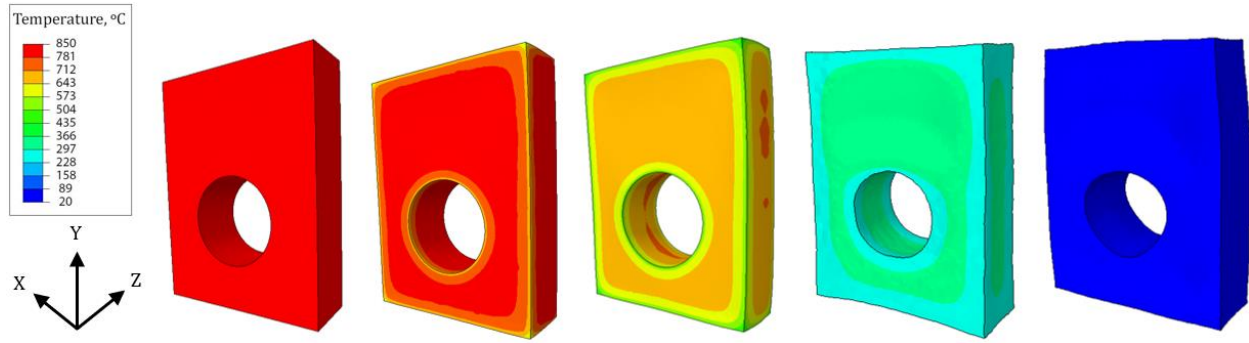


Figure 14: Heat transfer simulation of the rectangular specimen: quench along the z-axis.

The comparison between the shape of the circular hole before and after heat treatment simulation was conducted (Fig. 15 to Fig. 17). To identify the distortion, the displacement of each node was multiplied by sixty times. The change in radius at different locations around the circular hole with selected orientation is compared in Fig. 18. It shows that the distortion tendency and degree of the circular hole along the circumferential direction predicted by DANTE are similar regardless of the quenching orientation.

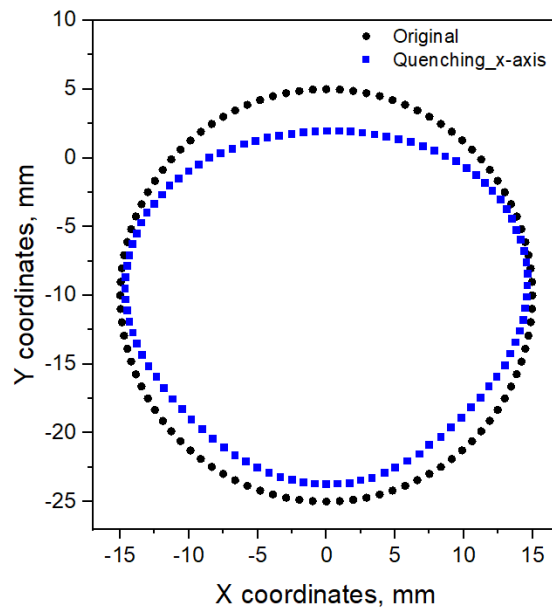


Figure 15: The coordinates of the circular hole before and after quenching (quench along the x-axis).

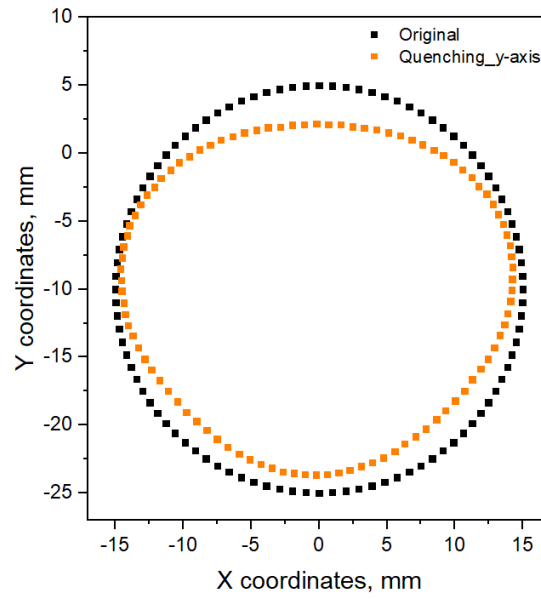


Figure 16: The coordinates of the circular hole before and after quenching (quench along the y-axis).

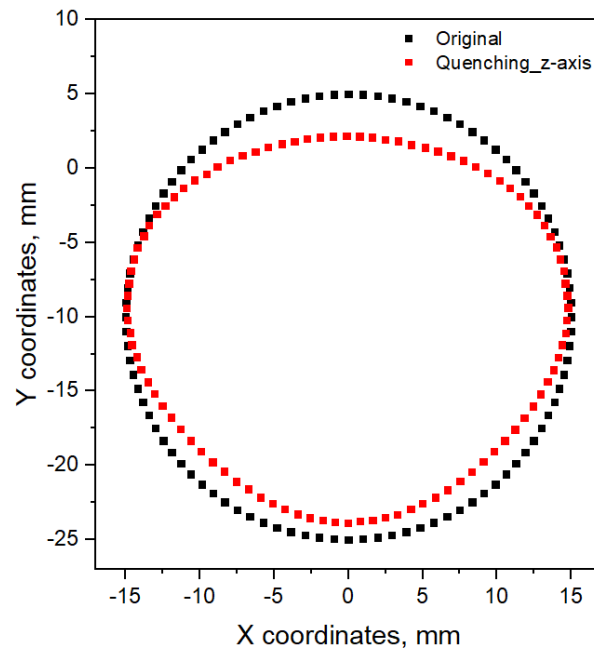


Figure 17: The coordinates of the circular hole before and after quenching (quench along the z-axis).

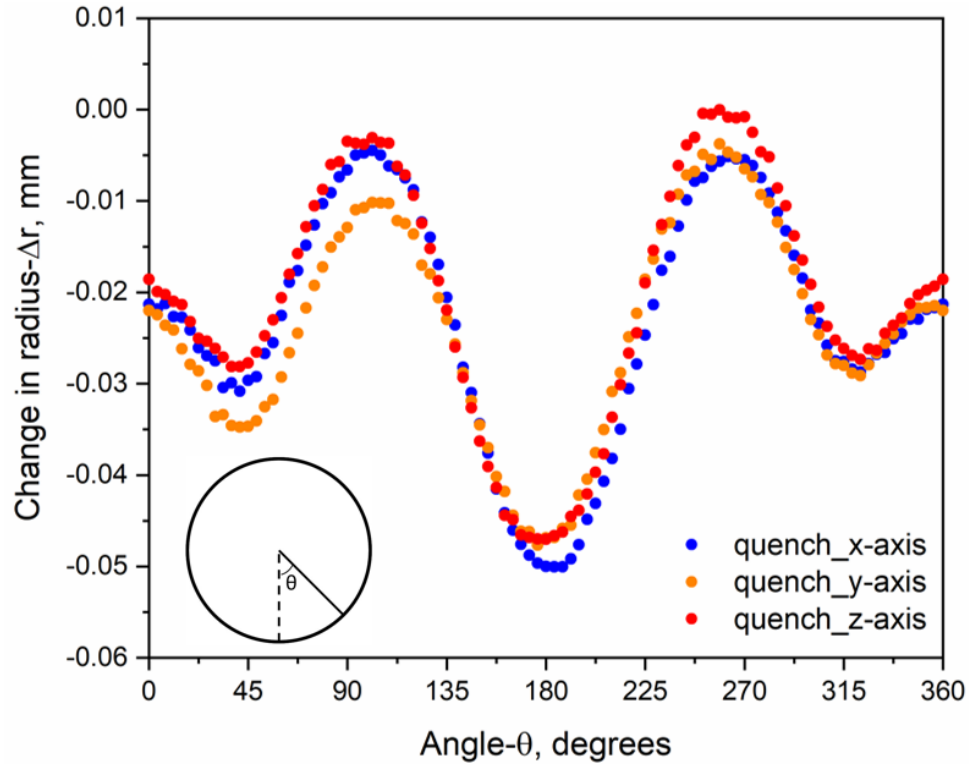


Figure 18: Change in radius at different locations around the hole with selected quenching orientations.

3.3 The effect of part thickness of rectangular specimen on quenching distortion

In order to study the effect of part sizes of the rectangular specimens on the quenching distortion, selected thickness (10mm, 20mm, 30mm) of the specimens were simulated to quench in alphaquench 5300 quenching oil at the pump speed of 25%. The finite element mesh for each rectangular specimen is shown in Fig. 19, and the quenching orientation is along the y-axis.

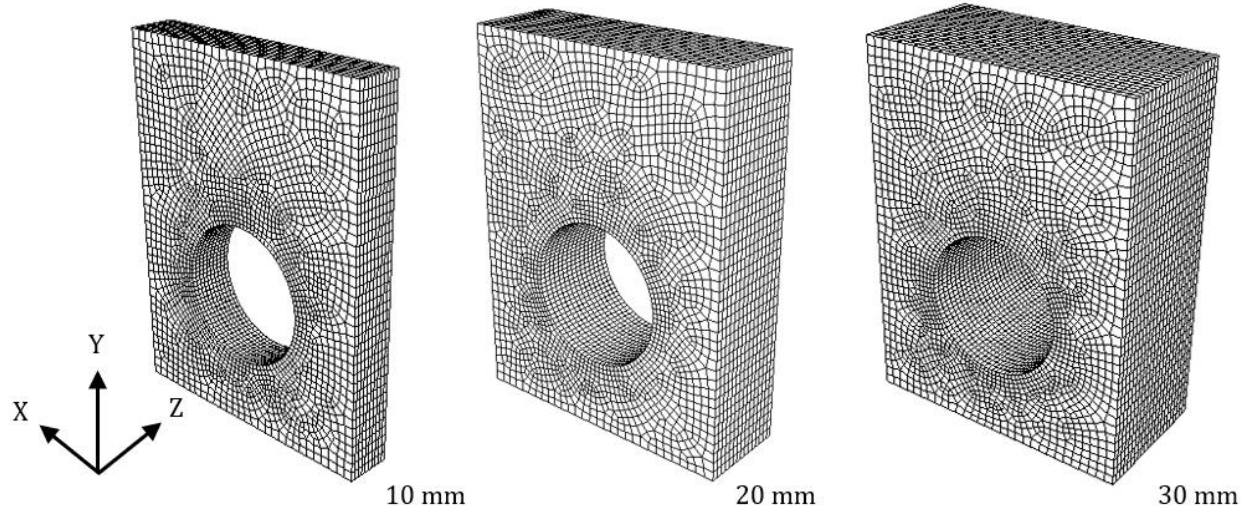


Figure 19: Finite element mesh of the rectangular specimens with selected thicknesses of 10mm, 20mm, and 30mm.

The shape of the distorted circular hole after quenching simulation is shown in Fig. 20. Compared to the part with higher thickness, the distortion of the hole with a thickness of 10mm is insignificant even with the magnification of sixty times. However, the shape of the circular hole with 30mm thickness is highly distorted. The changes in radius along the circumferential direction around the circular hole with selected thicknesses are compared in Fig. 21. It shows that increasing the thickness of the specimen can result in a larger distortion of the circular hole.

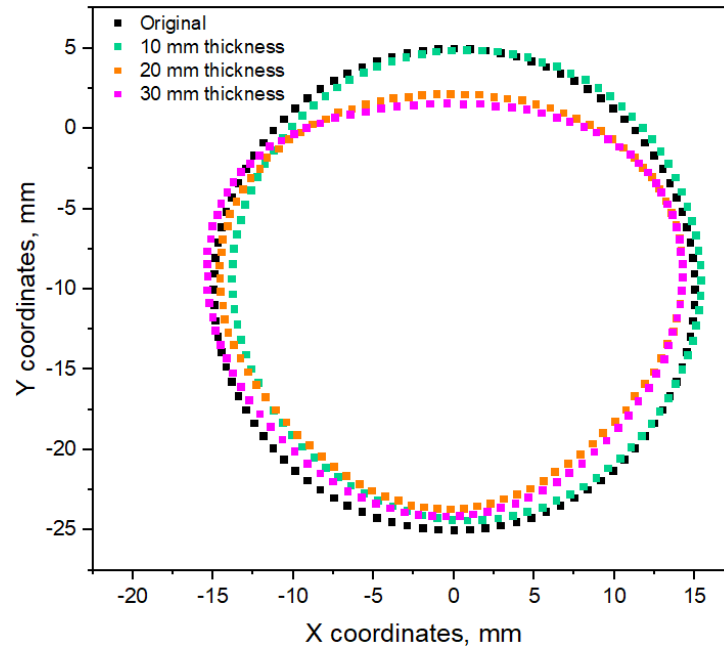


Figure 20: The coordinates of the circular hole before and after quenching.

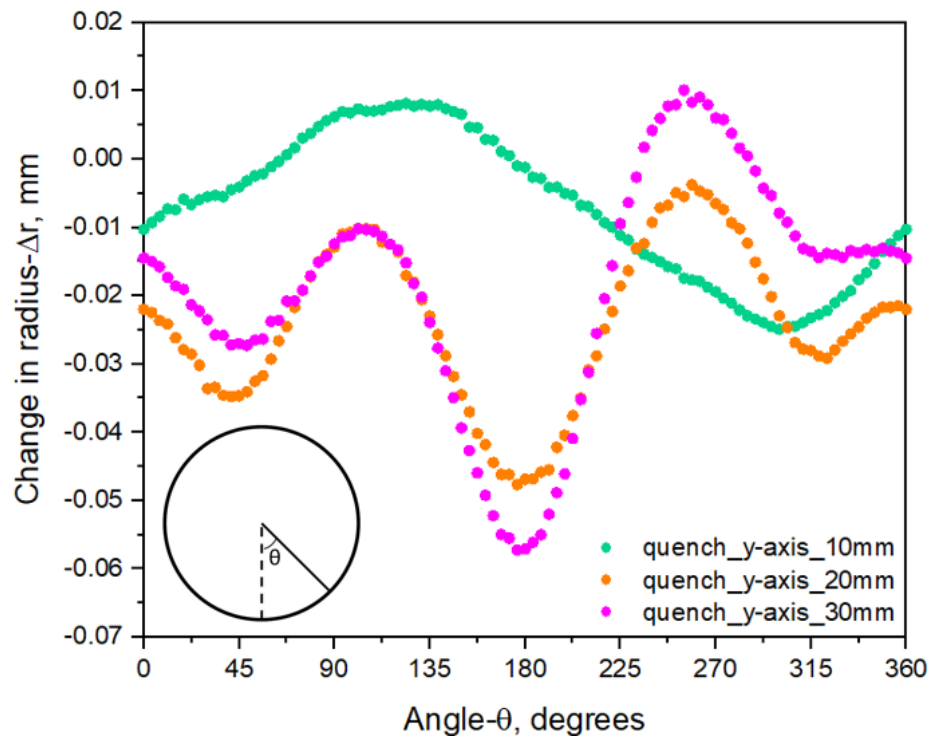


Figure 21: Change in radius at different locations around the hole with selected part thickness.

3.4 The effect of gravity on quenching induced distortion

In previous cases, the same heat transfer coefficient was applied to all sample surfaces. But in the actual experiment, it is harder for boiling bubbles that form on the upper face of the circular hole to escape compared to bubbles that form on the lower face due to the effect of gravity. Therefore, the HTC from the upper part of the circular hole should be lower than the HTC from the lower part of the circular hole. To simulate this case, the surface of the circular hole inside the rectangular specimen was divided into sixteen sections (Fig. 22), at which the values of HTC are different (H1, H2, H3...). The values of HTC at various circumferential locations are shown in Table 1, which increases gradually along the clockwise direction. Due to the symmetry, the HTC applied on the left half-section of the hole is equal to the right half-section. The distortion degree of the hole under identical HTC and various HTC along the circumferential direction are shown in Fig. 23. The distortion degree of the circular hole under both conditions has no significant difference. It is suggested that the difference of HTC at different locations for the rectangular specimen can be neglectable.

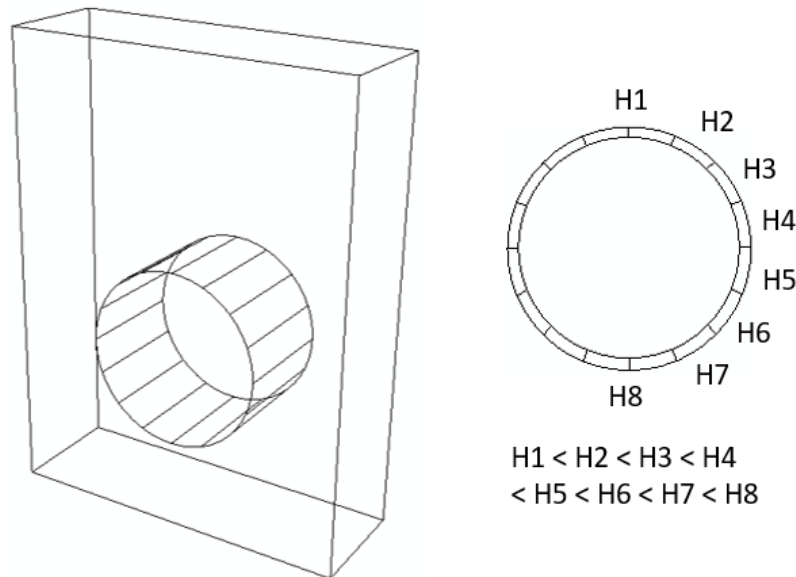


Figure 22: The schematic drawing of the circular hole divided by 16 sections.

Table 1: The HTC value for each section

	H1	H2	H3	H4	H5	H6	H7	H8
HTC value	1/8 H8	2/8 H8	3/8 H8	4/8 H8	5/8 H8	6/8 H8	7/8 H8	HTC of alphaquench 5300 with pump speed of 25%

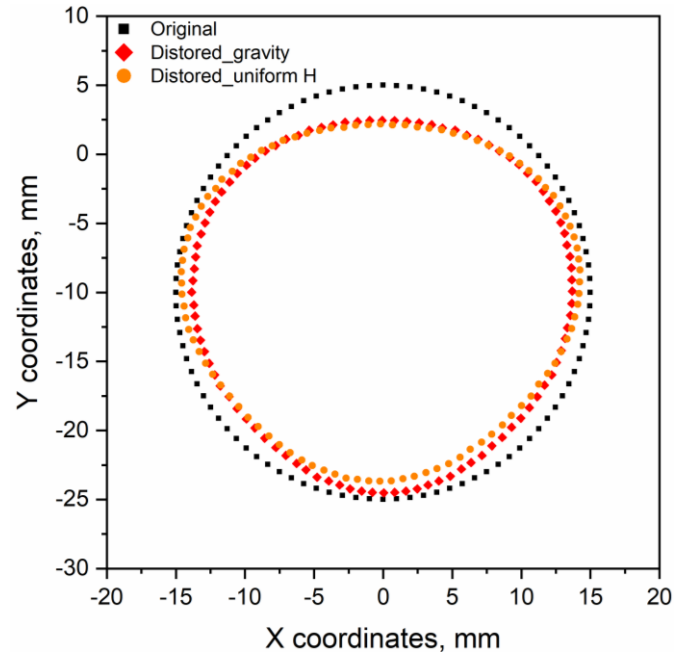


Figure 23: The coordinates of the circular hole before and after quenching considering gravity effect.

3.5 The effect of agitation on quenching induced distortion

To identify the effect of the agitation speed on distortion during quenching, the rectangular specimen was simulated to quench in the alphaquench 5300 quenching oil with selected pump speeds. From simulation results (Fig. 24), it shows that, with no agitation, the distortion of the central hole is very small, and the largest distortion is obtained at the highest pump speed.

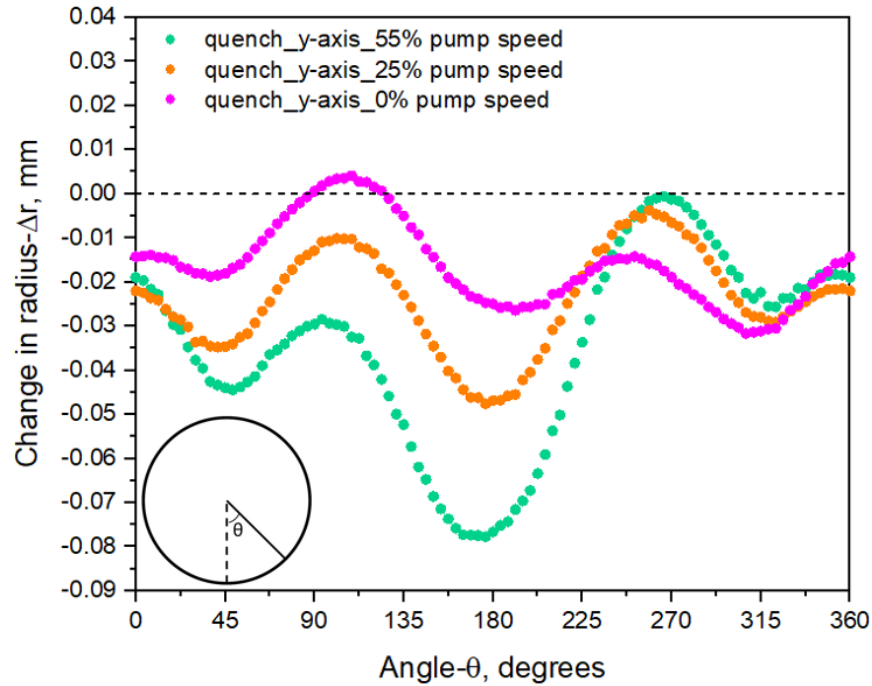


Figure 24: Change in radius at different locations around the hole with selected agitation speeds.

Furthermore, the circularity tolerance is also calculated to reveal the overall distortion of the hole after quenching. According to ASME Y14.5-1994 standard [17], the circularity tolerance can be expressed as a radial distance of two concentric circles, which cover the contour of the produced circle (Fig. 25):

$$\text{Circularity tolerance} = R_{\max} - R_{\min} \quad (1)$$

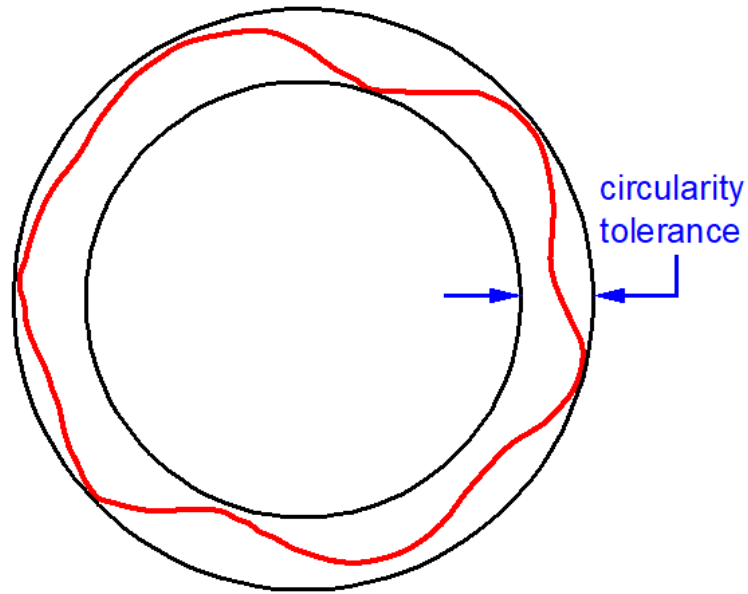


Figure 25: Schematic diagram to demonstrate circularity tolerance.

The closer the value to 0, the more perfect the circle is. The circularity tolerance of the distorted hole for each simulation with selected processing parameters was calculated and compared in Fig. 26. It shows that the agitation level and specimen geometry (thickness) have significant effects on the quenching induced distortion of the hole inside the specimen. On the other hand, quenching orientation and gravity effect have relatively less impact on the distortion of the hole.

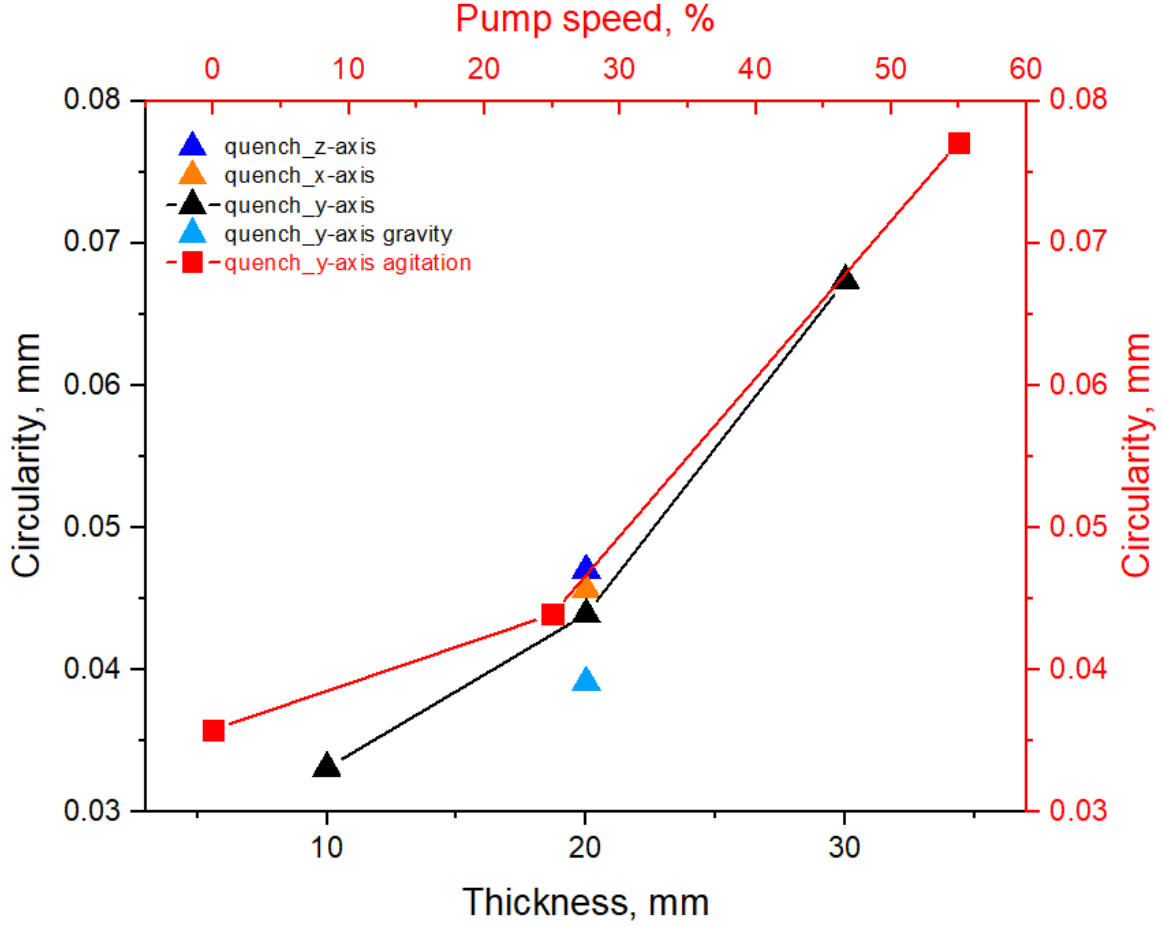


Figure 26: The circularity (CIR) with different quenching process parameters.

To study the relationship between selected processing parameters and distortion during quenching, the Biot number is used. The Biot number [18] is defined as the convective heat transfer coefficient multiplied by the characteristic length divided by the thermal conductivity of the body.

$$Bi = \frac{h(T) * L_c}{k(T)} \quad (1)$$

Where

$h(T)$ = film coefficient or convective heat transfer coefficient [$W/m^2 \cdot K$].

L_c = characteristic length, which is generally described as the volume of the body divided by the surface area of the body [m].

$k(T)$ = thermal conductivity of the body [$W/m \cdot K$]

The lower the Biot number, the lower the temperature gradient in the part cross-section. For Biot number less than 0.1, the temperature gradients are insignificant, and a lumped-capacity model may be used [18]. When the Biot number is larger than 1, the temperature gradients in the part cross-section is significant [18]. Table 2 shows the calculated Biot number at Ms temperature of the rectangular components with selected thickness. The martensite start temperature of AISI 4140 steel is used to calculate the HTC and thermal conductivity of the steel. From ASTM handbook [15], the thermal conductivity of austenite at Ms (326°C) is 21.7 W/m*K. From the calculation, the Biot numbers from all the cases are higher than 0.1, which means the temperature gradient within the rectangular component is not negligible. It also shows that with a higher Biot number, the circularity of the hole is higher, which means higher quenching distortion (Fig. 27).

Table 2: The Biot number of rectangular components with selected thickness at a temperature of 326°C

thickness, mm	pump speed, %	characteristic length, m	HTC at Ms, W/m ² *K	thermal conductivity, W/m*K	Biot number	Circularity, mm
10	25	0.003240	976	18.3	0.173	0.033
20	0	0.004999	735	18.3	0.201	0.036
20	25	0.004999	976	18.3	0.267	0.043
30	25	0.006104	976	18.3	0.326	0.067
20	55	0.004999	1700	18.3	0.464	0.077

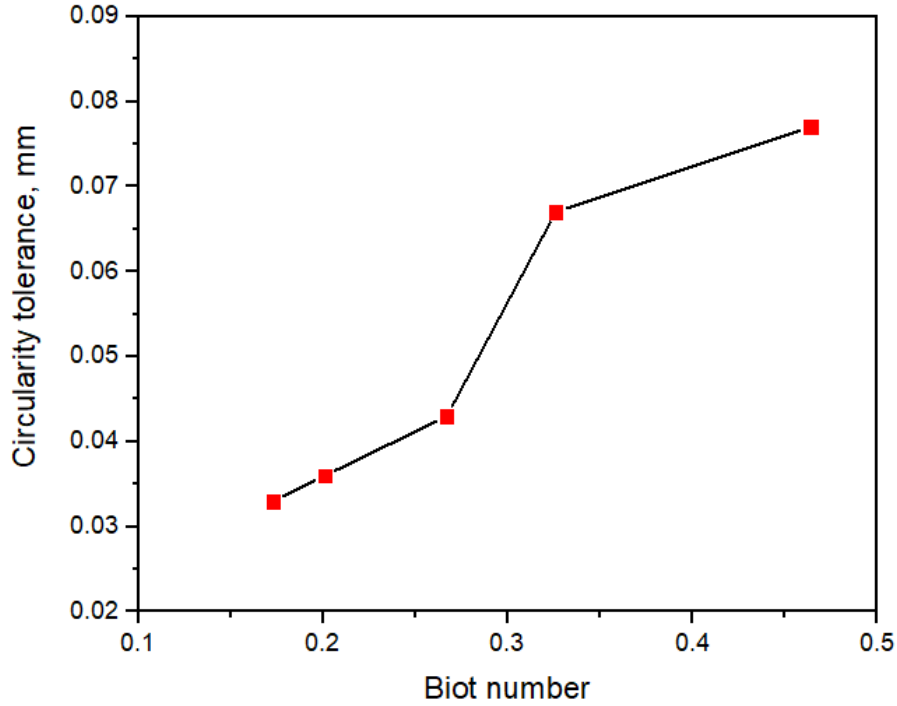


Figure 27: Circularity tolerance as a function of Biot number.

4 Navy C-ring specimen

4.1 The effect of specimen geometry and agitation speed on quenching induced distortion of Navy C-ring

The second distortion test part is the Navy C-ring specimen [2]. By measuring the gap opening percentage before and after the heat treatment, the distortion of the part can be identified. The heat treatment modeling of the Navy C-ring was carried out using finite element analysis (FEA) software ABAQUS coupled with heat treatment analysis software DANTE. In order to determine the part geometry effect on distortion, selected sizes of the Navy C-ring specimens are used for simulation (Fig. 28). The specimen on the left is the one-eighth size of the standard specimen, and the specimen on the right is eight times the size of the standard specimen. The quenching in alphaquench 5300 quenching oil with selected pump speeds has been simulated using DANTE. Constant HTC as a function of temperature was applied to all surfaces of the part. The gap opening% = (final gap – original gap)/original

gap*100%. Fig. 29 demonstrates that with higher pump speeds and large part size, the gap opening is increased.

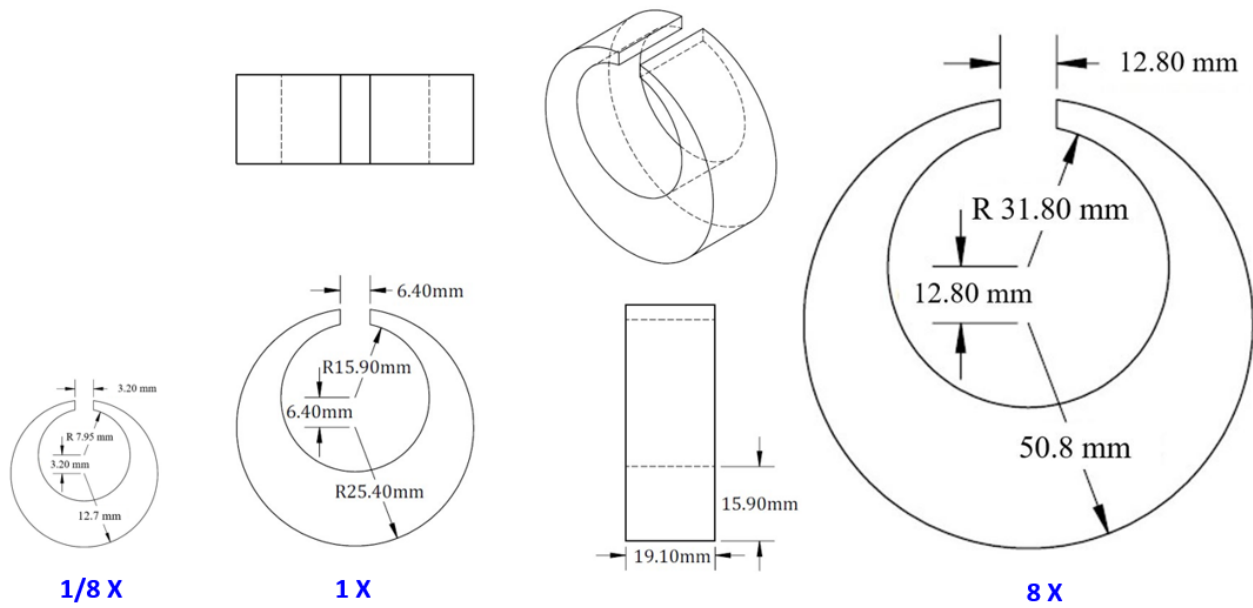


Figure 28: Dimensions of the Navy C-ring specimens with selected part geometries.

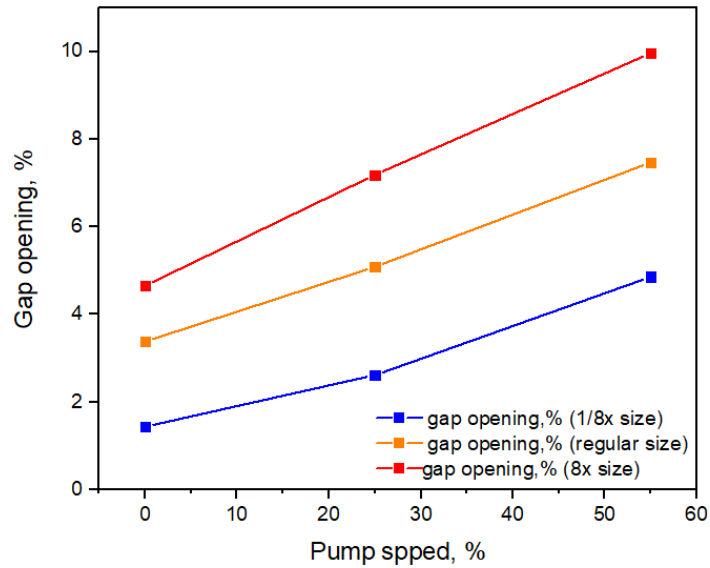


Figure 29: The gap opening with selected pump speed and part geometry.

In DANTE simulation, when the Von-Mises stress is higher than the yield stress of the steel during quenching, the plastic deformation will occur. The larger the effective plastic strain, the larger the distortion. Fig. 30 illustrates the final plastic strain of Navy C-ring specimen with selected part geometry after quenching with alphaquench 5300 quench oil at a pump speed of 25%. Larger part size can generate not only larger gap opening but also higher plastic strain. The bottom of the part has higher plastic strain than the gap regardless of the part size as seen in Fig. 30.

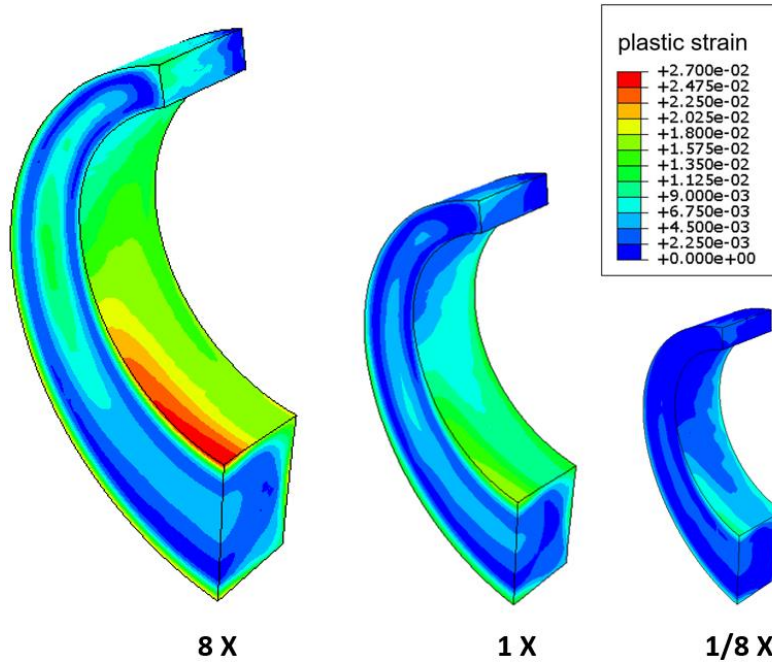


Figure 30: The plastic strain distribution of Navy C-ring after quenching with selected part size.

Part geometry and size play an important role in distortion. The geometry and size must be coupled with the temperature dependent heat transfer coefficient $h(T)$ during quenching. This system approach requires coupling of the geometry size and $h(T)$. This system approach may be accomplished with a location specific Biot number. The location specific Biot number can be defined in the same way as Biot number, except the characteristic length must be defined for at a specific location in the part. For example, in the Navy C-ring specimen, the thickness varies within the part. The Navy C-ring is divided into thirteen sections and the characteristic length of each section is calculated. The local Biot number during the quenching of the part in alphaquench 5300 quenching oil with pump speed of 25% at M_s temperature can be calculated as a function of angle. As illustrated in Fig. 31, local Biot number increases with larger part size and higher angle, which indicates a higher temperature gradient of the part during quenching. For the smaller size of the Navy C-ring (blue line), the biot number in most of the part is less than 0.1, which means the temperature gradient is negligible. For the larger part size of the specimen (red line), the biot number is larger than 0.1, which means the temperature gradient during quenching is significant. The

largest local biot number is obtained at the bottom of the specimen, which explained why the highest plastic strain is obtained at the bottom of the Navy C-ring specimen in Fig. 30.

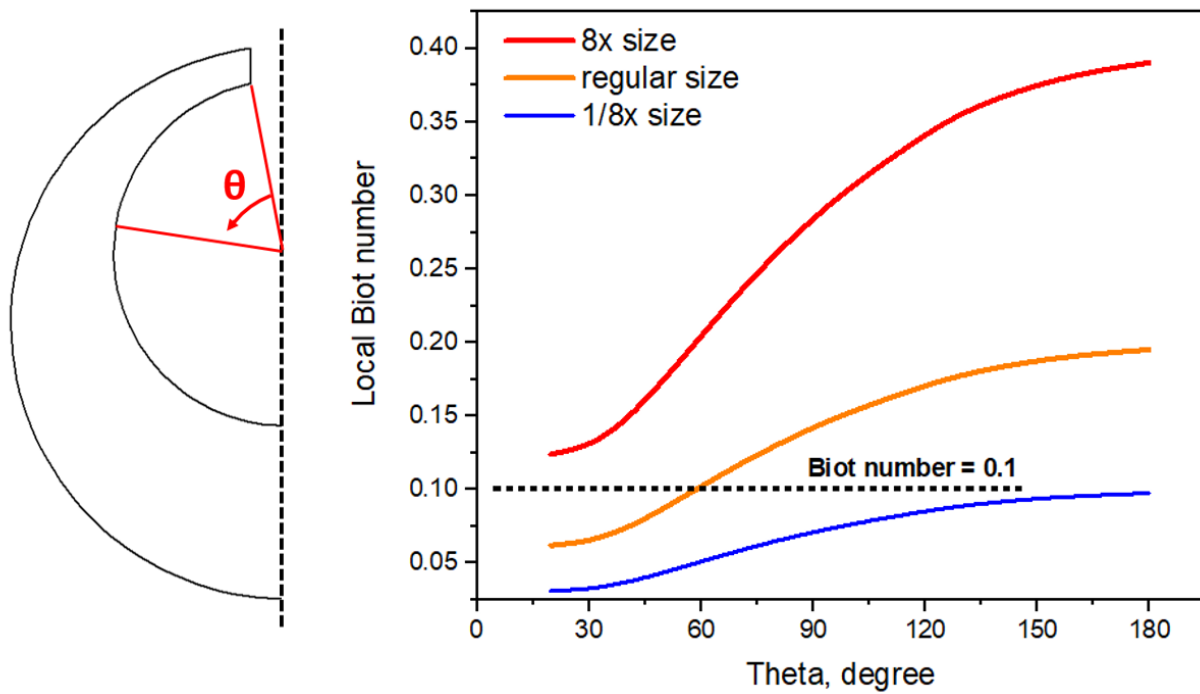


Figure 31: The local Biot number as a function of angle with selected part sizes.

4.2 Using DoE to determine the important processing parameters for distortion

As shown in Table 3, the statistical analysis of the full 2^6 factorial DoE plan was developed to assess the impact of the part geometry, quenching orientation, agitation speed, immersion rate, and quenchant temperature on quenching distortion of Navy C-ring specimen. Two levels were specified for each processing parameter. The results for each simulation are shown in appendix 1, Table 1.

Table 3: Full 2^6 factorial design for processing parameters on quenching distortion for the parts quenched in Houcto-Quench G quenching oil.

Symbol	Quenching parameters	Unit	Level 1	Level 2
A	Part geometry	--	Small	Large
B	Quenching orientation	--	Gap up	Gap down
C	Agitation level	rpm	0	800
D	Quench start temperature	°C	850	900
E	Immersion rate	mm/s	10	120
F	Quenchant temperature	°C	20	60

Table 4: Analysis of variance for gap opening.

	DF ^a	SS ^b	MS ^c	F ^d	P
Source					
Part geometry	1	87.047	87.047	241.77	0.000
Quenching orientation	1	0.563	0.563	1.56	0.216
Agitation level	1	134.471	134.471	373.48	0.000
Quench start T	1	0.148	0.148	0.41	0.524
Immersion rate	1	0.801	0.801	2.22	0.141
Quenchant T	1	0.323	0.323	0.90	0.348
Error	57	20.523	0.360		
Total	63	243.876			

^a Degree of freedom.

^b Sum of squares.

^c Mean squares

^d F ratio

Table 4 shows a summary of the analysis of variance (ANOVA) results using the software Minitab 18 (Minitab Ltd, Coventry, UK). In ANOVA, the p-values (probability of error) were used as criteria to determine which of the factors were statistically significant. P-value of less than 0.05 was identified as 'statistically significant' or 'statistically contributing' and vice versa. From the table, it shows that for the parts quenched in Hougto-Quench G quenching oil, part geometry, and agitation level have a significant effect on quenching distortion. On the other hand, quenching orientation, quench start temperature, quenchant temperature, and immersion rate have not significant effect on quenching distortion. A higher agitation speed results in larger gap opening because it can produce higher cooling rate in bottom section of the Navy C-ring and transform more austenite to martensite instead of lower bainite. A higher agitation speed produces higher HTC and increases the Biot number during quenching. Higher temperature gradient (higher Biot number) will result in a larger distortion of the part. The effect of part geometry on gap opening is significant. That is because the smaller size of the part has more uniform cooling (lower Biot number) whereas the larger one has a larger temperature gradient (higher Biot number)

during quenching due to the increased thickness. The quench starts temperatures does not have a significant effect on gap opening because it did not provide either the different cooling rate in the core nor Biot number of the Navy C-ring during quenching, which was also discussed in the previous chapter. Higher quenchant temperature can increase the HTC to a certain extent, but it is still not significant enough to provide the relatively higher cooling rate in the core of the C-ring. The effects of immersion rate and immersion orientation on gap opening are also not significant due to the relatively small size of the test part.

In order to identify the effect of quenchant on quenching induced distortion, another statistic analysis of full factorial DoE plan with 2^6 runs was conducted (Table 5). The HTC for water with selected quenchant temperature measured by Li et al. [19] is shown in Fig. 32. With a decreasing temperature of the water, the HTC increases. The result for each simulation is shown in appendix 1, table 2.

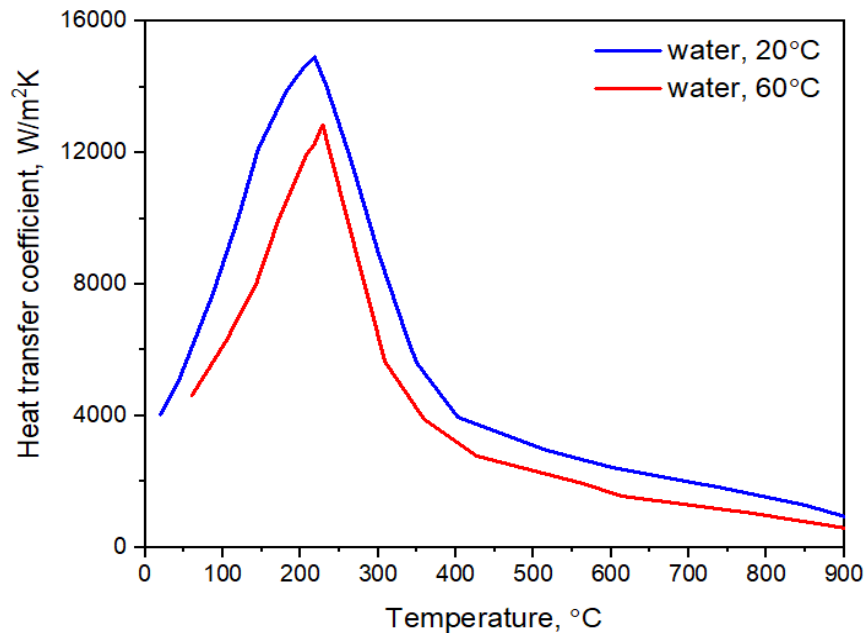


Figure 32: Heat transfer coefficients of water with selected temperatures [19].

Table 5: Full 2⁶ factorial design for processing parameters on quenching distortion for the parts quenched into two selected quenchants.

Symbol	Quenching parameters	Unit	Level 1	Level 2
A	Part geometry	--	Small	Large
B	Quenching orientation	--	Gap up	Gap down
C	Quench start temperature	°C	850	900
D	Immersion rate	mm/s	10	120
E	Quenchant	--	Hougto- Quench G Quenching Oil	Water
F	Quenchant temperature	°C	20	60

Table 6: Analysis of variance for gap opening.

	DF	SS	MS	F	P
Source					
Part geometry	1	39.825	39.825	113.96	0.000
Quenching orientation	1	4.083	4.083	11.68	0.001
Quench start T	1	1.243	1.243	3.56	0.064
Immersion rate	1	0.093	0.093	0.27	0.608
Quenchant T	1	3.227	3.227	9.23	0.004
Quenchant type	1	582.710	582.710	1667.43	0.000
Error	57	19.920	0.349		
Total	63	651.101			

^a Degree of freedom.

^b Sum of squares.

^c Mean squares

^d F ratio

From the ANOVA analysis (Table 6), it indicates that part geometry, quenching orientation, quenchant temperature, and quenchant type significantly affect the quenching induced distortion. On the other hand, quench starts temperature, and immersion rate have not a significant effect on distortion. Water has a higher HTC value than Houghto-Quench G quenching oil. During quenching, water can generate a higher cooling rate in the core of the part to form more martensite. Higher HTC of water can also result in a higher Biot number of the part during quenching, which enlarges the part distortion. Higher Biot number of the part during quenching is the result of the higher HTC of water, which can further increase by decreasing the temperature of the water.

The effect of quenching orientation on gap opening is significant when the part is quenched in water whereas, for oil, the orientation is not. This is because the relatively higher HTC of water makes the short immersion process matters due to the larger Biot number. A part which is quenched gap down will have a different resulting distortion, compared to a part which is quenched gap up.

With the help of Minitab 18, the processing parameters for quenching distortion were ranked based on their impact in Fig. 33. The ranking of the processing parameters is:

1. Quenchant selection
2. Agitation level
3. Part geometry
4. Quenching orientation
5. Quenchant temperature
6. Immersion rate
7. Quench starts temperature

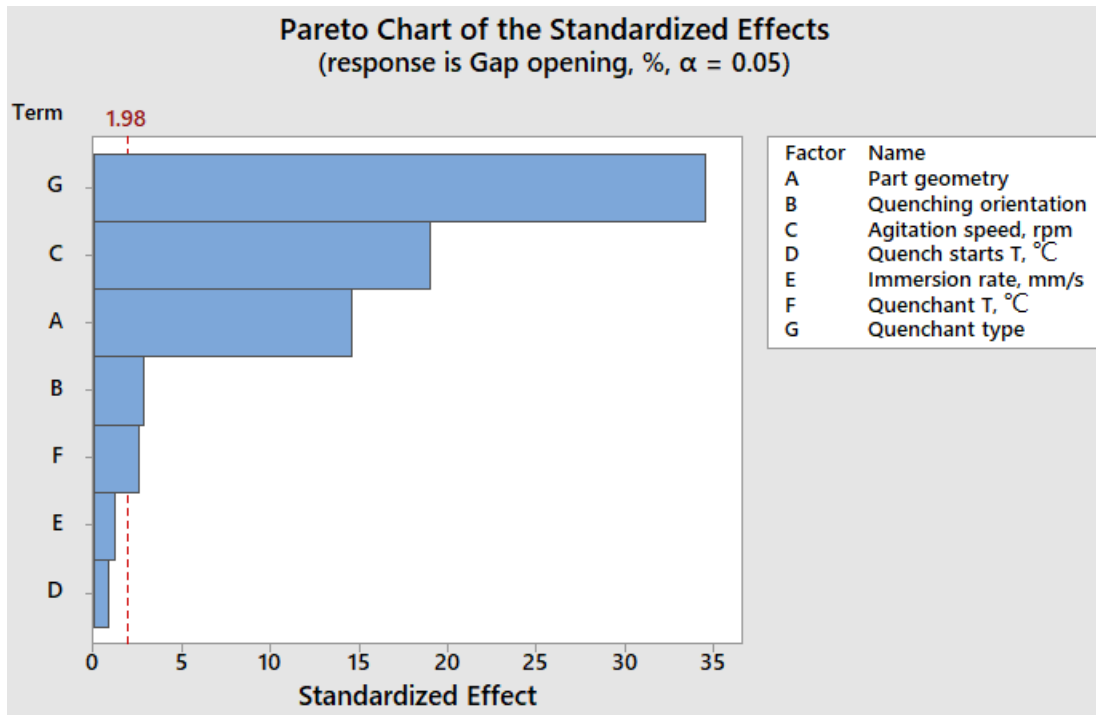


Figure 33: Pareto chart of the statistical analysis of selected processing parameters on the distortion of Navy C-ring specimen (error rate $\alpha=0.05$).

As it is shown in Fig. 34, the effective local Biot number of the bottom section of the Navy C-ring specimen with selected quenching parameters at martensite start temperature is calculated. With higher Biot number, the larger gap opening% is obtained.

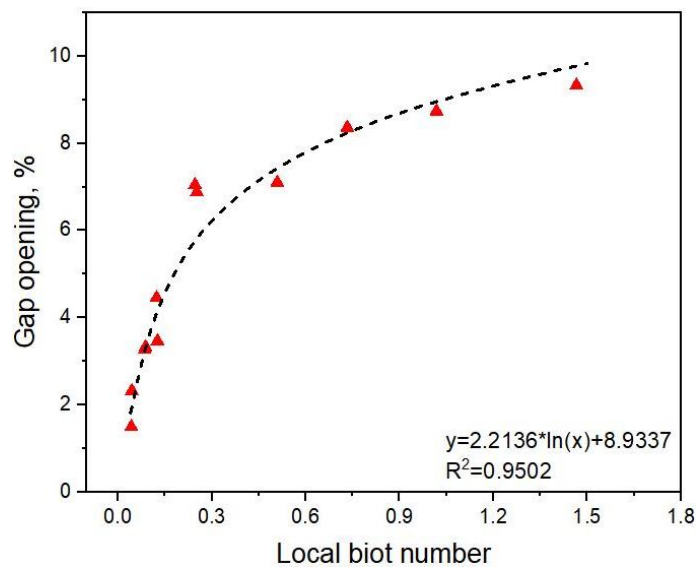


Figure 34: The gap opening% as a function of local Biot number.

5 Conclusions

In this study, the heat treatment modeling of AISI 4140 steel using DANTE on selected distortion coupons with different quenching conditions is conducted. Heat transfer coefficient of alphaquench 5300 and Hougto-Quench G quenching oil with selected agitation speed, quench start temperatures, and quenchant temperatures were measured by CHTE quench probe system. The rectangular specimen with a circular hole was simulated to quench in alphaquench 5300 quenching oil with selected quenching parameters. The simulation results indicated that agitation speed and part geometry significantly affect the distortion of the hole. Higher agitation speed and larger part geometry will increase the Biot number of the part during quenching and result in larger distortion.

Design of experiment (DoE) combined with analysis of variance (ANOVA) was used to identify the quenchant type, part geometry, agitation speed, quenchant temperature, and quenching orientation as the five most important processing parameters during quenching of Navy C-ring specimen. These processing parameters have the most impact on Biot number, where the greater the Biot number, the greater the distortion of the quenched part.

References

1. Ferguson, B. L., Li, Z., & Freborg, A. M. (2005). Modeling heat treatment of steel parts. *Computational Materials Science*, 34(3), 274-281.
2. Totten, G. E. (Ed.). (2002). *Handbook of residual stress and deformation of steel*. ASM international.
3. Maniruzzaman, M., Chaves, J., McGee, C., Ma, S., & Sisson Jr, R. (2002, July). CHTE quench probe system: a new quench characterization system. In *5th International Conference on Frontiers of Design and Manufacturing (ICFDM)* (pp. 619-625).
4. Ferguson, B. L., Li, Z., & Freborg, A. M. (2005). Modeling heat treatment of steel parts. *Computational Materials Science*, 34(3), 274-281.
5. Wallis, R. A., & Forgings, W. G. (2010). Modeling of quenching, residual-stress formation, and quench cracking. *ASM handbook*, 22, 547-585.
6. Arimoto, K. (1998). Development of heat treatment simulation system Deform-HT. In *Proceeding of 18th Heat Treating Conference, ASM International*, 1998.
7. Inoue, T. (1992). Metallo-thermo-mechanical Simulation of Quenching Process-Theory, and Implementation of Computer Code" HEARTS". In *Proc. 1st Int. Conf. Quenching and Control of Distortion*, 1992.
8. Jarvstrat, N., & Sjostrom, S. (1993, June). Current status of TRAST; a material model subroutine system for the calculation of quench stresses in steel. In *ABAQUS User's Conference Proceedings*.
9. Rani, R. M., & Seshan, S. (1998). Studies on abrasive jet machining through statistical design of Experiments. *Experimental techniques*, 22(2), 28-30.
10. Ross, P. J. (1996). *Taguchi techniques for quality engineering: loss function, orthogonal experiments, parameter and tolerance design*.
11. Macodiyo, D. O., & Soyama, H. (2006). Optimization of cavitation peening parameters for fatigue performance of carburized steel using Taguchi methods. *Journal of Materials Processing Technology*, 178(1-3), 234-240.
12. Dong, J., Epp, J., da Silva Rocha, A., Nunes, R. M., & Zoch, H. W. (2016). Investigation of the influence factors on distortion in induction-hardened steel shafts manufactured from cold-drawn rod. *Metallurgical and Materials Transactions A*, 47(2), 877-888.

13. Clausen, B., Frerichs, F., Kohlhoff, T., Lübben, T. H., Prinz, C., Rentsch, R., & Klein, D. (2009). Identification of process parameters affecting distortion of disks for gear manufacture Part I: casting, forming and machining. *Materialwissenschaft und Werkstofftechnik: Entwicklung, Fertigung, Prüfung, Eigenschaften und Anwendungen technischer Werkstoffe*, 40(5-6), 354-360.
14. https://www.houghtonintl.com/sites/default/files/data-sheets/houghton-quench_g_1311_us.pdf
15. J. R. Davis and S. R. Lampman, Eds., ASM Handbook Volume 1: Properties and Selection: Irons, Steels, and High-Performance Alloys, 10th ed. ASM International, 2004
16. Warke, V. S. (2008). *Predicting the response of powder metallurgy steel components to heat treatment*. Worcester Polytechnic Institute. Worcester, USA.
17. ASME Y14.5M-1994, "Dimensioning and tolerancing", American Society for Mechanical Engineers, NY, 1994.
18. Mills, A. F. Heat Transfer, 1992. Irwin, IL.
19. Li, H., Zhao, G., He, L., & Mu, Y. (2008). High-speed data acquisition of the cooling curves and evaluation of heat transfer coefficient in quenching process. *Measurement*, 41(6), 676-686.

CHAPTER 5 Paper III: The effect of heat transfer coefficient and martensite start temperature on distortion of the Navy C-ring specimen

Haixuan Yu · Richard D. Sisson, Jr

To be submitted to: HTM Journal of Heat Treatment and Materials

Highlights:

1. The simulation results indicated that higher HTC max and HTC at convection could enlarge the gap opening of the Navy C-ring.
2. The effect of carbon content on gap opening was also studied. Increasing carbon content corresponds to an increase in the gap opening. This trend continues up to carbon content of 0.5%, at which point the relationship is inverted due to the increase in retained austenite.
3. The effect of quenching parameters in decreasing order of importance were determined to be: Ms temperature, HTC at Ms, HTC max, HTC at convection, HTC at LF, and the temperature at HTC max.

The effect of heat transfer coefficient on distortion of Navy C-ring specimen

Haixuan Yu¹ · Richard D. Sisson, Jr.^{*1}

¹*Center for Heat Treating Excellence, Worcester Polytechnic Institute, 100 Institute Road, Worcester, MA 01609, USA*

hyu2@wpi.edu, yhxates@gmail.com (H. Yu)

sisson@wpi.edu (R.D. Sisson, Jr)

Abstract

Steel parts can become distorted during heat treating. To reduce distortion and meet the geometrical specification, it is crucial to understand and control the effects of heat transfer coefficient (HTC) during quenching on distortion. Heat treating simulation using DANTE [1], has been conducted on Navy C-ring specimen [2] to simulate the steel to be quenched. The effect of HTC and alloy selection on distortion was analyzed using design of experiments (DoE) coupled with analysis of variance (ANOVA). The effect of quenching parameters on distortion in decreasing order of importance were determined to be: Ms temperature, HTC at Ms, HTC max, HTC at convection, HTC at Leidenfrost (LF) temperature, and the temperature at HTC max. In this paper, the results of these simulations and statistical analysis are presented and discussed.

Keywords quenching distortion · FEM · heat transfer coefficient · Navy C-ring · DoE · ANOVA

1 Introduction

Steel parts that are used in the aerospace, automotive, construction, and heavy equipment industry rely on different heat-treating process, especially, quenching to acquire the desired mechanical properties. But rapid phase transformations and high thermal gradients that occur during quenching can cause distortion [1], which can lead to costly hard-machining and rejection.

Finite element analysis (FEA) is one of several effective methods to understand the mechanisms causing distortion and help develop a heat treatment procedure that can minimize distortion, cost as well as time [3]. Heat treatment analysis software including DANTE [1], DEFORM-HT [4], HEARTS [5], and SYSWELD [6] have been well developed to predict the microstructure and final distortion after heat treatment. In previous papers, the experimental results showed good agreement with the simulation results from DANTE. Therefore, the analysis is based on DANTE simulation.

As shown in Fig. 1, heat transfer during quenching with a liquid medium is a process, which is controlled by four distinct cooling stages [7, 8].

At the beginning of the quenching procedure, the hot surface becomes surrounded by a vapor blanket, which is shown in range A-B. The film boiling stage has the lowest heat transfer rate, and the heat transfer occurs mainly by radiation through the vapor blanket. The vapor film is stable, and it can be removed by speed improving additives or agitation during quenching [9].

The second phase of the quenching process is called transition boiling or partial film boiling, which is shown by range B-C. In the second phase, the vapor film becomes unstable, and the heat transfer coefficient increases. The onset of the partial film boiling stage is known as Leidenfrost point (LF).

The range C-D is the nucleate boiling regime. With a further decrease in temperature, the partial film collapses into numerous bubbles, and the quenchant contacts the part directly, which corresponds to rapid heat transfer. In this stage, the heat transfer rate reaches its maximum, which is known as critical heat flux (CHF). The nucleate boiling regime stops when the surface temperature of the part is lower than the boiling point of the liquid quenchant.

The fourth regime is the natural convection regime, where the heat is transferred by the convection of the liquid. Heat is removed by convection and is controlled by quenchant's conductivity and specific heat. The convection stage usually has the lowest heat transfer rate among the four stages of quenching.

The temperature dependent heat transfer coefficient (HTC) is the most important boundary condition for the quenching process simulation. To achieve proper mechanical properties of steel and minimize the distortion of the steel part after heat treatment, understand the effect of each regime of HTC curve is crucial. In this paper, the sensitivity analysis of the HTC and alloy selection on quenching distortion of Navy C-ring specimen using the DoE method is simulated and discussed.

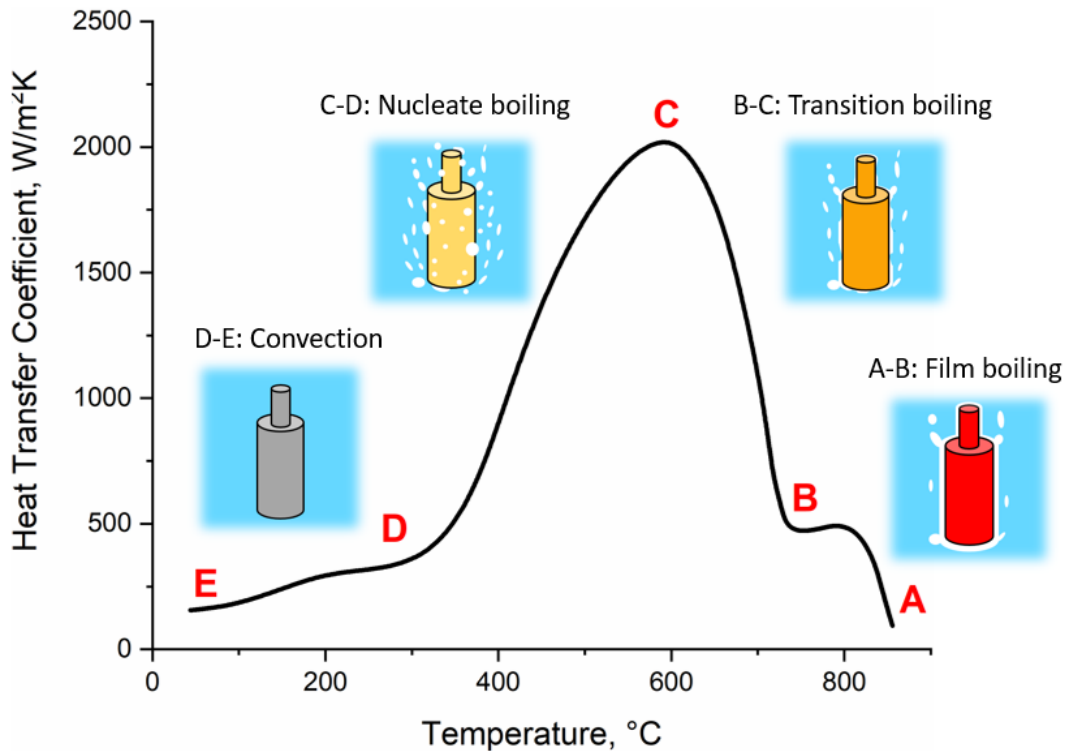


Figure 1: Stages of quenching in a liquid medium.

2 Numerical simulation

The heat treatment modeling of the Navy C-ring was carried out using finite element analysis (FEA) software ABAQUS coupled with heat treatment analysis software DANTE [1]. Fig. 2 presents the three-dimensional finite element (FE) model of the steel part for heat treatment simulation. In order to have accurate simulation results, a finer mesh was applied near the surface. Due to the symmetry of the specimen, only one-quarter of the part was simulated. The finite element mesh consisted of 21584 nodes and 18900 quad elements. Node A was used to measure the distortion of the gap after heat treatment simulation. The finite element (FE) input for the simulation is summarized in Table 1. An HTC as a function of temperature was applied to all surfaces of the part.

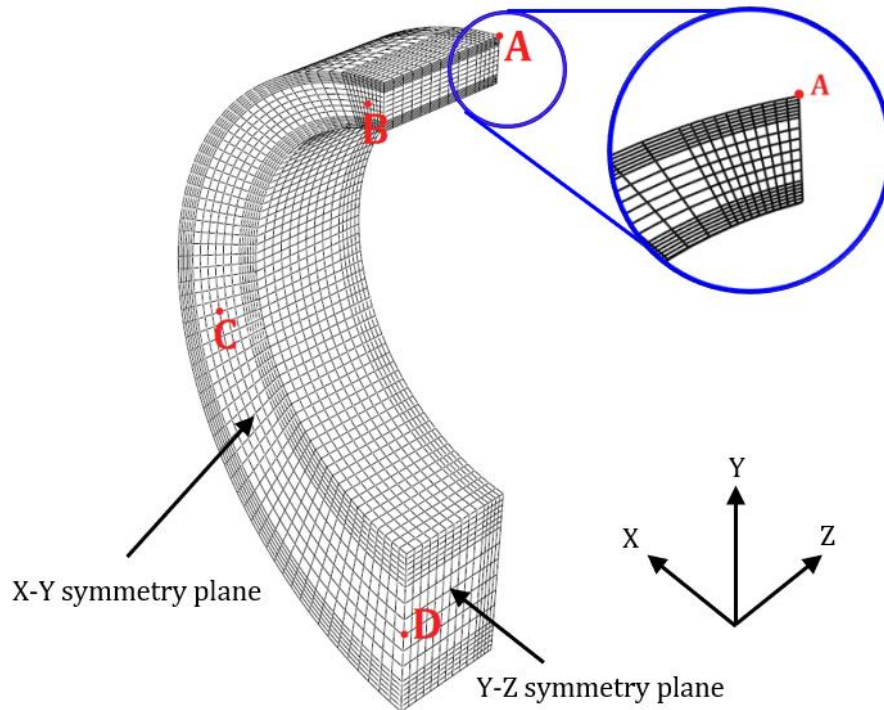


Figure 2: Solid model and finite element mesh used for heat treatment simulation.

Table 1: FE input for the simulations of Navy C-ring specimen.

Operation	Parameter	Value
Step 1: Heating	Code	DANTE
	Specimen geometry	Fig. 6
	Material Property	Selected steel from DANTE data base
	Initial temperature	20°C
	Austenitizing temperature	Selected quench starts T
	Time	40 minutes
Step 2: Air transfer	Code	DANTE
	Time	15 seconds
Step 3: Immersion quenching	Code	DANTE
	Time	2 seconds
Step 4: Quenching	Code	DANTE
	Heat transfer coefficient	Function of temperature
	Time	5 minutes

3 Results and Discussion

3.1 Sensitivity study of HTC value on distortion of Navy C-ring specimen during quenching

As shown in Fig. 3, five constant heat transfer coefficient values are used for the sensitivity study of HTC value on quenching induced distortion. The constant HTCs are a good simulation for high-pressure gas quenching [10]. By changing the gas pressure, gas velocity, and gas type, the HTC of the gas quenching can be increased [11]. The heat treatment of the Navy C-ring specimen made of AISI 4140 steel was simulated. The part was heated to 850°C, held for 40 minutes, and quenched with high-pressure gas, which had different HTC values from 1000 W/m²°C to 5000 W/m²°C.

Fig. 4 presents the relationship among gap opening, phase fraction of martensite, and lower bainite in Node D as a function of HTC. The gap opening of Navy C-ring specimens increased with increasing HTC value. That is because higher HTC value increased the cooling rate of part and formed more martensite at Node D instead of bainite. Due to a relatively lower density of martensite, the gap opening of the Navy C-ring increased with a higher fraction of martensite.

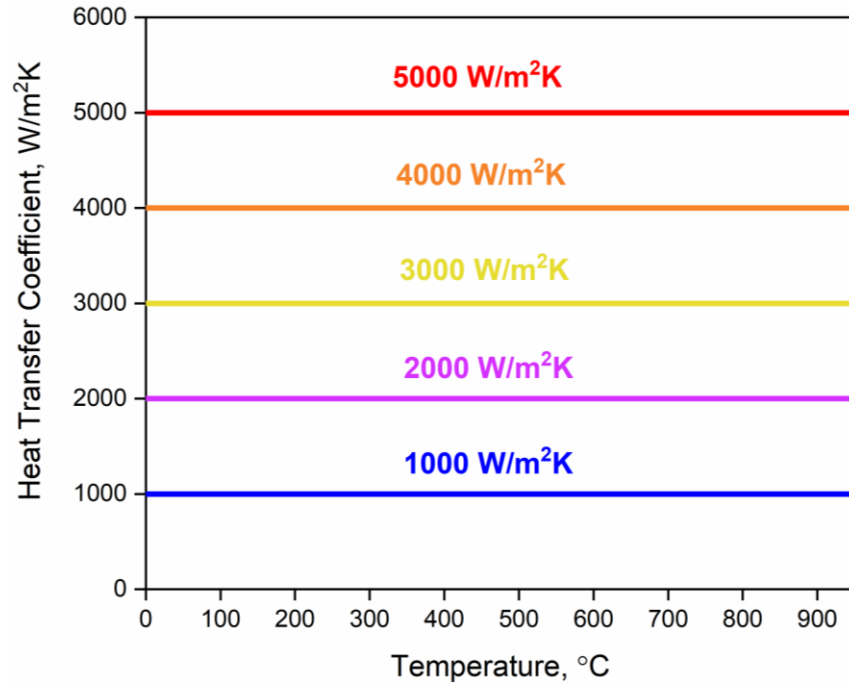


Figure 3: Selected constant HTC value used for heat treating simulation.

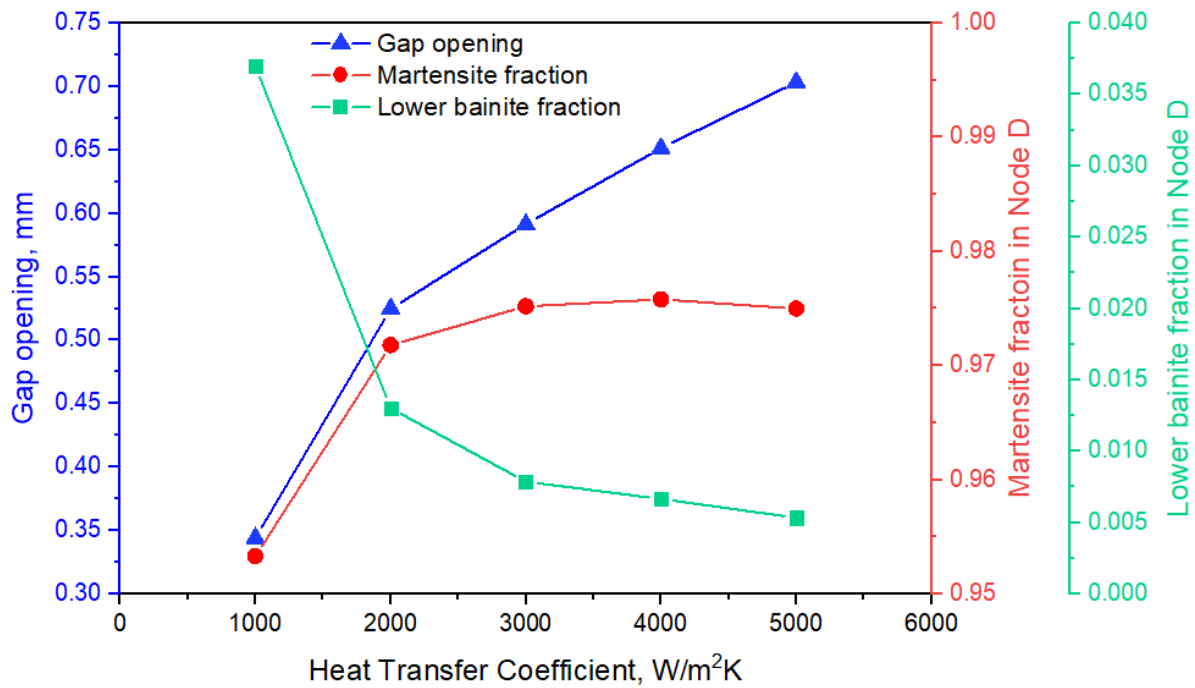


Figure 4: The relationship among gap opening, fraction of martensite, and fraction of lower bainite in Node D as a function of HTC value for high pressure gas quenching.

3.2 Sensitivity study of HTC max on distortion of Navy C-ring specimen during quenching

As it is shown in Fig. 5, eleven schematic heat transfer coefficient curves are used for the sensitivity study of HTC max on quenching induced distortion. The Navy C-ring specimens heat treatments were simulated by heating up to 850°C for 1 hour and quenching into the quenched, which had selected HTC max. In order to determine the distortion behavior for different alloys, AISI 4140, 4160, 4340, and 9310 steels were used for the simulation. As shown in Fig. 6, the gap opening of Navy C-ring specimens made of four alloys steel had the same trend. In the beginning, the distortion increased sharply with higher HTC max. When the HTC max was 7000 W/m²°C, the change of the gap opening was doubled for all the steels. The gap opening then decreased when HTC max higher than 7000 W/m²°K. This phenomenon is possibly due to the distortion mechanisms. When the HTC max is not very high, the phase transformation induced distortion dominate, which would generate tensile residual stress on the surface of the sample and make the gap open. On the other hand, after the HTC is high enough to through-hardened the part, a higher the HTC would bring the larger effect of thermal-induced distortion, which will bring compressive residual stress on the surface of the sample and make the gap close.

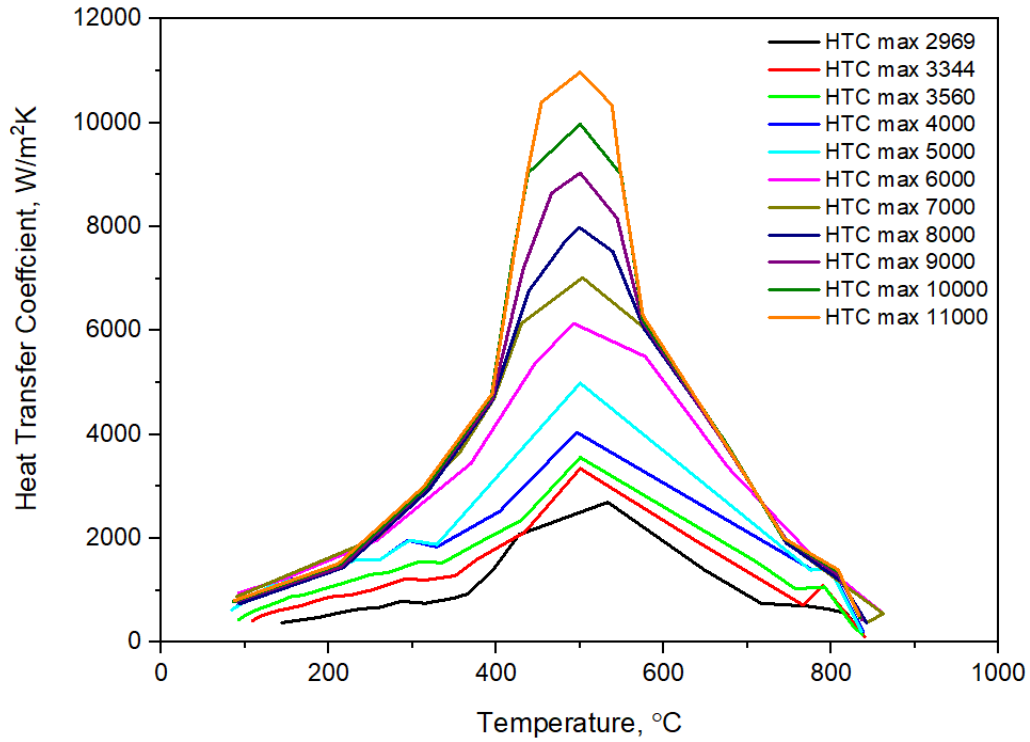


Figure 5: Selected HTC curves used for the sensitivity study of HTC max on distortion.

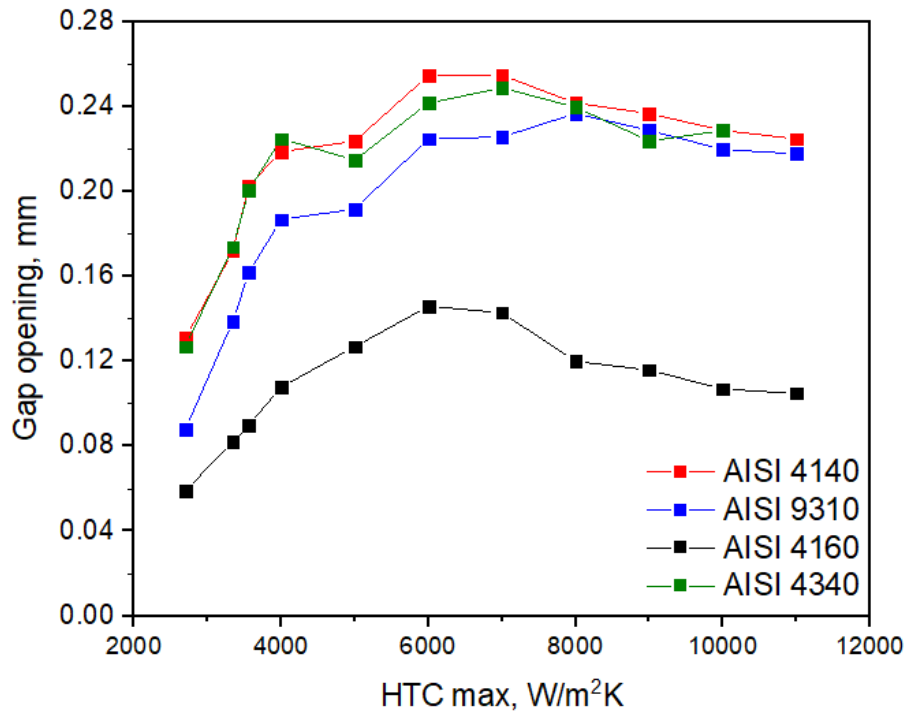


Figure 6: The gap opening of Navy C-ring specimens made of selected alloys with selected HTC max.

3.3 Sensitivity study of HTC at convection stage on distortion of Navy C-ring specimen during quenching

The sensitivity study of HTC at the convection stage was also studied in this paper. As shown in Fig. 7, four schematic heat transfer coefficient curves with the same HTC max but selected HTC at convection stage are used for simulation. As illustrated in Fig. 8, with higher HTC at convection stage, the gap opening of the Navy C-ring specimens increases. The same trend is also found with selected HTC max.

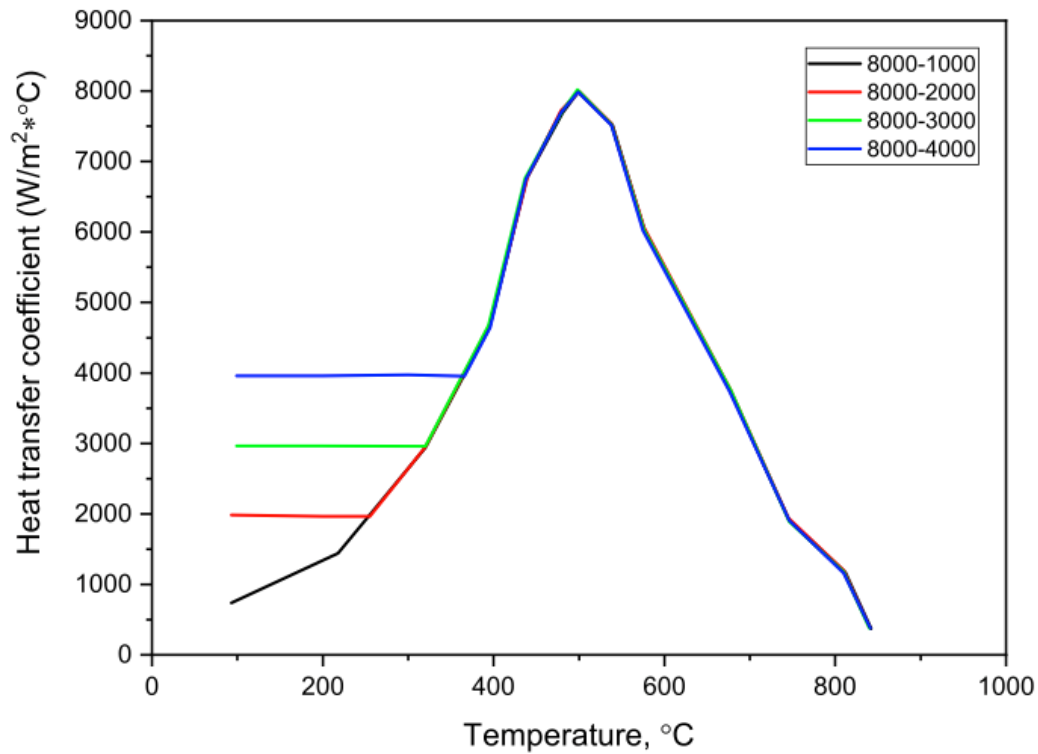


Figure 7: Selected HTC curves used for sensitivity study of HTC at convection on distortion (HTC max = 8000 W/m²K).

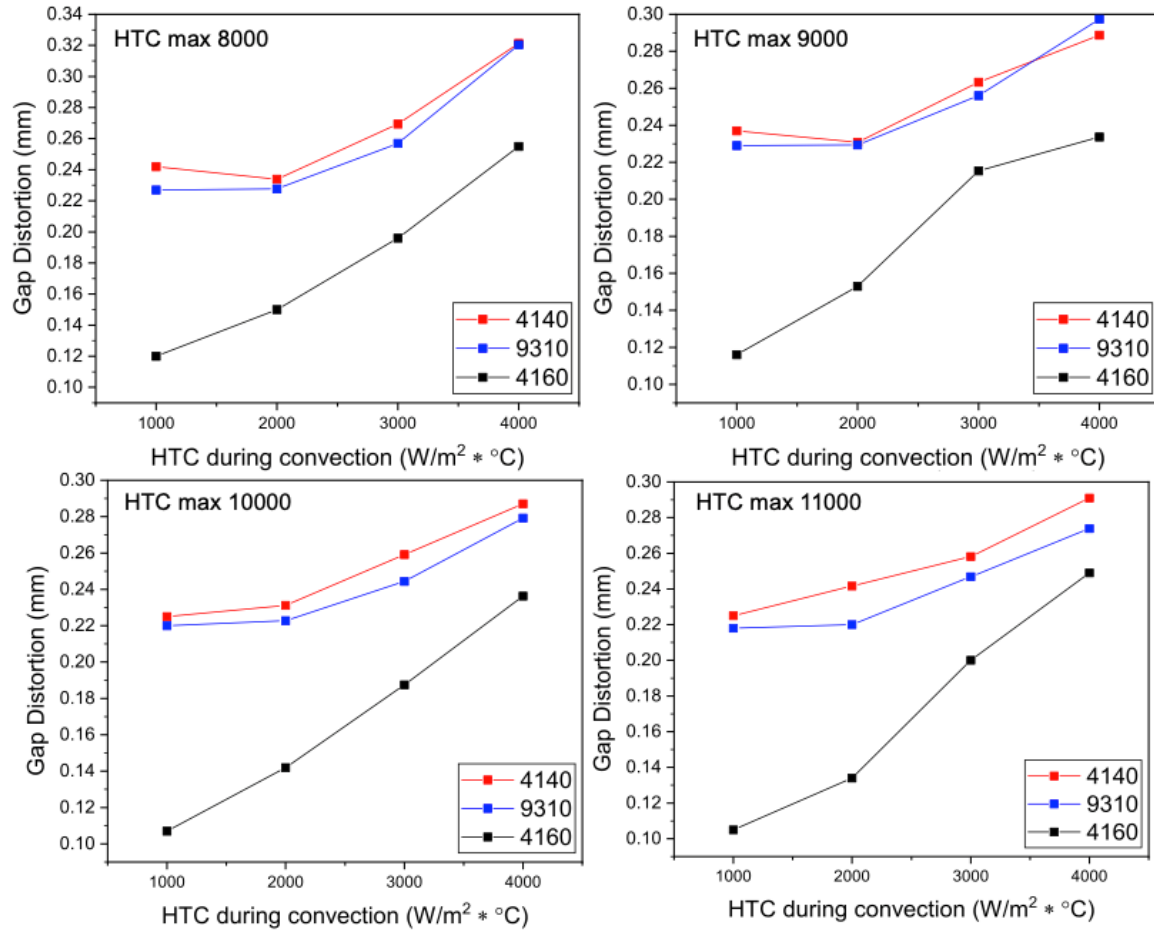


Figure 8: The gap openings of Navy C-ring specimens made of selected alloys with selected HTC max and selected HTC at convection stage.

3.4 Sensitivity study of quench starts temperature on distortion of Navy C-ring specimen during quenching

The effect of quench starts temperature was also studied in this report. The Navy C-ring specimen was simulated with the austenitizing temperature of 850°C, 870°C, 900°C, 930°C, 950°C, 980°C, and 1000°C followed by quenching in Houghto-Quench G quench oil with 1000 rpm agitation speed. From the result (Fig. 9), the quenching starts temperature has not significant effect on quenching induced distortion of Navy C-ring specimen made of selected alloy steel.

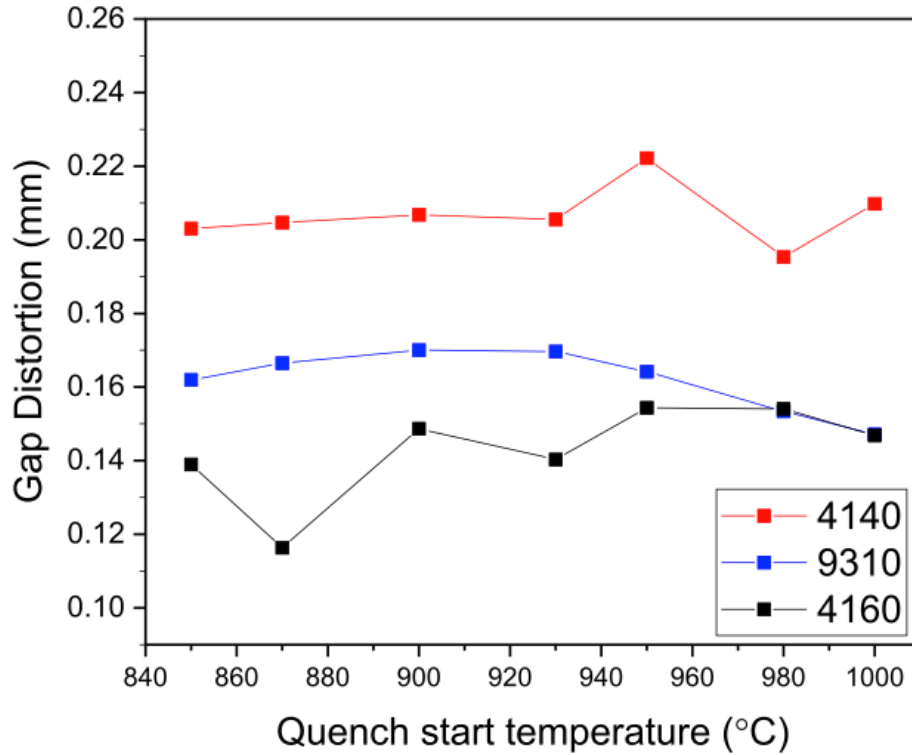


Figure 9: The effect of quench start temperature on quenching induced distortion of Navy C-ring specimen.

3.5 Sensitivity study of carbon content on distortion of Navy C-ring specimen during quenching

To study the effect of the carbon content of the steel on quenching induced distortion of Navy C-ring specimen, selected 41xx series steel with selected carbon concentration is simulated to quench into alphaquench 5300 quenching oil at the pump speed of 25%. With higher carbon content, the martensite starts temperature (M_s) of the steel decreases, and the hardenability of the steel increases. The alloy and their M_s temperatures with selected carbon content from the DANTE database are shown in Table 2. Fig. 10 shows the heat transfer coefficient of the quenchant as a function of temperature with corresponding M_s temperature of selected steel grades.

Table 2: Selected 41xx steels with their martensite start temperatures.

Material	Carbon content, %	Martensite start temperature, °C
AISI 4120	0.2	412
AISI 4130	0.3	370
AISI 4140	0.4	326
AISI 4150	0.5	289
AISI 4160	0.6	260

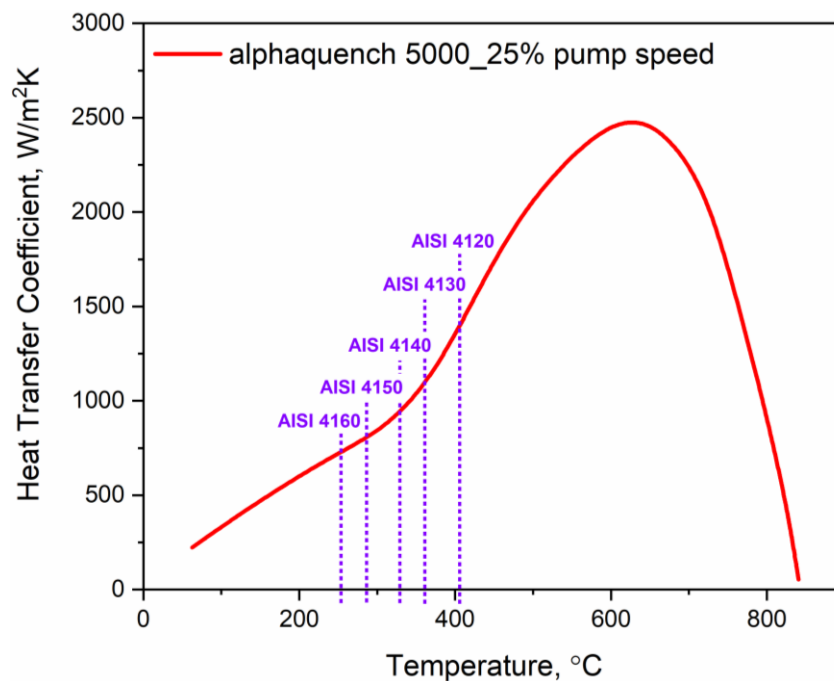


Figure 10: Heat transfer coefficient of alphaquenched 5300 quenching oil with corresponding Ms temperature of selected carbon content.

Fig. 11 presents the relationship between the gap opening and Ms temperature, where decreasing the Ms temperature corresponded to an increase in the gap opening. This trend continues up to the Ms temperature of 289 °C, at which point the relationship inverted. As it is shown in Fig. 80, increasing the carbon content will result in not only decrease the Ms temperature but also increasing the hardenability of steel (push the “knee” to the right, promoting the formation of martensite). Martensite is less dense than bainite, so increased martensite content corresponds to a larger gap opening.

When the carbon content reaches 0.5%C (Ms temperature of 289 °C), more retained austenite will form instead of martensite. Due to the relatively higher density of the austenite, the gap opening will decrease.

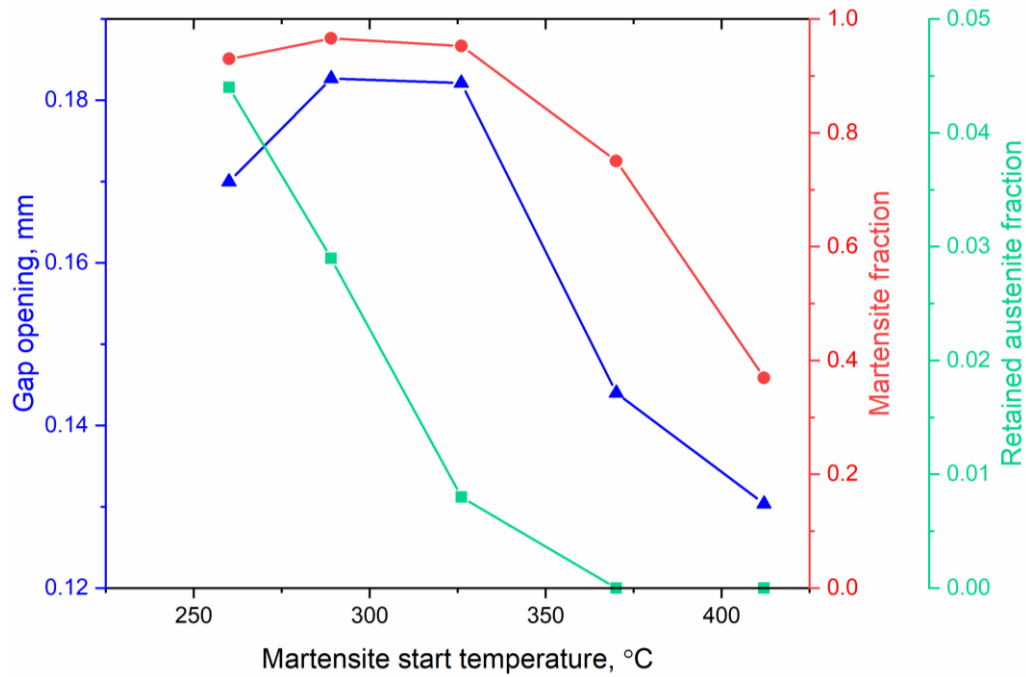


Figure 11: The correlation among gap opening, martensite fraction, and retained austenite fraction in Node D versus Ms temperature.

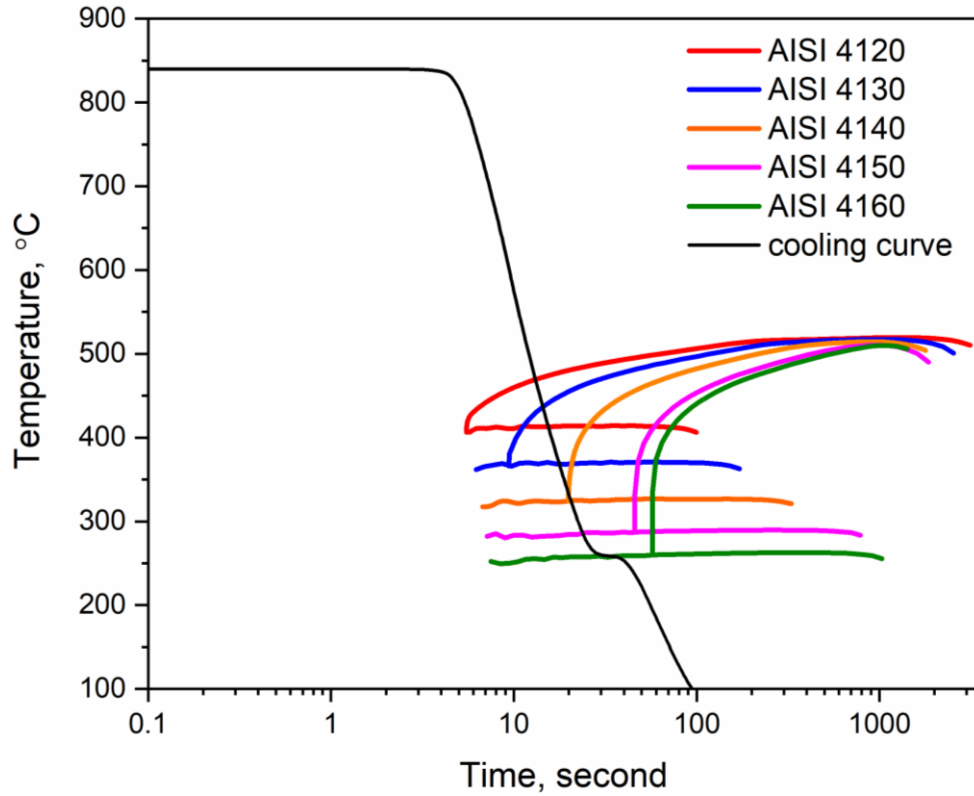


Figure 12: The cooling curve of Node D with CCT curves of selected carbon content.

3.6 The sensitivity study of the effect of the HTC curve on distortion of the Navy C-ring using the DoE method

3.6.1 Significant features of HTC curves

Varde et al. [12] identified the HTC curve with a few features, which are listed below and illustrated in Fig. 13:

- BP: The heat transfer coefficient at the boiling point of the quenchant. (From nucleate boiling to convection)
- LF: The Leidenfrost point at which the vapor blanket breaks down.
- MAX: The point of maximum heat transfer.
- Tmax: Temperature at which the maximum heat transfer is reached.
- MIN: The point of minimum heat transfer.
- SC: The point where slow cooling ends.

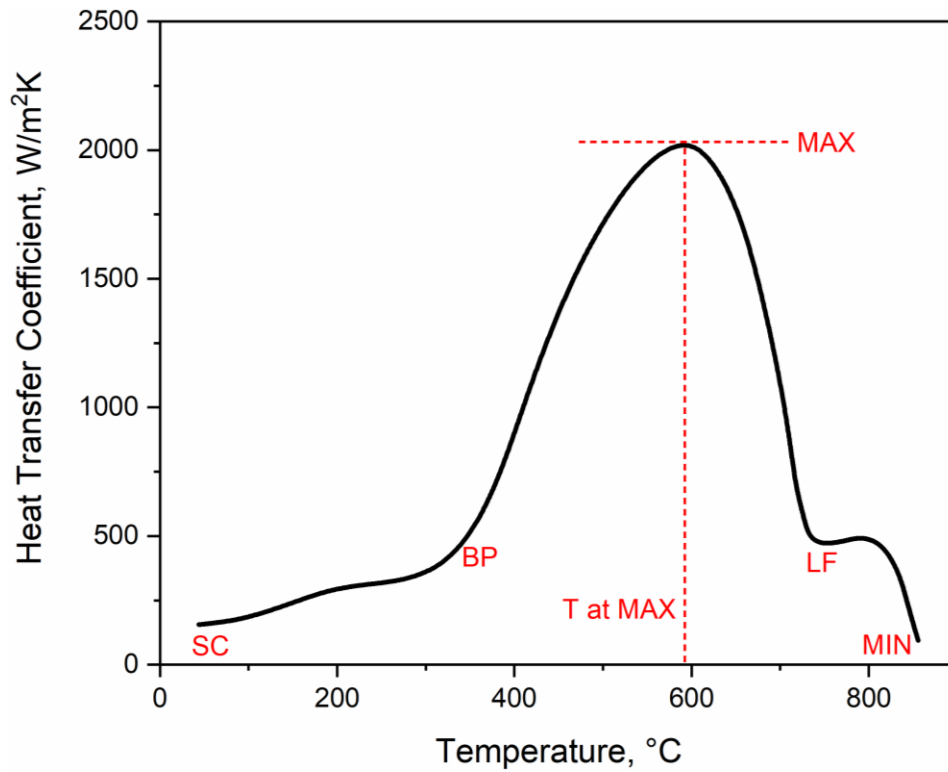


Figure 13: The HTC curve with its semantics.

To conduct the sensitivity analysis of the HTC on distortion of Navy C-ring specimen, the alloy itself must be considered. Based on the previous description of HTCs, five features of HTC plus the M_s temperature of the alloy are considered, as seen in Fig. 14.

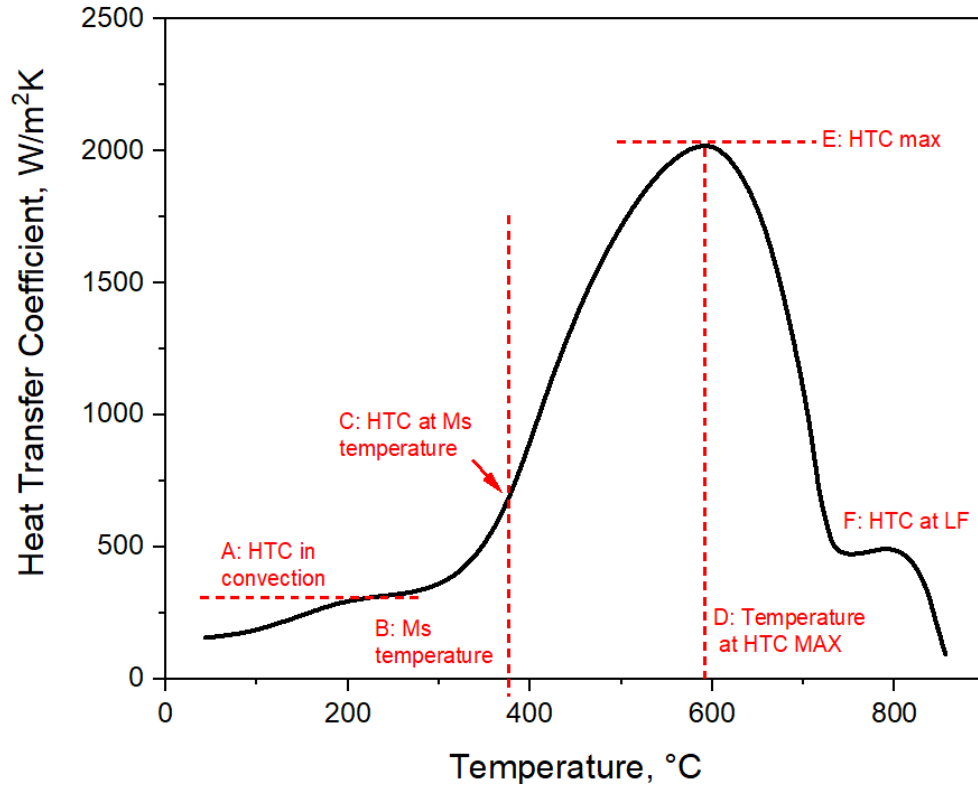


Figure 14: The Ms temperature and the HTC curve with its features.

3.6.2 Using DoE to determine the important processing parameters on distortion

As shown in Table 3 the statistical analysis of the fractional 2^5 factorial DoE plan was developed using the software Minitab 18 (Minitab Ltd, Coventry, UK) [13] to assess the impact of the HTC in convection, Ms temperature, HTC at Ms temperature, temperature at HTC max, HTC max and HTC at LF on distortion of Navy C-ring specimen. Two levels were specified for each processing parameter (Fig. 15). The result for each simulation is shown in appendix 2, Table 19.

Table 3: Fractional 2^5 factorial design of the sensitivity of the HTC curve on quenching distortion of the Navy C-ring.

Symbol		Unit	Level 1	Level 2
A	HTC in convection	W/m ² K	500	1000
B	Ms temperature	°C	326	412
C	HTC at Ms	W/m ² K	1000	2000
D	Temperature at HTC max (Tmax)	°C	500	700
E	HTC max	W/m ² K	3000	5000
F	HTC at LF	W/m ² K	500	1000

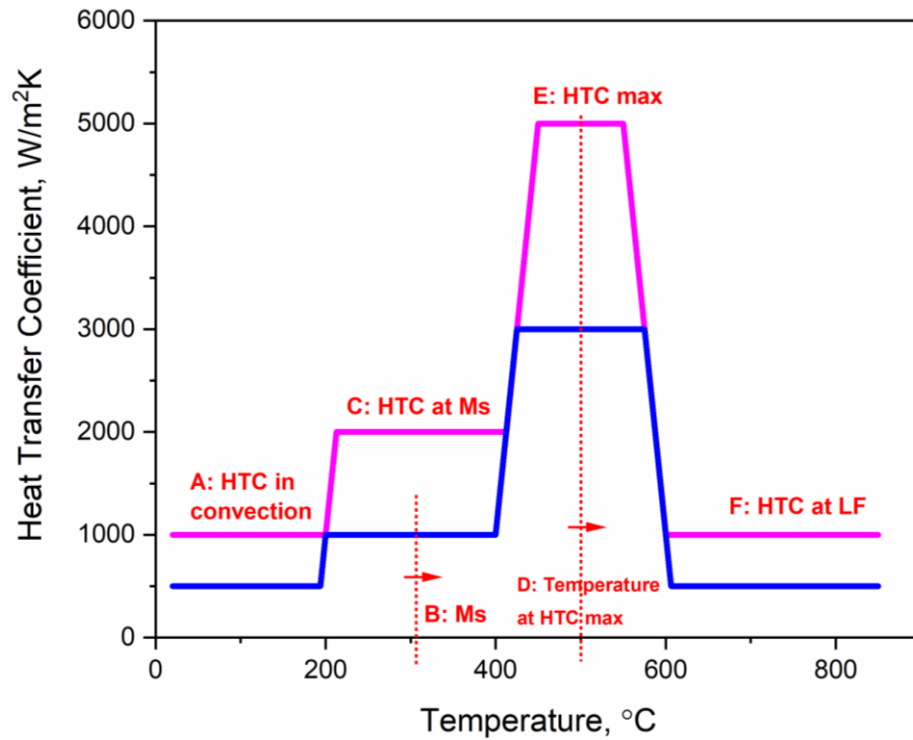


Figure 15: Selected HTC curves to determine the important processing parameters on distortion using DoE method.

Table 4 shows a summary of the analysis of variance (ANOVA) results using Minitab 18. In ANOVA, the p-values (probability of error) were used as criteria to determine which of the factors were statistically significant. P-value of less than 0.05 was identified as 'statistically significant' or 'statistically contributing' and vice versa. From the table, it shows that HTC in convection, Ms temperature, HTC at Ms, and HTC max has a significant effect on quenching distortion. On the other hand, temperature at HTC max and HTC at LF do not have a significant effect on quenching distortion. As illustrated in Fig. 16, any factors that pass the red line (significance threshold) means it is significant. The effect of these features of the HTC curve in decreasing order of importance was determined to be: Ms temperature, HTC at Ms, HTC max, HTC at convection, HTC at LF, and the temperature at HTC max.

Carbon content results in different Ms temperature and therefore hardenability of the steel. Higher hardenability of the steel can increase the volume fraction of martensite in the core of the Navy C-ring specimen, which will enlarge the gap opening. Higher HTC at Ms, convection regime, and nucleate boiling regime can increase the cooling rate, which can form more martensite in the core of the specimen and enlarge the gap opening. A high Biot number will result in larger temperature gradient across the C-ring and time variations to form martensite or bainite. A variation in microstructure (i.e. fraction of martensite, bainite, and austenite) in the cross-section will result in higher stresses and larger distortion.

Table 4: Analysis of variance for gap opening.

	DF ^a	Adj SS ^b	Adj MS ^c	F ^d	P
Source					
HTC in convection	1	0.00178	0.00178	7.17	0.013
Ms temperature	1	0.07402	0.07402	297.51	0.000
HTC at Ms	1	0.04710	0.04710	189.31	0.000
Temperature at MAX	1	0.00002	0.00002	0.08	0.777
HTC max	1	0.00244	0.00244	9.80	0.004
HTC at LF	1	0.00003	0.00003	0.10	0.749
Error	25	0.00622	0.00622		
Total	31	0.131606			

^a Degree of freedom.

^b Sum of squares.

^c Mean squares

^d F ratio

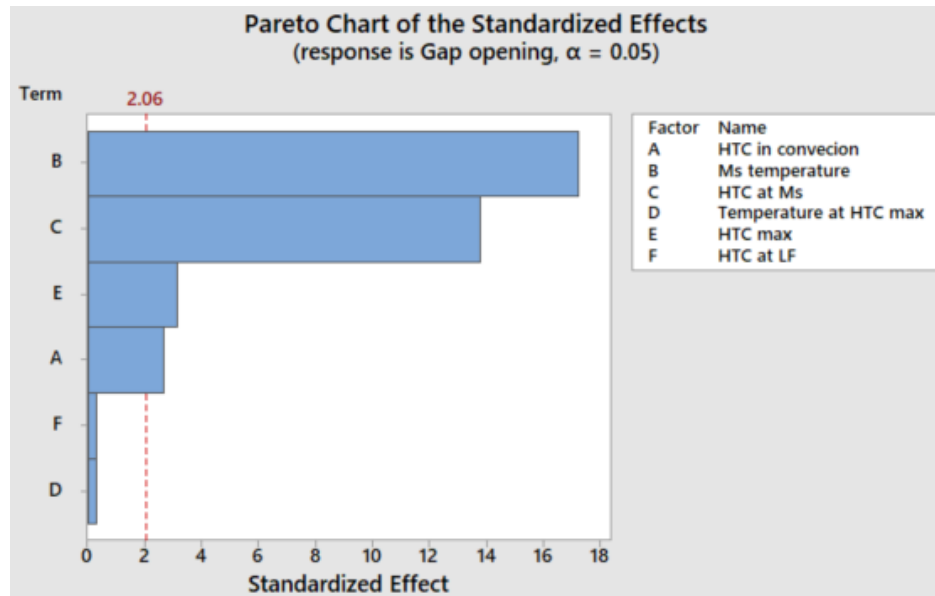


Figure 16: Pareto chart of the statistical analysis of HTC curves on distortion of Navy C-ring specimen (error rate $\alpha=0.05$).

4 Conclusions

In this study, the heat treatment modeling of Navy C-ring using DANTE with selected steel grades was conducted. The simulation results indicated that higher HTC max and HTC at convection could enlarge the gap opening of the Navy C-ring. On the other hand, the quench start temperature does not have a significant effect on quenching distortion of the Navy C-ring specimen. The effect of carbon content on gap opening was also studied. Increasing carbon content corresponds to an increase in the gap opening. This trend continues up to carbon content of 0.5%, at which point the relationship is inverted due to the increase in retained austenite. Design of experiment (DoE) combined with analysis of variance (ANOVA) was used to identify the important features of the HTC curve during quenching of Navy C-ring specimen. The effect of the materials and quenching parameters in decreasing order of importance were determined to be:

- Ms temperature
- HTC at Ms
- HTC max
- HTC at convection
- HTC at LF
- Temperature at HTC max.

References

1. Ferguson, B. L., Li, Z., & Freborg, A. M. (2005). Modeling heat treatment of steel parts. *Computational Materials Science*, 34(3), 274-281.
2. Totten, G. E. (Ed.). (2002). *Handbook of residual stress and deformation of steel*. ASM international.
3. Wallis, R. A., & Forgings, W. G. (2010). Modeling of quenching, residual-stress formation, and quench cracking. *ASM handbook*, 22, 547-585.
4. Arimoto, K. (1998). Development of heat treatment simulation system Deform-HT. In *Proceeding of 18th Heat Treating Conference, ASM International, 1998*.
5. Inoue, T. (1992). Metallo-thermo-mechanical Simulation of Quenching Process-Theory, and Implementation of Computer Code" HEARTS". In *Proc. 1st Int. Conf. Quenching and Control of Distortion, 1992*.
6. Jarvstrat, N., & Sjostrom, S. (1993, June). Current status of TRAST; a material model subroutine system for the calculation of quench stresses in steel. In *ABAQUS User's Conference Proceedings*.
7. Bergles, A. E. (1992). Elements of Boiling Heat Transfer. In *Boiling Heat Transfer* (pp. 389-445). Elsevier.
8. Totten, G. E., Bates, C. E., & Clinton, N. A. (1993). *Handbook of quenchants and quenching technology*. ASM international.
9. Faulkner, C. (2017, Oct). Aqueous quenchants for induction hardening. *Proceedings of the 29th Heat Treating Society Conference* (pp. 141-143). Columbus, Ohio, USA
10. Lu, Y., Sisson, R., & Pershing, M. (2017) "Gas Quenching: Linking Steel Hardenability and Furnace Cooling Capability Tests."
11. Liscic, B., Tensi, H. M., Canale, L. C. F. & Totten, G. E., (2011) *Quenching Theory and Technology*, Second Edition.
12. Varde, A., Takahashi, M., Maniruzzaman, M., & Sisson Jr, R. (2002, October). Web-based data mining for quenching analysis. In *Proceedings of the 13th Congress of the International Federation for Heat Treatment and Surface Engineering (IFHTSE) and ASM International Surface Engineering Congress, October* (pp. 7-10).
13. <http://www.minitab.com/en-US/default.aspx>

CHAPTER 6 Summary

In this thesis, the identification of the important process parameters for quenching induced distortion was investigated.

In summary, based on the results from simulation, experiment, and ANOVA, the most important processing parameters is HTC, which is a function of quenchant, agitation speed, quenchant temperature and quenching orientation. The second most important processing parameters is part geometry. The part geometry can be coupled with HTC to obtain the local effective Biot number, where the greater the Biot number, the greater temperature gradient and the potential distortion of the quenched part.

Distortion is a result of the interactions of the quenching system design, the part geometry and the alloy being heat treated.

The key to distortion control is the minimization/control of internal temperature gradients in the part being heat treated. As discussed previously, the reduction of internal temperature gradients may be accomplished by controlling and reducing the local Biot number. The local Biot number may be reduced by changing the part design and/or controlling the temperature dependent heat transfer coefficient (HTC) at selected locations at the surface of the part.

The change in part design may be limited due the requirements for the performance of the part. A set of “design guidelines” should be developed to aid the designer in “design for quenching”. The guidelines may include advice like: avoid large changes in part cross sections, avoid regions that restrict or channel flow, include fixture design in the quenching system process design.

The fixture design must also be included in quenching system process design and selection. The effects of the fixtures on the quench flow around the part must be considered. The mechanical constraints on the part expansion and contraction must also be included.

To reduce the HTC locally the flow rate of the quenchant at selected locations on the surface must be reduced. This reduction may be accomplished by local control of the flow rate from pumps, nozzles or water jets. This real time control during quenching will require an intelligent control system that is coupled with a real time software simulation model to rapidly and accurately direct and control rates. The reduction may also be achieved by fixture design to reduce or channel quenchant flow.

Another method to reduce the effective HTC is to mask selected regions of the part with an insulating coating. This coating may be painted on the part and cured before heat treating. The coating adhesion may be an issue. The effectiveness of this method may be simulated using heat treat modeling software.

The cooling rates within the part must be rapid enough to achieve the desired microstructure and mechanical properties but also slow enough to avoid distortion. The quenching system design and the part design should be tested using heat treat modeling software to iterate the designs to achieve the desired part performance.

The design of the quenching system will include the following:

1. Quenching tank geometry and quenchant volume
2. Quenchant composition
3. Quenchant temperature
4. Pumps, nozzles or jets and their location
5. Fixture design to support and constrain the part
6. Quenchant flow patterns and velocities around the part

CHAPTER 7 Recommendations for future work

- Investigate the effects of carburization on distortion and residual stress.
- Investigate the effect of intensive quenching on distortion and residual stress.
- Identify new geometries for simulation and testing.
- Test real gears – simulations and production results.

CHAPTER 8 Relevant presentations and publications

Publications:

- [1] Haixuan Yu, Mei Yang, and Richard D. Sisson Jr. "Applications of the Navy C-ring specimen to study the distortion during quenching." Accepted by *Metal Science and Heat Treatment*.
- [2] Haixuan Yu, Yuan Lu, Yangzi Xu, and Richard Sisson. "The Effect of Surface Preparation on Retained Austenite Measurement." In *100 Years of E04 Development of Metallography Standards*. ASTM International, 2019. **DOI:** 10.1520/STP160720170210
- [3] Yuan Lu, Haixuan Yu, and Richard D. Sisson Jr. "The effect of carbon content on the c/a ratio of as-quenched martensite in Fe-C alloys." *Materials Science and Engineering: A* 700 (2017): 592-597. **DOI:** 10.1016/j.msea.2017.05.094
- [4] Haixuan Yu, Mei Yang, Richard D. Sisson Jr. "Identification of the important parameters that control distortion during quenching of steel" *Heat treat 2019 (Detroit, MI)*
- [5] Haixuan Yu, Richard D. Sisson Jr. "Identification of the important process parameters to control distortion in heat treatment" *Thermal Processing in Motion 2018 (Spartanburg, SC)*
- [6] Haixuan Yu, Yuan Lu, Tianyi Zhou, and Richard D. Sisson Jr. "Identification of the important process parameters to control distortion and residual stress during heat treating" *Heat treat 2017 (Columbus, OH)*
- [7] Haixuan Yu, Yuan Lu, Xiaoqing Cai, and Richard D. Sisson Jr. "Microstructural analysis of carbides in steel by electrochemical extraction technique" *IFHTSE 2016 (Savannah, GA)*
- [8] Yuan Lu, Haixuan Yu, Xiaoqing Cai, Yiming Rong, and Richard D. Sisson Jr. "Martensite lattice parameter Measured by modern X-ray diffraction in Fe-C alloy" *IFHTSE 2016 (Savannah, GA)*
- [9] Haixuan Yu, Yuan Lu, Xiaoqing Cai, and Richard D. Sisson Jr. "The effect of tempering on the structure of martensite in 52100 steel" *Heat treat 2015 (Detroit, MI)*

Presentations:

- [1] Haixuan Yu, Mei Yang, Richard D. Sisson Jr. "Identification of the important parameters that control distortion during quenching of steel" *Heat Treat 2019 (Detroit, MI)*
- [2] Haixuan Yu, Richard D. Sisson Jr. "Understanding and controlling residual stress and distortion in heat treated steels" *Furnaces North America 2018 (Indianapolis, IN)*
- [3] Haixuan Yu, Richard D. Sisson Jr. "Identification of the important process parameters to control distortion in heat treatment" *Thermal Processing in Motion 2018 (Spartanburg, SC)*
- [4] Haixuan Yu, Yuan Lu, Tianyi Zhou, and Richard D. Sisson Jr. "Identification of the important process parameters to control distortion and residual stress during heat treating" *Heat Treat 2017 (Columbus, OH)*
- [5] Haixuan Yu, Yuan Lu, and Richard D. Sisson Jr. "Identification of the important material and process parameters that control distortion and residual stress in heat treatment" *Material Science & Technology 2017 (Pittsburgh, PA)*
- [6] Haixuan Yu, Yuan Lu, Xiaoqing Cai, and Richard D. Sisson Jr. "Microstructural analysis of carbides in steel by electrochemical extraction technique" *IFHTSE 2016 (Savannah, GA)*
- [7] Haixuan Yu, Yuan Lu, Xiaoqing Cai, and Richard D. Sisson Jr. "The effect of tempering on the structure of martensite in 52100 steel" *Heat treat 2015 (Detroit, MI)*

Appendix 1: Full factorial design table to identify the important processing parameters on quenching distortion

Table 1: Results of full 2⁶ factorial design for processing parameters on quenching distortion for the parts quenched in Hougto-Quench G quenching oil.

Test No.	Processing parameters						Results
	Part geometry	Quenching orientation	Agitation speed, rpm	Quench starts T, °C	Immersion rate, mm/s	Quenchant T, °C	Gap opening, %
1	small	gap down	800	850	120	60	3.319
2	small	gap down	0	900	10	60	0.123
3	big	gap down	800	850	10	20	6.283
4	big	gap up	0	900	10	20	2.200
5	small	gap up	800	850	10	60	2.690
6	big	gap up	0	850	120	20	3.262
7	big	gap down	800	900	10	60	6.096
8	big	gap up	0	900	120	20	3.002
9	small	gap up	0	850	120	60	2.315
10	small	gap down	0	850	120	20	1.162
11	small	gap down	800	900	120	20	3.539
12	small	gap up	800	850	10	20	2.658
13	small	gap down	0	850	10	60	1.256
14	big	gap up	800	900	120	60	6.322
15	big	gap up	800	850	10	60	6.070
16	big	gap up	800	850	10	20	6.934
17	big	gap down	0	900	120	20	3.075
18	small	gap up	0	850	10	60	1.268
19	big	gap up	0	850	10	20	2.908
20	small	gap down	800	850	120	20	3.331
21	big	gap up	800	850	120	60	6.878
22	big	gap down	0	900	120	60	2.142
23	small	gap up	0	850	10	20	1.994
24	big	gap up	0	900	10	60	2.292

25	small	gap up	800	900	120	60	3.374
26	small	gap down	0	900	10	20	0.708
27	small	gap up	0	900	10	20	0.714
28	big	gap up	800	900	10	60	5.939
29	small	gap down	800	850	10	60	3.362
30	small	gap up	0	900	120	60	0.901
31	small	gap up	0	900	120	20	1.727
32	big	gap down	0	850	10	20	2.644
33	big	gap down	0	900	10	60	3.347
34	small	gap down	800	850	10	20	4.031
35	small	gap up	0	900	10	60	2.234
36	big	gap down	800	900	10	20	6.440
37	small	gap down	800	900	10	60	3.602
38	big	gap down	0	850	10	60	2.417
39	big	gap down	800	900	120	60	7.006
40	big	gap up	0	900	120	60	3.207
41	small	gap up	800	900	10	60	3.459
42	big	gap up	0	850	120	60	3.323
43	small	gap down	0	850	120	60	1.608
44	big	gap up	800	850	120	20	7.047
45	small	gap down	0	900	120	60	1.272
46	small	gap up	800	850	120	60	3.458
47	big	gap up	800	900	120	20	6.656
48	big	gap down	0	850	120	60	3.102
49	big	gap down	800	850	120	20	6.966
50	small	gap up	0	850	120	20	1.492
51	big	gap down	800	900	120	20	6.742
52	small	gap up	800	850	120	20	4.451
53	small	gap down	0	850	10	20	0.657
54	small	gap up	800	900	120	20	3.538
55	big	gap up	800	900	10	20	6.573
56	small	gap up	800	900	10	20	4.173

57	big	gap down	800	850	120	60	6.356
58	big	gap down	800	850	10	60	5.779
59	big	gap down	0	900	10	20	3.794
60	big	gap up	0	850	10	60	3.728
61	small	gap down	800	900	120	60	3.269
62	small	gap down	0	900	120	20	0.949
63	big	gap down	0	850	120	20	2.577
64	small	gap down	800	900	10	20	3.832

Table 2: Results of full 2⁶ factorial design for processing parameters on quenching distortion for the parts quenched into two selected quenchants.

Test No.	Processing parameters						Results
	Part geometry	Quenching orientation	Immersion rate, mm/s	Quench starts T, °C	Quenchant T, °C	Quenchant type	Gap opening, %
1	big	gap up	120	900	60	Water	8.198
2	big	gap down	120	850	20	Oil	2.577
3	small	gap up	10	850	20	Water	9.254
4	small	gap down	120	900	60	Oil	1.272
5	big	gap up	120	850	20	Water	9.332
6	small	gap down	10	850	20	Oil	0.657
7	small	gap down	120	900	20	Water	8.231
8	small	gap down	120	850	20	Oil	1.162
9	small	gap up	120	900	20	Water	8.100
10	big	gap down	10	900	60	Water	7.721
11	big	gap down	120	850	60	Oil	3.102
12	small	gap up	120	850	20	Water	7.980
13	big	gap down	10	900	20	Oil	3.794
14	small	gap down	10	850	60	Water	6.281
15	small	gap up	10	850	60	Water	7.408
16	small	gap up	120	850	20	Oil	1.492
17	small	gap up	120	900	20	Oil	1.727
18	small	gap up	10	850	60	Oil	1.268
19	big	gap down	120	900	20	Oil	3.075
20	small	gap down	10	900	20	Water	6.689
21	big	gap down	10	900	20	Water	8.857
22	big	gap up	120	850	60	Oil	3.323
23	small	gap down	120	850	20	Water	8.164
24	small	gap up	120	900	60	Oil	0.901
25	big	gap up	10	900	20	Oil	2.200
26	small	gap up	120	850	60	Water	7.104
27	small	gap up	10	900	60	Oil	2.234

28	big	gap up	120	900	20	Water	8.939
29	small	gap up	10	900	20	Water	8.931
30	small	gap down	10	850	60	Oil	1.256
31	small	gap down	10	900	60	Water	5.847
32	big	gap up	120	850	60	Water	8.741
33	big	gap down	120	900	60	Oil	2.142
34	small	gap down	10	850	20	Water	6.958
35	big	gap down	10	850	60	Water	8.216
36	small	gap up	120	850	60	Oil	2.315
37	big	gap up	10	900	20	Water	9.560
38	big	gap down	120	850	60	Water	8.140
39	small	gap up	10	850	20	Oil	1.994
40	big	gap down	10	850	60	Oil	2.417
41	big	gap up	10	900	60	Water	8.927
42	big	gap up	10	850	60	Water	9.616
43	big	gap down	120	900	60	Water	8.650
44	big	gap down	120	850	20	Water	9.196
45	big	gap down	10	850	20	Water	9.524
46	small	gap up	10	900	20	Oil	0.714
47	big	gap up	10	900	60	Oil	2.292
48	big	gap up	10	850	20	Oil	2.908
49	big	gap down	10	900	60	Oil	3.347
50	big	gap up	120	850	20	Oil	3.262
51	small	gap down	10	900	60	Oil	0.123
52	small	gap up	10	900	60	Water	6.946
53	big	gap up	10	850	60	Oil	3.728
54	small	gap down	120	850	60	Water	7.073
55	big	gap down	10	850	20	Oil	2.644
56	small	gap down	10	900	20	Oil	0.708
57	big	gap up	10	850	20	Water	9.717
58	small	gap down	120	900	60	Water	6.651
59	big	gap down	120	900	20	Water	8.844

60	big	gap up	120	900	60	Oil	3.207
61	big	gap up	120	900	20	Oil	3.002
62	small	gap down	120	900	20	Oil	0.949
63	small	gap down	120	850	60	Oil	1.608
64	small	gap up	120	900	60	Water	6.719

Appendix 2: Fractional factorial design table to study the effect of HTC curve on quenching distortion of the Navy C-ring specimen

Table 1: Results of 2^5 fractional factorial design for processing parameters on quenching distortion for the parts quenched in Hougto-Quench G quenching oil.

Test No.	Parameters						Results
	HTC in convection, W/m^2K	Ms temperature, $^{\circ}C$	HTC Ms, W/m^2K	at Temperature at HTC max, $^{\circ}C$	HTC max, W/m^2K	HTC LF, W/m^2K	at Gap opening, mm
1	500	326	2000	700	3000	500	6.903
2	1000	412	2000	700	5000	1000	5.002
3	1000	326	2000	700	5000	500	8.404
4	1000	412	1000	500	5000	1000	2.502
5	500	412	2000	500	5000	1000	4.128
6	1000	412	2000	700	3000	500	5.402
7	1000	326	2000	500	3000	500	7.587
8	1000	326	1000	500	5000	500	5.744
9	1000	412	1000	700	3000	1000	1.904
10	1000	326	1000	500	3000	1000	5.078
11	500	412	1000	700	5000	1000	2.153
12	1000	326	2000	500	5000	1000	8.409
13	1000	326	2000	700	3000	1000	7.684
14	500	412	1000	700	3000	500	2.865
15	500	326	1000	500	5000	1000	6.182
16	500	326	2000	500	5000	500	7.278
17	1000	412	1000	700	5000	500	2.446
18	1000	412	2000	500	3000	1000	5.028
19	500	326	1000	700	3000	1000	5.279
20	1000	326	1000	700	5000	1000	5.945
21	1000	412	1000	500	3000	500	2.417
22	500	326	1000	700	5000	500	4.913
23	500	326	2000	500	3000	1000	6.912
24	1000	412	2000	500	5000	500	5.877

25	500	326	2000	700	5000	1000	8.716
26	500	412	2000	500	3000	500	4.153
27	500	412	2000	700	3000	1000	3.581
28	500	412	2000	700	5000	500	4.899
29	500	326	1000	500	3000	500	4.710
30	1000	326	1000	700	3000	500	5.084
31	500	412	1000	500	3000	1000	1.828
32	500	412	1000	500	5000	500	2.549
